CARBON, NITROGEN, AND SULFUR CYCLING INTERACTIONS IN ORGANIC CARBON RICH EXTREME ENVIRONMENTS

by Marshall W. Bowles

(under the supervision of Samantha B. Joye)

ABSTRACT

The interactions of dissimilatory processes were studied in organic carbon rich extreme environments, on the basis of geochemical signatures, molecular microbiology, and microbial activity assessments. In cold seep and hydrothermally-altered sediments dissimilatory processes such as nitrate reduction (DNF), sulfate reduction (SR), anaerobic oxidation of methane (AOM), and bicarbonate reduction based-methanogenesis (MOG) were measured. Sediments with bacterial mats and exposed gas hydrates, which are surficial features associated with the active seepage of reduced compounds (e.g. sulfide and methane), were targeted during this work and typify the general sample description. In a Gulf of Mexico cold seep we measured the highest reported rates of SR, and noted a large disparity in comparison to the lower AOM rates. These findings led to a global compilation of all *ex situ* rates of simultaneously reported SR and AOM rates. The current process based understanding of AOM suggests that the ratio of SR to AOM should be 1:1 based on the reaction stoichiometry of one mol sulfate reduced and methane oxidized. In the global compilation (n = 53 cores) of *ex situ* rates the median ratio of SR to AOM was 10.7:1. The median global integrated rate of AOM, representing a general cold seep AOM rate, was only 5% of the previously published estimate for AOM rates at cold seeps. These *ex situ* AOM rate estimates are performed at atmospheric

pressure, where saturated methane concentrations might be significantly lower than methane concentrations *in situ*. Based on reaction kinetics at higher methane concentrations rates of AOM should be higher. To address these issues we developed a novel method wherein *in situ* methane concentrations could be achieved by applying pressure to a sample amended with gaseous headspace. The method was described and a pressure and methane concentration effect was seen for processes such as SR, AOM, and MOG in samples from cold seeps in the Gulf of Mexico and Monterey Bay. These results explicitly show that degassed sediments used for *ex situ* rate estimates do not describe microbial activities in deep sea sediments, particularly methane rich environments.

INDEX WORDS: Cold seep, Hydrothermal vent, Sulfate reduction, Anaerobic oxidation of methane, Methanogenesis, Denitrification, Beggiatoa sp., High pressure, Biogeochemistry, Molecular Ecology, Lipid biomarkers, Gas hydrate, Thermodynamics, Carbon fixation

CARBON, NITROGEN, AND SULFUR CYCLING INTERACTIONS IN ORGANIC CARBON RICH EXTREME ENVIRONMENTS

by

MARSHALL WAYNE BOWLES

B.S. Integrated Science and Technology, James Madison University, 2003

M.E.M. Water and Air Resources, Duke University, 2005

A Dissertation Submitted to the Graduate Faculty of the University of Georgia in Partial Fulfillment of the Requirements for the Degree

DOCTOR OF PHILOSOPHY

ATHENS, GEORGIA

2011

CARBON, NITROGEN, AND SULFUR CYCLING INTERACTIONS IN ORGANIC CARBON RICH EXTREME ENVIRONMENTS

by

MARSHALL WAYNE BOWLES

Major Professor: Samantha B. Joye

Committee: Jeff Chanton
Mary Ann Moran
Bess Ward
William Whitman

Electronic Version Approved:
Maureen Grasso
Dean of the Graduate School
The University of Georgia
May 2011

DEDICATION

This work is dedicated to my parents:

Wayne and Debbie Bowles

Thank you for everything.

ACKNOWLEDGEMENTS

The dissertation presented here was made possible by the kind, good-spirited, collaborative and always cooperative nature of many individuals. First I would like to thank my major advisor Mandy Joye. Her endless encouragement, support, and excitement nurtured my interest and never put limits on my curiosity or abilities. As a mentor and friend she has made a lasting impression on me. I thank Vladimir Samarkin for constantly training my 'hands' and mind. First a colleague and later a друг, Vladimir was always involved in this work by teaching about biogeochemistry and life. Christof Meile and Nick Hayman (Duke University) played a similar role in this work at different times. Nick believed in me years ago and pushed me in this career path. Christof pushed me to always know a little more, on the most fundamental level, and in addition his truly generous attitude gave me much to aspire to. The tough-love support given by both was pivotal to the beginning and the completion of this work. Kim Hunter, Bill Porubsky, and Christelle Hyacinthe were all closely associated with this work, but most importantly were great friends throughout. Finally I would like to thank the Joye Lab throughout the years for keeping things light and sharing lots of good times: Charles Schutte, Melitza Crespo-Medina, Antje Vossmeyer, Meghan Hill, Kate Segarra, Beth Orcutt, Laura Palomo, Chris Comerford, Laura Potter, Amy Saupe, Steve Bell, Rachel Luther, Julie Slaughter.

Many field research trips were made during the course of this work and I thank the many that helped during these expeditions. Carol Lutken and the Hydrate Research

Consortium helped by generously supplying samples on many occasions. I thank Andreas Teske for graciously providing samples from Guaymas Basin. I thank Michael Madigan for allowing me to help him in the field, and his continued support.

I thank my committee; Mary Ann Moran, Barny Whitman, Jeff Chanton, and Bess Ward they provided advice at a critical stage in this work. They were also extremely cooperative and made all interactions very pleasant. Jay Brandes participated actively as an unofficial committee member through parts of the work, and his advice was greatly appreciated.

Finally, I would like to thank my family and friends for continued support and help over the years: Wayne and Debbie Bowles, William and Shirley Daughtrey, Kathy Bowles, Jenny Bailey, Ken Bradshaw, and Tim Brinkley.

TABLE OF CONTENTS

Page

LIST OF TABLES

Page

LIST OF FIGURES

Page

CHAPTER 1

INTRODUCTION and LITERATURE REVIEW

Biogeochemists have long attempted to relate prokaryotic activity to geochemical parameters, and likewise link molecular signatures to both activity and chemical patterns (Vernadsky, 1926). The work presented here represents a holistic approach of describing geochemical patterns, prokaryotic activities, and molecular biology as applied to better understand the cycling of elements and molecules critical as nutrients (C, N, and S) and energy sources (e.g. methane, nitrate, and sulfate) in deep-sea sediments. Little is known of how microorganisms assimilate nutrients or to what extent dissimilatory, or energy gaining reactions, are performed in deep-sea sediments. As such assimilatory and dissimilatory processes were examined in this work, within cold-seep and hydrothermally-altered sediments.

Cold seep and hydrothermally-altered sediments are typically methane rich, and defined by high rates of sulfate reduction (SR) and coupled anaerobic methane oxidation (AOM) (Joye et al., 2004, Arvidson et al., 2004; Kallmeyer and Boetius, 2004). In particular SR rates from a cold seep environment are the highest recorded rates in a natural environment (Arvidson et al., 2004). Sulfate reduction at these sites is driven by the oxidation of organic carbon deposited to the seafloor (Berner, 1980; Canfield, 1991), the anaerobic oxidation of methane (Reeburgh 1980; Valentine and Reeburgh, 2000 *and references therein*), or to oxidation of other hydrocarbons (Kniemeyer et al., 2007; Widdel et al., 2006 *and references therein*). Previous work in Gulf of Mexico cold seeps

has documented SR rates that exceed rates of AOM, and this was hypothesized to be a result of SR driven by abundant sources of labile carbon (Joye et al., 2004, Orcutt et al., 2005). Generally the view has been that these processes are linked and occur in a 1:1 ratio in accordance with the stoichiometry of the process (Hinrichs and Boetius, 2002 *and references therein*). If SR rates greatly exceed AOM rates then the efficiency of methane oxidation in advection dominated cold seep systems is greatly diminished.

In **Chapter 1** I describe rates of SR and AOM, geochemistry, and molecular biology in oily and gassy Gulf of Mexico cold seep sediments. At the Gulf of Mexico study site elevated rates of SR in comparison to AOM rates led to a global compilation of all simultaneous rate measurements of SR and AOM reported in literature. The global compilation was used to determine a new median cold seep AOM rate, which was substantially lower than the previous estimate (Hinrichs and Boetius, 2002). Enhanced sulfate removal via rigorous SR, coupled to observations of low AOM rates led to the assessment that perhaps the sediment biofilter of methane was not as strong as previously suspected.

The low rates of AOM compiled during the global survey developed into an investigation of factors that might increase AOM rates, namely higher methane concentrations and *in situ* pressures. The caveat with traditional rate assay methodology is that these all occur at *ex situ* conditions, i.e. sediments are recovered by a surface vessel and radiotracers are used to estimate rates at *in situ* temperature, but at atmospheric pressure (Jørgensen, 2006). The importance of pressure to date has only been considered in a cursory way, because a pressure of about 200 bar (2000 meters below sea level, *hereafter* mbsl) is required to influence or form a pressure-specific

signature on microbial distributions/activity (Overmann, 2006 *and references therein*), i.e. barophilism. However as depth increases pressures rise rapidly (10 bar per 100 mbsl), and pressure greatly influences the solubility biologically important gases (e.g. methane, butane, propane, and hydrogen). For example at atmospheric pressure (1 bar) methane solubility is only 1-2 mM, whereas at 1000 mbsl, or at a pressure of 100 bar, excluding hydrate formation methane solubility is predicted to be >120 mM (Duan and Mao, 2006). Therefore a need for a method which would allow incubations to be performed at *in situ* pressure and gas concentrations was realized.

In general microbiological processes and organisms have been studied at elevated pressure, but gas concentrations are not typically considered (Jannasch and Taylor, 1984, Kim and Kato, 2010 *and references therein*). The techniques that have allowed for either the maintenance of *in situ* gases or the restoration of typical environmental gas concentrations have not been directly amenable to measuring multiple processes on environmental samples (Weber et al., 2001, Nauhaus et al., 2005). In particular the previously used methods are restricted to processes without gaseous reactants and products. Specifically the processes of AOM and bicarbonate based methanogenesis (MOG) have never before been directly measured at *in situ* pressures and methane concentrations.

In **Chapter 2** I outline the development of a new method that allows rate assays to be performed for numerous processes at *in situ* pressures and gas concentrations. The method uses modified hungate tubes in conjunction with plungers to complete a sample vessel that makes possible the compression of amended gas and sediment as pressure is applied. The sampling vessels allow for numerous processes to be evaluated, because the

vessels are self-contained and gas tight. The method was evaluated for SR, AOM, and MOG in cold seep sediments from the Gulf of Mexico and California coast. In the method evaluation, all rates were influenced by methane and pressure, even considering all sediments were from depths significantly more shallow than 2000 mbsl.

Overlying water and sediments from cold seeps and hydrothermal vents can contain methane concentrations much higher than saturation at atmospheric pressure (Wankel et al., 2006, Lapham et al., 2008, Whelan et al., 1988). To date all estimations of microbial processes were performed at atmospheric pressure in degassed samples from both environments. Only one estimate of methane's influence on AOM exists, and this estimate is based entirely on SR rates used as a proxy for AOM rates (Nauhaus et al., 2005). Systematic studies on the influence of methane concentration on microbial processes do not exist.

Methane concentrations can influence many processes in cold seep and hydrothermally-altered sediments. As methane concentrations increase AOM becomes more favorable thermodynamically and rates should increase. As AOM rates increase sulfur cycling should be intensified through sulfate reduction (Hoehler et al., 1995). Conversely, MOG should become less favorable thermodynamically, and rates decrease, as methane concentrations increase. The final and fundamental consideration is the effect of methane concentration on carbon assimilation pathways. Microorganisms performing AOM and MOG have both been shown to assimilate bicarbonate (Whitman et al., 2006, Wegener et al., 2008), while some speculate methane assimilation by anaerobic methanotrophs (Hinrichs et al., 1999). Some sulfate reducing prokaryotes are autotrophic, using bicarbonate for carbon, while others are heterotrophic (Rabus et al., 2006).

In **Chapter 3** the influence of methane concentration on microbial processes in cold seep and hydrothermally altered sediments is explored. Sediments from the Gulf of Mexico, Monterey Bay, and Guaymas Basin were subjected to various treatments of methane concentration, while rates of SR, AOM, MOG, and methane and bicarbonate derived particulate organic carbon formation, as a proxy measure for carbon assimilation, were measured. SR and AOM rates both responded positively to methane concentrations in all sediments. In sediments from the Gulf of Mexico and Guaymas Basin rates of AOM exceeded SR by as much as 6 times. These data represent a complete reversal of the previous *ex situ* observations.

The only other process directly linked to methane oxidation is denitrification (DNF) (Raghoebarsing et al., 2006, Ettwig et al., 2010). Though DNF alone could not support the observed AOM rates from pressure experiments, because of nitrate limitation, the process of dissimilatory nitrate reduction can occur in cold seep sediments, though to date it is not documented. Prokaryotes capable of DNF have metabolic similarities to sulfate reducing bacteria. Perhaps most relevant is their ability to utilize numerous hydrocarbons (Widdel and Rabus, 2001). Seawater overlying cold seep sediments often maintains ~20-30 μM nitrate that diffuses into sediments (Joye et al., 2004). In addition giant sulfur oxidizing bacteria (e.g. *Beggiatoa*) that are commonplace in cold seep sediments concentrate nitrate in their vacuoles and might intensify nitrogen cycling in these sediments (Joye et al., 2004).

In **Chapter 4** I explored the potential for total nitrate removal and heterotrophic potential DNF in cold seep sediments from the Gulf of Mexico. Specifically in cold seep sediments inhabited by *Beggiatoa* I investigated nitrate removal in an upper horizon

populated by *Beggiatoa*, and a lower horizon without visible filaments. This chapter represents the first quantification of DNF rates within cold seep sediment.

References

Arvidson, R. S., Morse, J. W., and Joye, S. B., 2004. The sulfur biogeochemistry of chemosynthetic cold seep communities, Gulf of Mexico, USA. *Marine Chemistry* **87**, 97-119.

Berner, R. A., 1980. *Early Diagenesis: A theoretical approach.* Princeton University Press, Princeton, New Jersey.

Canfield, D. E., 1991. Sulfate reduction in deep-sea sediments. *American Journal of Science* **291**, 177-188.

Duan Z.H. and S.D. Mao. 2006. A thermodynamic model for calculating methane solubility, density and gas phase composition of methane -bearing aqueous fluids from 273 to 523 K and from 1 to 2000 bar. *Geochim. Cosmochim. Acta.* **70** (13): 3369-3386.

Ettwig, K.F., Butler, M.K., Le Paslier, D., Pelletier, E., Mangenot, S., Kuypers, M.M., Schreiber, F., Dutilh, B.E., Zedelius, J., de Beer, D., Gloerich, J., Wessels, H.J., van Alen, T., Luesken, F., Wu, M.L., van de Pas-Schoonen, K.T., Op den Camp, H.J., Janssen-Megens, E.M., Francoijs, K.J., Stunnenberg, H., Weissenbach, J., Jetten, M.S., Strous, M., 2010. Nitrite-driven anaerobic methane oxidation by oxygenic bacteria. *Nature* **464**, 543–548.

Hinrichs, K.-U., Hayes, J. M., Sylva, S. P., Brewer, P. G., and DeLong, E. F., 1999. Methane-consuming archaebacteria in marine sediments. *Nature* **398**, 802-805.

Hinrichs, K.-U. and Boetius, A., 2002. *The anaerobic oxidation of methane: new insights in microbial ecology and biogeochemistry.* Springer-Verlag, Berlin, Germany.

Hoehler, T.M., M.J. Alperin, D.B. Albert, and C.S. Martens. 1994. Field and laboratory studies of methane oxidation in an anoxic marine sediment: evidence for a methanogen-sulfate reducer consortium. *Global Biogeochem. Cycles* **8**: 451-463.

Jannasch, H.W. and C.D. Taylor. 1984. Deep-sea Microbiology. Ann. Rev. Microbiol. **38**: 487-513.

Jørgensen, B.B. *Bacteria and marine biogeochemistry.* H. D. S. a. M. Zabel, Ed., Marine Geochemistry (Springer, Berlin, ed. 2nd ed., 2006).

Joye, S. B., A. Boetius, B.N. Orcutt, J.P. Montoya, H.N. Schulz, M.J. Erickson, and S.K. Lugo. 2004. The anaerobic oxidation of methane and sulfate reduction in sediments from Gulf of Mexico cold seeps. *Chem. Geol.* **205**: 219-238.

Kallmeyer, J. and Boetius, A. (2000) Effects of Temperature and Pressure on Sulfate Reduction and Anaerobic Oxidation of Methane in Hydrothermal Sediments of Guaymas Basin. *Applied Environmental Microbiology.* 1231-1233.

Kim, S.-J. and C. Kato. 2010. 40 Sampling, Isolation, Cultivation, and Characterization of Piezophilic Microbes. In K.N. Timmis ed., Handbook of Hydrocarbon and Lipid Microbiology. Berlin: Springer- Verlag, p. 3869-3881.

Kniemeyer, O., Musat, F., Sievert, S. M., Knittel, K., Wilkes, H., Blumenberg, M., Michaelis, W., Classen, A., Bolm, C., Joye, S. B., and Widdel, F., 2007. Anaerobic oxidation of short-chain hydrocarbons by marine sulphate-reducing bacteria. *Nature* **449**, 898-901.

Lapham, L. L., J.P. Chanton, C.S. Martens, P.D. Higley, H.W. Jannasch, and J.R. Woolsey. 2008. Measuring Temporal Variability in Pore-Fluid Chemistry To Assess Gas Hydrate Stability: Development of a Continuous Pore-Fluid Array. *Environ. Sci. Technol.* **42**(19): 7368-7373.

Nauhaus, K., A. Boetius, M. Kruger, and F. Widdel. 2002. *In vitro* demonstration anaerobic oxidation of methane oxidation coupled to sulfate reduction in sediment from a marine gas hydrate area. *Environ. Microbiol.* **4**(5): 296-305.

Orcutt, B., M. Elvert, V.A. Samarkin, and S.B. Joye. 2005. Molecular biogeochemistry of sulfate reduction , methanogenesis, and the anaerobic oxidation of methane at Gulf of Mexico cold seeps. *Geochim. Cosmochim. Acta.* **69**(17): 4267-4281.

Overmann, J. (2006) Principles of Enrichment, Isolation, Cultivation and Preservation of Prokaryotes. *The Prokaryotes*: 80-136.

Rabus, R., Hansen, T.A., Widdel, F. (2006) Dissimilatory Sulfate- and Sulfur-Reducing Prokaryotes. *The Prokaryotes*: 659-768.

Raghoebarsing, A.A., Pol, A., van de Pas-Schoonen, K.T., Smolders, A.J., Ettwig, K.F., Rijpstra, W.I., Schouten, S., Damste, J.S., Op den Camp, H.J., Jetten, M.S., Strous, M., 2006. A microbial consortium couples anaerobic methane oxidation to denitrification. *Nature* **440**, 918–921.

Reeburgh, W.S., 1980. Anaerobic methane oxidation: Rate depth distributions in Skan Bay sediments. *Earth Planetary Science Letters* **47**, 345-352.

Vernadsky, V.I. (1926) Nauchnoe khimiko-tekhnicheskoe izdatel'stvo, *Biosfera*, Leningrad (in Russian).

Wankel, S.D., S.B. Joye, V.A. Samarkin, S. Shah, G. Friderich, J. Melas-Kryiazi, and P.R. Girguis. 2010. New constraints of diffusive methane fluxes and rates of anaerobic methane oxidation in a Gulf of Mexico brine pool through the use of a deep sea *in situ* mass spectrometer. *Deep Sea Research I*, doi:10.1016/j.dsr2.2010.05.009.

Weber, A., W. Riess, F. Wenzhoefer, and B.B. Jørgensen. 2001. Sulfate reduction in Black Sea sediments: in situ and laboratory radiotracer measurements from the shelf to 2000m depth. *Deep-Sea Research I* **48**: 2073-2096.

Wegener, G., Niemann, H., Elvert, M., Hinrichs, K.-U., and Boetius, A., 2008. Assimilation of methane and inorganic carbon by microbial communities mediating the anaerobic oxidation of methane. *Environmental Microbiology* **10**, 2287-2298.

Welhan, J.A. 1988. Origins of methane in hydrothermal systems. *Chem. Geol.* **71**: 183 198.

Whitman, W., Bowen, T., and Boone, D. (2006) The Methanogenic Bacteria. *The Prokaryotes*, Springer, New York.

Widdel F, Rabus R. (2001). Anaerobic biodegradation of saturated and aromatic hydrocarbons. *Curr. Opin. Biotechnol.* **12**: 259–276.

Widdel, F., Boetius, A., and Rabus, R., 2006. Anaerobic Biodegradation of Hydrocarbons Including Methane. *The Prokaryotes*, Springer, New York.

CHAPTER 2

WEAK COUPLING BETWEEN SULFATE REDUCTION AND THE ANAEROBIC OXIDATION OF METHANE IN METHANE-RICH SEAFLOOR SEDIMENTS DURING *EX SITU* INCUBATION[1]

[1] Bowles, M.W., Samarkin, V.A., Bowles, K.M., and S.B. Joye. 2010. *Geochimica Cosmochimica et Acta*. 75: 500-519, doi:10.1016/j.gca.2010.09.043. Reprinted here with permission of the publisher.

Abstract

We investigated coupling between sulfate reduction (SR) and anaerobic oxidation of methane (AOM) by quantifying porewater geochemical profiles, determining rates of microbial processes, and examining microbial community structure at two sites within Mississippi Canyon lease block 118 (MC118) in the Northern Gulf of Mexico. Sediments from the northwest seep contained high concentrations of methane while sediments from the southwest seep contained methane, gaseous *n*-alkanes and liquid hydrocarbons and had abundant surficial accumulations of gas hydrate. Volumetric (21.5 μmol cm^{-3} d^{-1}) and integrated (1429 mmol m^{-2} d^{-1}) rates of SR at MC118 in *ex situ* incubations are the highest reported thus far for seafloor environments. AOM rates were small in comparison, with volumetric rates ranging from 0.1 to 12.6 nmol cm^{-3} d^{-1}. Diffusion cannot adequately supply the sulfate required to support these high SR rates so additional mechanisms, possibly biological sulfide oxidation and/or downward advection, play important roles in supplying sulfate at these sites. The microbial communities at MC118 included sulfate-reducing bacteria phylogenetically associated with *Desulfobacterium anilini,* which is capable of complex hydrocarbon degradation. Despite low AOM rates, the majority of archaea identified were phylogenetically related to previously described methane oxidizing archaea. To evaluate whether weak coupling between SR and AOM occurs in habitats lacking the complex hydrocarbon milieu present at MC118, we compiled available SR and AOM rates and found that the global median ratio of SR to AOM was 10.7:1 rather than the expected 1:1. The global median integrated AOM rate

was used to refine global estimates for AOM rates at cold seeps; these new estimates are only 5% of the previous estimate.

1. Introduction

Sulfate is the most abundant dissolved electron acceptor in seawater and microbial sulfate reduction is often the dominant anaerobic terminal metabolic process in marine sediments. Sulfate reduction (*hereafter* SR) can be coupled to the oxidation of organic carbon deposited to the seafloor (Berner, 1980; Canfield, 1991), the anaerobic oxidation of methane (Reeburgh 1980; Valentine and Reeburgh, 2000 *and references therein*), or to oxidation of other hydrocarbons (Kniemeyer et al., 2007; Widdel et al., 2006 *and references therein*). Cold seep ecosystems uniquely support SR coupled to all ofthese reductants, with SR rates among the highest recorded for natural systems (Arvidsonet al. 2004; Joye et al. 2004).

The extraordinarily high SR rates at cold seeps are fueled by the focused seepage of reduced substrates, including gaseous and liquid hydrocarbons. However, such high SR rates are ultimately self-limiting because the sulfate pool is depleted rapidly in the absence of reduced sulfur recycling via oxidation to sulfate or accelerated rates of sulfate transport. Sulfate can be replenished by three mechanisms: chemical oxidation, downward advection of sulfate-rich seawater, and biological oxidation. Chemical (abiotic) oxidation is supported by Fe and Mn oxides or by O_2 transported into sediments via sedimentation or diffusion, respectively (Schippers and Jørgensen, 2001; Preisler et al., 2007). Fluid or bubble-induced mixing of pore waters (O'Hara et al., 1995; Sahling et al., 2009) can increase supplies of sulfate to sulfate reducing bacteria (*hereafter* SRB) and thereby sustain/fuel high rates of SR. Biological sulfide oxidation coupled to the

reduction of molecular oxygen or nitrate is common in sulfidic environments like cold seeps (Otte et al., 1999; Høgslund et al., 2009).

The diversity of sulfate reducing bacteria (SRB) and methane cycling archaea at cold seeps is high (Knittel et al., 2003, 2005). Though most previous assessments of SRB diversity were conducted at cold seeps lacking gaseous *n*-alkanes > C_1 and/or liquid hydrocarbons and oil (see e.g. Knittel et al., 2003, 2005), known SRB can utilize a wide range of organic substrates that are present at cold seeps; including, simple volatile fatty acids (e.g. acetate; Widdel and Pfennig, 1981; Sørensen et al., 1981), complex organic molecules, e.g. long-chain hydrocarbons and aromatic hydrocarbons (Widdel and Rabus, 2001), and gases, e.g. propane and butane (Kniemeyer et al., 2007; Orcutt et al., 2010). Distinct clades of so-called *an*aerobic *me*thanotrophs (ANME) may co-occur with specific SRB and appear to mediate the anaerobic oxidation of methane (AOM). The ANMEs (ANME-1, ANME-2, and ANME-3) occur as aggregates with SRB, individual cells, clusters, or chains of cells (Orphan et al., 2002; Orcutt et al., 2005; Lösekann et al., 2007). Oftentimes, ANME-1 and ANME-2 co-occur with clades *Desufosarcina*/ *Desulfococcus*, whereas ANME-3 co-occurs with the clade *Desulfobulbus*. Though ANME and associated SRB clades occur at higher alkane and oil rich cold seeps like MC118 (Orcutt et al., 2005; Orcutt et al., 2010), AOM activity is low relative to rates of sulfate reduction (Joye et al., 2004; Joye et al., 2010).

Our objective in this work was to evaluate further the impact of non-methane organic carbon on microbial activity and community composition. We present here measurements of microbial activity, microbial community composition, and sediment

geochemistry for a cold seep in the Northern Gulf of Mexico (*hereafter* GOM). We also assembled data from the literature from cold seeps around the globe to evaluate broadly the relationship between SR and AOM at seeps characterized by a range of carbon inputs and better constrain the efficiency of AOM as a biofilter for methane in the environment.

2. Materials and Methods

2.1 Study Site

Sediment samples were collected from Mississippi Canyon lease block 118 (*hereafter* MC118), which is located offshore of Louisiana (28°51.47 N, 88°29.52 W) beneath 880 meters of water (Figure 1). At MC118 surface breaching gas hydrate, chemosynthetic mussels, and *Beggiatoa* mats occur along a topographic high associated with seepage of oil and gas (Lapham et al., 2008). The site overlies a salt diapir (~500m subbottom), and a complex fault networks connect deep subsurface and surficial habitats (McGee et al., 2008). Sediments from the northwest seep at MC118 (*hereafter* gassy seep) were gas-charged and overlain by *Beggiatoa* mats. Sediments from the southwest seep (*hereafter* oily seep) were characterized by *Beggiatoa* mats, oil staining, gas bubble streams, and surface breaching gas hydrate (Table 1). The abundance of *Beggiatoa* mats at MC118 underscores the active nature of seepage of this site; however, the site lacks the signatures of mature seepage (i.e. tubeworms, clams, and extensive carbonate pavement; Levin, 2005) suggesting that active seepage is a recent phenomenon.

2.2. Sample description and sample collection.

Samples were collected in September 2006 using the manned submersible *Johnson SeaLink II* during a research cruise on board the R/V Seward Johnson II. At each coring

site, at least two cores were collected, one core for geochemical characterization and a paired core for microbial rate assays and microbiology. A total of 12 cores were analyzed and included sediments characterized as: gassy with white *Beggiatoa* (gassy-1), gas-laden (gassy-2), oil-stained adjacent to a gas hydrate mound (oily-1), oil-stained and carbonate-rich (oily-2), oil-stained and gassy (oily-3), and oil-stained and gas-laden with white *Beggiatoa* (oily-4) (Table 1). Upon return to the surface, cores were immediately transported to a 4°C cold room and processed. Porewaters were collected using a mechanical porewater squeezer similar in design to that of Reeburgh (1967).

2.3. Geochemistry

2.3.1. Gases, salts, and carbon

Cores were sectioned at 2 cm or 3 cm intervals and sub-samples for gas analysis (C_1-C_5, e.g. methane, ethane, propane, iso-butane, butane, and pentane) were collected immediately as a new sediment section was extruded. For dissolved gas quantification, a 2 cm^{-3} sediment sub-sample was fixed with 3 mL anoxic (He-purged) 2M NaOH in headspace vials, crimp sealed with butyl rubber septa, and stored upside down. Samples were analyzed on a Shimadzu Gas Chromatograph using Flame Ionization Detector (GC-FID) (Joye et al., 2004). Gaseous hydrocarbon concentrations are conservative because degassing occurred during return to the surface and during manipulation at atmospheric pressure. Stable isotopic analysis of methane and standardization was carried out using isotope ratio monitoring mass spectrometry as described in Joye et al. (2010). For hydrogen (H_2) analysis, a 3 cm^{-3} sub-sample was transferred into a He-purged headspace vial, was capped with a thick rubber septa, crimp sealed, and re-purged with He. The

headspace was allowed to reach equilibrium by incubation at *in situ* temperature (8ºC) for four to five days (Hoehler et al., 1994) and then H_2 concentration was determined on a Reduced Gas Analyzer (RGA) (Peak Performer™, Peak Laboratories, California, USA) calibrated using a certified H_2 standard (1% H_2 in a balance of He; Scott Specialty Gases, Plumsteadville, Pennsylvania, USA). The detection limit was 800 parts per trillion (~sub-picomolar H_2 concentration); the standard precision was 3%.

The remaining sediment was transferred to an argon flushed squeezer cup, pressure was applied, and the displaced porewater (~30 mL) collected into argon-purged syringes. Immediately after collection, pore water samples were filtered (0.2 µm Target® filters) and transferred to different vials. Prior to subsampling the sample pH was measured using a Thermo Scientific, Inc. Orion 4 Star™ pH electrode that was calibrated with NBS buffers (pH=4, 7, and 10). Subsamples (0.5 to 2 mL) for hydrogen sulfide (H_2S) were transferred into a tube containing 1 mL of 20 weight percent zinc acetate; H_2S concentration was determined using the methylene blue method (precision of 3-5%; Cline, 1969). Anion subsamples (sulfate (SO_4^{2-}) and chloride (Cl^-)) were preserved by addition of nitric acid (0.1 µM final concentration) and concentrations quantified on a Dionex® Ion Chromatograph (Joye et al., 2004); analytical precision was between 1.5% and 7%. All nutrient samples (NO_x^- = nitrate (NO_3^-) + nitrite (NO_2^-), ammonium (NH_4^+) and phosphate (PO_4^{3-})) were collected, stored, and analyzed as described previously (Joye et al., 2004). Subsamples were also collected and immediately frozen for measurement of dissolved organic carbon (DOC), which was quantified using a Shimadzu® TOCV (Weston and Joye, 2005) with an analytical precision of 2-5%.

Dissolved inorganic carbon (DIC) samples were preserved with saturated $HgCl_2$ and concentrations were determined using infrared detection (precision 0.5-2%).

2.3.2. Solid Phase Carbon and Nitrogen

An aliquot of frozen sediment was dried, and then crushed with a mortar and pestle. About 15 mg of crushed dry sediment was weighed using a microbalance, placed in a miniature silver tin, and fumed with concentrated HCl for 24 hrs to remove carbonates. Afterwards, samples were re-dried and analyzed on a ThermoFinnigan FlashEA 1112 series NC analyzer (Weston et al., 2006). Total organic carbon (TOC) and total nitrogen (TN) content is expressed as weight percent C or N.

2.3.3. Aliphatic hydrocarbon fraction

The aliphatic hydrocarbon fraction (AHF) was extracted from wet sediments following Elvert et al. (2000) with some modifications. Briefly, sediments were ultrasonically extracted, successively, with 25 ml of dichloromethane/methanol (1:2, v/v), 25 ml of dichloromethane/methanol (2:1, v/v), and twice with 25 ml of dichloromethane. Different lipid fractions were chromatographically separated using silica solid-phase extraction (Si-SPE) cartridges (500 mg, 3 ml, Supelco®) and aliphatic hydrocarbons were eluted with 9 ml of *n*-hexane. Upon elution the sample was evaporated to dryness and the AHF mass was determined gravimetrically. Gas chromatographic analyses of the AHF was performed using an Rtx-1 silica column (30 m x 0.25 mm ID and 0.25 !m film thickness; Restek Scientific) via an on-column injector and a GC-FID using H_2 as a carrier gas (4.0 ml/min flow rate). Samples were reconstituted with *n*-hexane prior to injection in the GC-FID. Samples were analyzed using an initial oven temperature of 50°C, followed

by a ramp of 20°C/min to 170°C, and a final ramp of 3°C/min to 310°C, where the temperature was held for 10 min. The chromatographs were used to evaluate the relative degree of microbial alteration of oil-derived materials, as noted by the loss of labile lipid components such as *n*-alkanes and isoprenoids, and the appearance of a broad peak (the "unresolved complex mixture" or UCM).

2.4. Microbial activity

Samples for SR and AOM rate measurements were injected, incubated and preserved on board the ship. For SR, the $^{35}SO_4^{2-}$ tracer solution (0.83 MBq) was injected through the butyl rubber stopper and samples were placed in an N_2 atmosphere for incubation at *in situ* temperature (8ºC) for 24 hours. Replicates (n=2) and a killed control were run for each depth horizon in each core assayed. To halt microbial activity, the sample was ejected into a 50 mL centrifuge tube containing 10 mL of 20 weight percent zinc acetate. To recover the radioactive sulfide produced, samples were rinsed of sulfate by centrifuging and amendment with anoxic seawater (repeated 3x). After the first rinse, a sub-sample was collected to quantify the $^{35}SO_4^{2-}$ activity. Samples were then stored in ethanol at -20°C until distillation. Samples were distilled via a one-step wet-acid reduction and sulfide was trapped in 20 weight percent zinc acetate (Canfield et al., 1986; Fossing and Jørgensen, 1989). The radioactivity of sulfate and sulfide samples was measured using Scintiverse BD (Fisher®) and Scintisafe Gel (Fisher®) scintillation cocktails, respectively. Rates of SR were estimated using equation (1).

$$\text{SR Rate}=[SO_4^{2-}]\times \alpha_{SO4}/t \times(\text{DPM-}H_2{}^{35}S/(\text{DPM-}{}^{35}SO_4+\text{DPM-}{}^{35}H_2S)) \quad (1)$$

Here, the SR rate (nmol cm^{-3} day^{-1}) is the rate of sulfate reduction; [SO_4^{2-}] is the porewater sulfate concentration (nmol cm^{-3} wet sediment; obtained by multiplying the porewater sulfate concentration times the sediment porosity); α is the fractionation factor (1.06; Jørgensen, 1978), *t* is the time of incubations (days); $H_2{}^{35}S$ is the radioactivity of sulfide generated (minus activity in killed controls); and $^{35}SO_4^{2-}$+$H_2{}^{35}S$ reflects the total tracer radioactivity injected. Recovered radioactivity from the sulfide pool exceeded 50% of injected radioactivity in the extreme high activity samples.

Samples for AOM rate determination (approximately 2 cm^{-3}) were amended with dissolved $^{14}CH_4$ (4.2 kBq) and incubated for 24 hours, after which time, samples were fixed by extruding the sample into a 50 mL centrifuge tube containing 5 mL of 2M NaOH. Samples were processed via active acid distillation in round bottom flasks with ground glass fitted condensers containing 15 mL of ethanol. Hydrochloric acid (final concentration of ~10%) was added, the samples were purged with nitrogen, and $^{14}CO_2$ was trapped directly into a mixture of CarboSorb E® and PermaFluor®. Samples were distilled for 1-hr and the recoveries, as determined from $NaH^{14}CO_3$, averaged 99%. Rates of AOM were calculated using equation (2)

$$\text{AOM Rate}=[CH_4]\times \alpha_{CH_4}/t \times(\text{DPM-}^{14}CO_2/\text{DPM-}^{14}CH_4) \qquad (2)$$

Here, the AOM rate (nmol cm^{-3} day^{-1}) is the rate of methane oxidation, [CH_4] is the concentration of methane (nmol cm^{-3} of wet sediment), α is the fractionation factor (1.06; Alperin et al., 1988), *t* is the time of incubations (days), $^{14}CO_2$ is the radioactivity of carbon dioxide generated minus activity from controls, and $^{14}CH_4$ reflects the ^{14}C tracer radioactivity injected.

Rates of SR and AOM are expressed volumetrically (nmol cm^{-3} day^{-1}) and as an integrated rate (mmol m^{-2} d^{-1}), which was obtained by trapezoidal integration of the depth-specific volumetric activity rates (Table 1). Turnover times of sulfate and methane were calculated as the integrated substrate pool divided by the integrated activity rate (Table 1).

2.5. Molecular Analysis

2.5.1. DNA extraction and Polymerase Chain Reaction

Samples for clone library construction targeted zones with maximum sulfate reduction rates (1.5 cm in gassy-1 and 5 cm in oily-4 cores). Approximately 30 mg of sediment was used for DNA extraction with the MOBIO™ (Carlsbad, CA) Ultrapure Soil DNA extraction kit as specified by the manufacturer. The PCR master mix consisted of (50 µL): 2 µL of template DNA, 0.5 µL of forward and reverse primers (100 µmol L^{-1}), 10 µL of 5x PCR buffer, 1.25 µL of bovine serum albumin (10 mg/mL), 1 µL of deoxynucleoside triphosphate (10 mM dATP, 10 mM of dCTP, 10 mM dGTP, 10 mM dTTP), 5 µL of $MgCl_2$ (25 mM), and 0.25 µL of Taq DNA (20 U/µL), and the balance as sterile H_2O. The *dsrAB* and 16S rRNA bacterial and archaeal gene PCR cycles began with an initial denaturation of 10 minutes at 94°C followed by 30 cycles of 1.5 minutes of denaturation at 94°C, 30 s of annealing at 55°C, 30 s of elongation at 72°C, ending with 7 minutes of elongation at 72°C. Primers specific to the functional gene *dsrAB*, *dsr1f* (ACSCAYTGGAAGCACG) and *dsr4r* (GTGTAGCAGTTACCGCA), were used for amplification of the alpha and beta subunits (Wagner et al., 1998). For the amplification of the16S rDNA region of bacteria the eubacterial specific primer B27f

(AGAGTTTGATCCTGGCTCAG) and the universal reverse primer U1492r (GGTTACCTTGTTACGACTT) were used (Orphan et al., 2001a). The 16S rDNA region of archaea was amplified by the combination of 3 primers: ARCH20f (TTCCGGTTGATCCYGCCRG), ARCH958r (YCCGGCGTTGAMTCCAATT), and UNI1392r (ACGGGCGGTGTGTRCA) (Orphan et al., 2001a; Teske and Sørensen, 2008).

2.5.2. Cloning

All PCR products were verified to contain the gene of interest and subsequently purified using a Qiagen Gel Extraction Kit, as specified by the manufacturer. The gene of interest was then ligated into a pCR4 vector (Invitrogen) and transformed into *E. coli* using the specifications of the manufacturer. All colonies were screened for ampicillin resistance and *lacZ* expression. Sequencing was carried out starting at the M13F primer within the pCR4 vector.

2.5.3. Phylogenetic analysis

For *dsrAB* gene analysis, sequences were converted to amino acids and verified to be on the correct reading frame using the Open Reading Frame (ORF) finder (NCBI). The *dsrAB* gene was aligned using Clustal W and the alignment (~200 amino acids) was then manually edited (Larkin et al., 2007). All 16S rRNA gene sequences were screened first using blastn (NCBI), and next were aligned using the *S*ilva *In*cremental *A*ligner (SINA) (Pruesse et al., 2007). After alignment, all 16S rDNA clones were tested for chimeras using Bellerophon (Huber et al., 2004). Following the chimera check, sequences (600 bp) were imported to ARB and the quality of the alignment was verified and manually

adjusted in ARB_EDIT (Ludwig et al., 2004). Mega4 was used to create *dsrAB* and 16S rDNA phylogenetic trees (Tamura et al., 2007). The *dsrAB* functional gene tree was created using minimum evolution with complete deletion and verification of alignment by bootstrap analysis (n=1000). Phylogenetic trees for 16S rRNA were made using neighbor joining, with a Jukes-Cantor model for distance correction, and tree topology was verified by bootstrap analysis (n=1000). Similarity cutoffs for operational taxonomic units (OTUs) were >90% and 97% similar for clones of the *dsrAB* and 16S rRNA genes, respectively.

2.6. Constraining Diffusive Fluxes

Diffusive sulfate delivery to depth was estimated using Fick's first law, (equation 3),

$$J = -D\frac{\partial C}{\partial x} \qquad (3)$$

where J is the diffusive flux of sulfate into sediments (mmol cm^{-2} y^{-1}), Φ is the porosity at 0.80, D_s is the diffusion coefficient corrected for tortuosity (112.5 cm^2 y^{-1}) and $\partial C/\partial x$ is the concentration gradient (mmol cm^{-4}). The sulfate concentration gradient between the upper sediment horizon (top 2 cm) and the overlying seawater was used to calculate the flux. To determine D_s we used the following equation (Iversen and Jørgensen, 1993):

$$D_s = \frac{D}{1 + n(1-\phi)} \qquad (4)$$

where D is the diffusion coefficient of the solute from (Schulz, 2000), sulfate in seawater, and n is porosity dependent constant of 3.

2.7. Free Energy of Reaction Estimates

The Gibb's Free Energy of reaction (ΔG) was determined for SR coupled to various electron donors, including methane, and methanogenesis (MOG) from acetate and bicarbonate. The ΔG^{o} values were obtained from published ΔG_f values (Table 3; Canfield et al., 2005, *unless otherwise noted*) and used to calculate ΔG (kJ mol^{-1}) for each reaction under *in situ* conditions, using equation (5).

$$\Delta G = \Delta G^{\circ} + RT \times \ln\left(\frac{[A]_{P_n}^{S_n}}{[A]_{R_n}^{S_n}}\right) \qquad (5)$$

Here, R is the gas constant (0.008314 kJ $mol^{-1}K^{-1}$), T is the *in situ* temperature (278°K), and A is the activity of the respective product (P) or reactant (R), which was approximated as the environmental concentration of that compound (Table 3). The activities for each compound (n) were corrected by the stoichiometric factor (S) for the respective reaction. The stoichiometrically corrected activities of products and reactants for each respective reaction were multiplied, and are represented here as $[A]_{P_n}^{S_n}$ and $[A]_{R_n}^{S_n}$ (Table 4). The balanced equations and determined ΔG^{o} values are presented in Table 4. Since the intermediate or electron carrier for coupled SR-AOM is not known, the ΔG was calculated for the net reaction.

3. Results

3.1. Geochemistry

3.1.1. Gases, Salt, and Carbon

Cores collected from the two seeps had similar concentrations of anions, DIC, and DOC, but differing concentrations and compositions of dissolved gases (Table 1).

Chloride concentrations were similar to seawater values (~550 mM). Sulfate consumption over depth was observed but only one core from each site (gassy-1 and oily-3) showed substantial sulfate depletion, which we conservatively define as $[SO_4^{2-}] < 2$ mM based on Boudreau and Westrich (1984) (Table 1, Figure 2). Sulfide concentrations increased with depth and ranged from 0 to 28 mM. Methane concentrations ranged from 17.3 μM to ~1.4 mM, which is about saturation at 1 atm, and generally increased with depth. Oily-2 sediments, collected near an authigenic carbonate outcrop away from a gas hydrate mound, had the lowest overall CH_4 concentration (72.1μM; Table 1). The average $\delta^{13}C$-CH_4 was -46‰ and -44‰ for gassy-1 and oily-4 sediments, respectively (Figure 2). The range of $\delta^{13}C$-CH_4 values in gassy-1 (-42 to -51‰) and oily-4 (-38 to -64‰) sediments was similar. Only two cores, oily-3 and oily-4, contained significant amounts of gaseous alkanes (C_2-C_5); the maximum alkane concentration (Σ alkanes=C_2+C_3+C_4+iso-C_4+C_5) was ~14 mM (Figure 2). In gassy-1 sediments, individual C_2-C_5 alkane concentrations were no greater than 20 μM (Figure 2). Hydrogen concentrations were variable and ranged from 3.3 to 57 nM, and averaged 14 nM (Table 1). Dissolved inorganic carbon concentrations increased with depth to 16 mM for all cores, except oily-2, which was short compared to the other cores. The depth specific DIC concentrations in this core were comparable to those observed in the other cores. Dissolved organic carbon concentrations also increased with depth; the highest DOC concentration was 3.3 mM (adjacent to a gas hydrate mound). Porewater pH ranged between 7.3 and 8.2.

3.1.2. Dissolved Inorganic Nutrients

Dissolved inorganic nitrogen (DIN=NO_x^- + NH_4^+) and dissolved inorganic phosphate (DIP=PO_4^{3-}) concentrations varied between cores.Concentrations of NO_x^- ranged from 0 to above 280 μM and were highest in sedimentsoverlain by *Beggiatoa* mats (gassy-1 and oily-4). All sediments except core oily-2 contained a secondary NO_x^- peak at depth. Ammonium concentrations were lowest inoverlying seawater and increased with depth from 74.1 to 821.3 μM. Cores containing *Beggiatoa* (gassy-1 and oily-4) contained relatively higher NH_4^+ concentration. Phosphate concentrations ranged from 0.7 to 21.4 μM and exhibited no consistent trend over depth (Table 1).

3.1.3. Solid Phase Carbon and Nitrogen

TOC and TN values ranged from 0.86 to 5.25 and 0.07 to 0.37 % by weight, respectively. Oily, gassy sediments contained the highest content of TOC and TN. All sediments had maximum TOC and TN content close to the sediment water interface and less at depth.

3.1.4. Aliphatic Hydrocarbon Fraction

The highest concentrations of aliphatic hydrocarbons (310 - 7429 μg/g wet sediment; Table 2) were found in oily seep sediments.Representative chromatograms of the AHF (Figure 3A-D) show the UCM characteristic of oily sediments (Gouch et al., 1992). In contrast, sediments from the gassy seep had the lowest concentrations of aliphatic hydrocarbons, with a maximum of 127 μg/g wet sediment (Table 2).

Hydrocarbon profiles from the gassy seep show clearly resolved peaks, indicating a lesser degree of microbial degradation (Figure 3E,F).

3.2. Microbial Activity

3.2.1. Sulfate Reduction

Oily-4 and oily-3 sediments exhibited the highest rates of SR at 19 and 21.5 μmol cm^{-3} d^{-1}, respectively. The highest rate of SR amongst gassy sediments was observed in a *Beggiatoa* core (gassy-1), and was an order of magnitude lower, 1.9 μmol cm^{-3} d^{-1} (Table 1). Integrated SR rates ranged from 2 to 1429 mmol m^{-2} d^{-1}. Highest integrated rates of SR were observed in oily-3 and oily-4, but *Beggiatoa* sediments from both sites, gassy-1 and oily-4, exhibited high integrated rates of SR (35 and 1205 mmol m^{-2} d^{-1}). Sediment collected at the gassy seep at 1.5 m from a gas hydrate mound (oily-1) and those collected near carbonate (oily-2) exhibited lower SR rates, ranging from 3.1 to 5.3 mmol m^{-2} d^{-1} (Table 1).

3.2.2. Anaerobic oxidation of methane

Volumetric AOM rates were generally lower in oily seep sediments, with only the *Beggiatoa*-inhabited sediment (oily-4) exhibiting rates (maximum 9.1 nmol cm^{-3} d^{-1}) being comparable to those in gassy sediments (Figure 2, Table1). Most oily seep samples exhibited low AOM rates, from 0.3 to 2.8 nmol cm^{-3} d^{-1} while rates in gassy seep sediments ranged from 0.8 to 12.6 nmol cm^{-3} d^{-1} (Table 1). At the oily seep, integrated AOM rates ranged from 0.1 to 0.3 mmol m^{-2} d^{-1} while at gassy seep, rates were slightly higher, 0.5 to 0.8 mmol m^{-2} d^{-1}.

3.3. Microbial Communities

3.3.1. Bacterial clone libraries

The bacterial communities from oily and gassy seeps were similar in composition. The majority of clones from gassy seep (46%) and oily seep (32%) belonged to the epsilonproteobacteria (Table 5). The next largest cluster of environmental clones was affiliated with the deltaproteobacteria (20% at gassy seep and 17% at oily seep). Alpha and gamma proteobacteria were less abundant and accounted for a maximum of only 6% of the clones. The gassy seep library contained two clones from the *Planctomycetes* and three clones that aligned closely with the *Actinobacteria* (Figure 4). The oily seep library contained three clones affiliated with *Chloriflexi* and four affiliates of the *Aquificae/Acidobacteria.* Both gassy and oily seep libraries contained clones representing OD1 (Harris et al., 2004) and JS1 (Blazejak and Schippers, 2010), which are groups with no cultured representatives.

3.3.2. Archaeal clone libraries

Archaeal clone libraries from MC118 show extensive diversity within certain clades and there was no obvious difference between the two sites (Figure 5, Table 6). Clones affiliated with the *Methanosarcinales* dominated clone libraries from gassy seep (91%) and oily seep (78%). Most of the gassy seep archaeal clones were most closely related to the ANME-1 clade of anaerobic methanotrophs (53%). The oily seep archaeal library was dominated by clones most closely associated with the ANME-2 group (53%). The gassy seep library contained representatives from all ANME-2 groups and ANME-

1, but no ANME-3. The oily seep library contained only ANME-1, ANME-2a and ANME-2c relatives and lacked ANME-2b or ANME-3. The oily seep library contained representatives related to the Gulf of Mexico specific clades GoM Arc 1 and GoM Arc 2. Oily seep contained relatively more Crenarchaeota (17%) than gassy seep (4%), and also a larger fraction of unclassified Crenarchaeota and Euryarchaeota (18%).

3.3.3. dsrAB functional gene

Functional gene analysis of sulfate reducing bacteria revealed sequences affiliated with the *Desulfovibrionaceae* and *Desulfobacteraceae* (Figure 6, Table 7). The *Desulfobacterium anilini* branch is listed separately (Table 5), since this groups cultured member's exhibit unique metabolic capabilities. *D. anilini*-like clones were well represented in clone libraries from both gassy (12%) and oily (10%) seeps. *Syntrophobacteraceae* and *Desulfobulbaceae* were represented in both clone libraries, though in lower relative proportion (maximum 7%). Finally, some clones at both sites were affiliated with the Guaymas Basin/Group IV sulfate reducing bacterial clade. A single *dsrAB* gene from the gassy seep was similar to an archaeal sulfate reducer (Figure 6, Table 7).

4. Discussion

4.1. Drivers of Sulfate Reduction

The SR rates in oily-3 and oily-4 sediments are the highest volumetric rates, maximum 21.5 μmol cm^{-3} d^{-1}, reported to date for a natural environment. The previous high for a cold seep, 14 μmol cm^{-3} d^{-1}, was reported at another Gulf of Mexico habitat (Arvidson et al., 2004). Unlike most shelf and slope environments where sedimentation of

organic matter from the water column fuels benthic sulfate reduction (Canfield, 1991), SR at cold seeps is driven by reductants upward advection of deeply-sourced, oil and gas rich, fluids (Aharon and Fu, 2000; Joye et al., 2004). These reductants, including oil, higher alkanes, and methane, fuel high rates of SR. Differences in the composition of advecting fluids may generate different patterns in microbial activity. For example, the lack of oil at the gassy seep resulted in lower SR rates compared to the extremely high rates of SR observed in oily seep sediments (integrated SR rate >200 mmol m^{-2} d^{-1} in oily-3 and oily-4; Table 1). Thus at oily seeps, most of the SR is fueled by oil and non-methane hydrocarbon oxidation, rather than by methane oxidation (Joye et al., 2004).

We quantified organic carbon in several different fractions (i.e., DOC, TOC, gaseous alkanes, AHF). The major contrast between gassy and oily seep was the composition and concentration of gaseous and aliphatic hydrocarbon fractions. Compared to methane oxidation, the oxidation of non-methane hydrocarbons provides a higher energy yield for SRB. The oxidation of methane coupled to sulfate reduction provides a meager energy yield (-34.4 kJ mol^{-1}; Table 3, 4) that must be split between the two partner microorganisms. Oxidation of higher alkanes (e.g. propane, -51.4 kJ mol^{-1}; Table 3, 4) or hexadecane (-62.9 kJ mol^{-1}; Table 3, 4; Widdel and Rabus, 2001) provide far more energy per sulfate reduced. Aliphatic hydrocarbons, which are abundant, particularly at the oily seep (Table 2, Figure 3), are also more energy-yielding electron donors.

The presence of alkane and aliphatic degrading microorganisms (e.g., *Desulfobacterium anilini* relatives) in the clone libraries supports the contention that SR

at MC118 is driven by utilization of non-methane hydrocarbons. In addition to *D. anilini* related SRB, a number of clones were related to SRB from other cold seep and hydrothermal environments with rich hydrocarbon stocks (e.g. Green Canyon, Gulf of Mexico; Orcutt et al., 2010, and Guaymas Basin, Dhillon et al., 2003). Despite the geochemical differences noted for gassy and oily seeps, no differences in the major microbial groups recovered in clone libraries was observed.

4.2. Role of reduced sulfur oxidation

Exceptionally short turnover times of sulfate (~1 day) in high activity oily cores (oily-3 and oily-4) (Table 1) underscore the requirement for tightly coupled sulfur reduction and oxidation and/or transport of sulfate to the sulfate reduction zone. For example in oily-3 sediments, diffusion supplied 0.4 μmol SO_4^{2-} per cm^2 from the overlying seawater to the upper sediment layer (2 cm below the surface) per day which represents only ~3% of the daily sulfate demand of SR (14 μmol SO_4^{2-} cm^{-2}). Clearly, molecular diffusion alone cannot support the observed high gross rates of SR. Additional mechanisms to support elevated SR rates include biological sulfide oxidation, chemical sulfide oxidation, and advective sulfate delivery.

Iron-oxide mediated (abiotic) oxidation was proposed as the primary mechanism of sulfide oxidation in coastal sediments inhabited by *Beggiatoa* (Preisler et al., 2007). However, in GOM surficial sediments, insufficient oxidized iron is present to support the required rates of sulfide oxidation. The largest reducible (HCl extractable) iron concentration reported for GOM cold seeps (~86 μmol cm^{-3}, calculated using data from Arvidson et al., 2004) could support the required level of sulfide oxidation for only 12

and 82 days for oily-3 and oily-4 cores, respectively, assuming that all available Fe was utilized for sulfide oxidation. Gordon and Goñi (2004) estimate sedimentation rates in the GOM ranging from 0.012 to 0.31 cm y^{-1}. Assuming the iron flux is proportional to sedimentation rate (i.e. Fe concentrations are uniform in upper horizons and Fe is introduced solely through sedimentation), 3.2 to 83 yrs are required to accumulate 86 μmol Fe, equating to an accumulation rate of 0.003 to 0.07 μmol Fe d^{-1}. Even at a the high end rate of Fe accumulation (0.07 μmol Fe d^{-1}), only 1% of the required sulfide oxidation could be supported by iron(III)-linked oxidation, assuming a stoichiometry of 2 moles iron(III) required to oxidize 1 mol of sulfide. Moreover, internal reoxidation of iron(II) requires oxidizing equivalents (likely either molecular oxygen or manganese oxides; Janzen et al., 2000, Schippers and Jørgensen, 2001), which would directly compete with oxygen utilization via sulfide oxidation. Abiotic iron-mediated sulfide oxidation thus appears to be an insufficient mechanism for meeting the high sulfatedemand of these sediments.

The imbalance of sulfate input by diffusion and the limited role of abiotic ironmediated sulfide oxidation suggest that biological sulfide oxidation is important. A variety of sulfide oxidizing prokaryotes inhabit seep environments (Teske et al., 2000) and rates of sulfide oxidation in sediments are substantial (as quantified by radiotracer ($H_2{}^{35}S$) incubations; Jørgensen and Bak, 1991). Biological processes may provide a critical internal source of sulfate and thiosulfate (Jørgensen and Bak, 1991; Sayama et al., 2005; Dale et al., 2009). In GOM seep sediments, the importance of biologicallymediated sulfide oxidation was invoked to explain observed $\delta^{34}S$ and $\delta^{18}O$ distributions in sulfate (Aharon and Fu, 2003); other studies (Arvidson et al., 2004; Joye et al., 2004)

invoked biological sulfide oxidation as a way to support high SR rates in similar seep sediments. In diffusion-dominated sediments off the coast of Namibia, Dale and coworkers (2009) suggest that 96% of SR is fueled by sulfate derived from biological sulfide oxidation.

Biological sulfide oxidation is often significant in *Beggiatoa*-containing surface sediments but these sediments also contained many epsilonproteobacteria clones that may also be capable of sulfide oxidation (Table 5). *Beggiatoa* mats were present in both oily and gassy sediments, and SR rates were extremely elevated in oily *Beggiatoa* sediments. *Beggiatoa* accumulate nitrate in their vacuoles (Sweerts et al., 1999), and elevated concentrations of NO_x^- were observed in MC118 sediment porewaters from *Beggiatoa* cores (see NO_x^- in Figure 2 and Bowles and Joye, 2010). *Beggiatoa* can couple sulfide oxidation to the reduction of nitrate or molecular oxygen (Sweerts et al., 1999; Sayama et al., 2005). At present, there are no reports of nitrate reduction rates at GOM sites; however, in coastal sediments from Aarhus Bay, approximately 35 nmol cm^{-2} h^{-1} of N (as N_2) were generated in *Beggiatoa* inhabited sediments (Sayama et al., 2005). Assuming a stoichiometry 4 moles NO_3^- required to oxidize 3 moles H_2S, this denitrification rate would translate into the generation of 0.63 μmol sulfate cm^{-2} d^{-1}, which could supply 31% of the sulfate required for sulfate reduction in oily-4 sediments. Thus, biological sulfide oxidation could be an important source of sulfate fueling the high SR rates at seeps; the potential sulfide oxidizing activity of epsilonproteobacteria offers an addition sulfate source.

Another mechanism potentially important for replenishing sulfate pools is the downward advective transport of sulfate. Complex 3-dimensional flow regimes driven by bubble-induced mixing can facilitate the delivery of sulfate-rich seawater to depth (O'Hara et al., 1995). The passage of bubbles through sediments leads to channel formation, which can further accelerate sulfate delivery to depth (Boudreau et al., 2005). Quantitative data constraining sulfate delivery via advective mechanisms at cold seeps is lacking at present, but O'Hara et al. (1995) suggest that bubble-induced mixing of pore fluids could enhance fluid delivery to depth by two orders of magnitude or more, which could support a substantial fraction of the SR sulfate demand observed at MC118 seeps.

4.3. Unexpected Microbial Distributions and Activities

At MC118, archaeal clone libraries were dominated by ANMEs (at least 71% of individual clone libraries; Table 6). Previously, Orcutt et al. (2005) observed similar ANME dominance with a different approach (CARD-FISH) in gas hydrate rich sediments, where ANME-1+ANME-2 accounted for about 92% of the archaea. In that study, AOM rates were very low compared to SR rates. The ANME dominance of the archaeal clone libraries in light of the observed extremely low rates of AOM is perplexing. ANMEs may perform methanogenesis under some conditions (Orcutt et al., 2005; House et al., 2009) and recent arguments suggest that ANMEs may be predominantly methanogenic (Alperin and Hoehler, 2009a). While we have not yet measured methanogenesis (MOG) rates at MC118, MOG rates at other seep sites were sometimes comparable to or even higher than AOM rates (Orcutt et al., 2005; Knab et al., 2009; Joye et al., 2009). Available data and energetic calculations suggest that methanogenesis,

possibly mediated by ANMEs, may be more common at cold seeps that previously realized. Below we consider several types of data used to characterize ANMEs as methanotrophic and discuss whether this same evidence could instead be used to argue that ANMEs are methanogenic.

The discovery by Hinrichs et al. (1999) of the ANMEs and the proposal that they mediate AOM, was based on their $\delta^{13}C$-depleted lipids, which suggested assimilation of a ^{13}C-depleted carbon source, presumably methane. Subsequent biomarker and whole-cell C isotopic data from ANME communities (Niemann and Elvert, 2008; Niemann et al., 2005; Orphan et al., 2001b; Orphan et al., 2002) documented depleted ^{13}C biomarkers and/or cells/consortia and concluded that the ANMEs utilized a ^{13}C -depleted carbon source, methane. However, in many habitats where isotopically depleted ANME biomarkers have been recovered, the $\delta^{13}C$ of methane (-40 to -50 ‰) is much heavier than that of the observed ANME-specific biomarkers (-80 to -110 ‰), meaning the biomarkers were fractionated significantly during biosynthesis (e.g. Orcutt et al., 2005, Orphan et al., 2001b). Furthermore, many of the biomarkers commonly linked to the ANMEs, such as archaeol, *sn*2-hydroxyarchaeol, some isoprenoids (e.g. 15,19-pentamethyleicosane, PMI), and glycerol dialkyl glycerol tetraethers (GDGTs), also occur in methanogenic archaea (see Niemann and Elvert, 2008 and Alperin and Hoehler, 2009b *for further discussion*). Previous (Summons et al., 1998) and recent (Londry et al., 2008) pure culture data highlight the complexities of interpreting the $\delta^{13}C$ signatures of archaeal lipid biomarkers. Perhaps most importantly, Londry et al. (2008) show that archaeol, a biomarker often associated with ANMEs, often exhibits the most substantial

fractionation relative to the source. Clearly, the presence of an isotopically depleted lipid biomarker cannot conclusively affirm the involvement of a microorganism in AOM (Alperin and Hoehler, 2009b).

The low energy yield of the putative AOM consortium (Orcutt and Meile, 2008) and the inability of energetic models to reproduce measured rates of coupled SR and AOM in seep habitats (Alperin and Hoehler, 2009a) suggest that ANMEs may be utilizing alternate metabolisms (methanogenic or perhaps fermentative) under some environmentally relevant conditions. The occurrence of methanogenesis in methane-rich cold seep sediments might at first appear counter-intuitive, as elevated methane concentrations could be assumed to represent an energetic barrier for MOG. However, the relative energy yields for AOM and MOG at the substrate concentrations observed at MC118 show that bicarbonate based MOG is exergonic over a surprising range of methane concentrations (Figure 7). The energy yield for bicarbonate based MOG is highly sensitive to H_2 concentrations. At the average H_2 concentration (14 nM) at MC118, bicarbonate based MOG is more exergonic than AOM up to 50 mM CH_4 (Figure 7). The highest methane concentration documented at MC118 using an *in situ* probe (14 mM; Lapham et al., 2008) were well below this level. At an H_2 concentration of 20 nM, which was observed in several samples from MC118, MOG is more exergonic than AOM at CH_4 concentrations exceeding 100 mM (Figure 7). Furthermore, the abundance of other reduced carbon substrates at MC118 seeps could select against AOM coupled to SR and favor an alternate metabolic strategy for the ANMEs.

4.4. Global Comparison of SR and AOM rates

We compiled data from cold seeps, including those characterized by gas hydrate, mud volcanoes, and brine flows, as well non-seep continental margin (Chilean margin) or estuarine (Eckernförde Bay) sediments, where SR and AOM rates and ancillary geochemical data were available (Table 8). From the 52 available data sets, the median ratio of SR to AOM was 10.7 (Table 8); the predicted 1:1 stoichiometry was rarely observed. We further divided sites into classifications of C_2-C_5 or oil containing, brine containing (Cl^- >580; *hereafter* brine), or simply high methane flux areas, to evaluate whether distinct patterns of the SR:AOM ratio emerged.

The median ratio of SR to AOM at these three classifications exhibited little variation relative to the range of ratios observed overall (Table 8). The SR:AOM ratio in sediments containing C_2-C_5 or oil, similar to MC118 oily cores, was 5.9. In brine-rich sediments, the median SR:AOM ratio was slightly lower (4.9). Surprisingly, the median SR:AOM ratio for gas-rich sites was 9.3. The SR:AOM ratios (up to >1000) at MC118 do not align with the global averages.

The median integrated SR rate across these sites was 7.8 mmol m^{-2} d^{-1}, and SR rates varied across the three classifications. The highest median SR rate, 10.1 mmol m^{-2} d^{-1}, was observed in C_2-C_5 or oil containing sediments. Rates at MC118 and many other oily GOM seeps exceeded the median significantly (see Table 8), likely due to differences in the amount, or type of aliphatic hydrocarbons and the availability of sulfate. Brine sediments exhibited the lowest integrated SR rates, at a median of 2.5 mmol m^{-2} d^{-1}, which was likely related to the rapid upward advection of sulfate-free brine (Orcutt et al.,

2005; Joye et al., 2009; Joye et al. 2010). The median SR rate in gassy sediments, 9.2 mmol m^{-2} d^{-1}, was comparable to the rates observed at the MC118 gassy seep.

Integrated AOM rates were much lower than SR rates across these three habitat types and medians ranged from 0.4 to 1 mmol m^{-2} d^{-1} (overall median: 0.5 mmol m^{-2} d^{-1}). Sediments containing C_2-C_5 hydrocarbons or oil exhibited the highest median AOM rate, 1 mmol m^{-2} d^{-1}, which greatly exceeded rates observed at MC118 (0.1-0.8 mmol m^{-2} d^{-1}). Briney sediments exhibited the lowest median integrated AOM rates (0.4 mmol m^{-2} d^{-1}) and were lower than the median of gassy sediments (0.8 mmol m^{-2} d^{-1}).

Globally, AOM rates ranged from 0.1 to 16.2 mmol m^{-2} d^{-1}, averaged 2.1 mmol m^{-2} d^{-1}; the median was 0.8 mmol m^{-2} d^{-1}. Hinrichs and Boetius (2002) presented an average cold seep AOM rate of 18 mmol m^{-2} d^{-1}. However, at that time, a limited number of direct AOM rate measurements were available (n = 5) and two of the available AOM rates were obtained by assuming that AOM was 70% of the measured SR rate. Hinrichs and Boetius (2002) presented a global integrated annual AOM rate for cold seeps of 4.9 x 10^{12} mol CH_4 y^{-1}. Applying the median AOM rate reported here to the estimated cold seep area (0.75 x 10^{12} m^2; Hinrichs and Boetius, 2002) gives a new cold seep global annual AOM rate of 0.22 x10^{12} mol y^{-1}, which is about 5% of the original estimate. This global average includes 49 sites and represents the largest, most inclusive collection of AOM rate data for oceanic environments.

Could methane consumption at cold seeps be higher than the above calculation suggests? Given the high metabolic rates observed at cold seeps, sulfate is rapidly depleted (<2 mM) within the upper 26 cm (which is the average integration length for the

available data set). Across this global data set in advection-dominated seeps, sulfate depletion was reached by 21 cm in 34% of the cores. In the absence of rapid sulfate replenishment, the presence of 2 mM sulfate would restrict the amount of AOM coupled to SR in methane-rich sediments. While the available data indicate that AOM consumes only a small fraction of the methane flux at active seeps dominated by advective methane transport, we note that all of these published rates were conducted under *ex situ* conditions, e.g., 1 atmosphere and thus degassed sediment cores; therefore, it is possible, and perhaps likely, that AOM rates at *in situ* pressure and gas concentration are appreciably higher.

Judd (2004) compiled data from seeps over an estimated area of 2,500 km^2. For these seeps, he determined a seafloor to water column methane flux of 0.0775 Tg y^{-1}. The median AOM rate applied to this area yields a methane sink of 0.001 Tg y^{-1}, which is only 1.5% of the observed methane flux from the sediments to the water column. Inefficient AOM-based consumption of methane in sediments means that aerobic methane oxidation in the water column is likely to play a key role in methane consumption at cold seeps, potentially limiting the flux of seafloor-derived methane to the atmosphere.

5. Conclusions

At MC118, extremely high rates of SR are coupled to anaerobic hydrocarbon metabolism. In oily sediments, SR rates were the highest ever reported for a cold seep. The combined impacts of biological sulfide oxidation and advection-fueled seawater injection likely account for the bulk of sulfate supply to depth. A global survey of SR rates revealed that SR is greatly enhanced by the presence of aliphatic hydrocarbons or gaseous alkanes. The ratio of SR to AOM greatly exceeds 1, even in seep sediments with high methane concentrations, but lacking higher alkanes and oil and in nearshore gassy sediments. At seep sites, an improved average integrated global AOM rate was much lower than previously reported (Hinrichs and Boetius, 2002) and the median AOM rate consumed only 1.5% of the methane flux from advection-dominated seeps. Despite low AOM rates 16S rDNA libraries at MC118 were dominated by ANMEs, suggesting that ANME perform another metabolism, possibly methanogenesis or fermentation, in these sediments.

Acknowledgments. This research was supported by the NOAA National Institute for Undersea Science and Technology (award numbers 06-09-018, 07-10-028 and 08-10-031). The Gulf of Mexico Gas Hydrate Research Consortium provided ship time and at-sea logistical support. We thank C. Lutken, L. Lapham and J. Knapp for sharing geological information about MC118. J. Brooks and B. Bernard aided by providing a summarization of lipid data from the Gulf of Mexico. H. Niemann provided background geochemical data for the global comparison. We thank C. Meile, E. Howard, E. Biers, and R. Newton for useful discussions; C. Meile for providing comments that significantly improved an earlier version of this paper; and K. Hunter for assistance with geochemical analyses. J.J. Middelburg, A. Stadnitskaia, and two anonymous reviewers provided comments that significantly improved the paper.

Table 2.1. Geochemical and microbial activity analysis of samples from MC118. Where (-) reflects no data, (Σ) is depth integrated, (cm) is centimeters below sediment surface and (-1) represents overlying seawater.

		Depth	CH_4	DIC	H_2	H_2S	SO_4^{2-}	Cl^-	NH_4^+	NO_3^-	PO_4^{3-}	DOC	TOC	TN	pH	SR Rate	AOM Rate	SO_4^{2-}	CH_4	Σ SRR	Σ AOM	Σ SRR/ Σ AOM
Gassy Seep		cm	μM	mM	nM	mM	mM	mM	μM	μM	μM	μM	(% weight)	(% weight)		nmol cm^3 d^{-1}	nmol cm^3 d^{-1}	turnover (d)	turnover (d)	mmol m^2 d^{-1}	mmol m^2 d^{-1}	
Gassy-1		-1.0	268.9	2.5	-	0.2	24.6	486.6	119.2	10.3	1.5	1176.0	-	-	7.3	-	-					
sediments hosting white Beggiatoa spp.		1.5	99.7	5.9	12.7	1.5	21.3	543.9	202.9	132.7	19.4	2509.8	1.24	0.13	7.9	1541.3	12.6	18.8	2355.1	35.4	0.5	72
		4.5	570.4	16.4	6.9	10.0	7.0	549.4	318.9	31.5	12.5	2319.5	0.90	0.08	7.9	377.4	6.5					
		7.5	648.2	17.7	4.9	15.7	1.9	556.3	505.7	27.1	11.0	2226.2	0.91	0.08	8.0	28.2	0.8					
		10.5	535.1	21.9	6.0	16.1	1.0	552.1	789.1	16.8	5.0	-	0.99	0.09	7.9	3.1	1.0					
		13.5	780.1	16.7	57.9	14.4	1.0	552.8	686.0	34.2	6.1	-	0.90	0.07	8.0	1.7	1.3					
		16.5	864.8	18.3	4.8	16.3	1.1	462.7	769.8	18.6	7.0	-	0.89	0.07	7.9	1.6	-					
Gassy-2		-1.0	222	2.6	-	0.0	27.5	560.7	112.7	0.0	0.7	422.1	-	-	7.6	-	-					
sediments collected near chimney		1.5	308.5	9.3	5.3	3.6	18.0	549.5	157.8	68.7	19.4	1264.0	1.54	0.17	7.9	36.3	10.7	523.6	1351.3	2.0	0.8	3
		4.5	498.7	9.6	6.3	11.3	8.7	542.9	376.8	20.7	10.2	1027.4	1.18	0.11	7.9	12.5	6.7					
		7.5	617.6	17.0	1.6	15.3	6.5	561.7	293.1	19.4	9.6	1269.3	0.95	0.09	7.9	14.4	2.7					
		10.5	643.4	18.4	8.8	18.7	4.1	555.8	518.6	17.3	9.3	-	0.98	0.09	7.9	5.9	2.9					
		13.5	656.7	18.2	13.1	20.0	3.2	544.8	454.1	32.3	8.1	1890.3	0.88	0.09	7.8	3.9	3.6					
		16.5	635.8	16.5	9.5	28.1	3.6	548.0	550.8	17.4	6.1	1223.7	0.86	0.08	7.8	8.5	3.2					
Oily Seep																						
Oily-1		-1.0	17.1	2.1	3.4	0.0	28.6	534.7	108.0	15.2	0.7	610.8	-	-	7.9	-	-					
sediments adjacent to hydrate		1.0	16.4	-	7.3	0.0	28.4	536.3	125.6	33.0	3.8	1708.9	2.21	0.24	7.4	48.6	1.9	728.0	3735.6	3.1	0.1	24
		3.0	31.0	3.1	9.3	0.2	27.7	548.5	235.1	22.9	11.0	1569.3	2.17	0.24	7.7	53.9	1.1					
		5.0	43.7	6.2	10.1	2.3	23.7	548.2	177.1	14.5	19.1	2099.3	1.97	0.20	8.0	41.4	1.3					
		7.0	41.5	7.7	13.6	5.8	18.8	542.6	473.5	35.0	21.4	2408.3	1.83	0.16	7.9	17.5	0.1					
		9.0	197.9	9.5	18.2	6.6	15.6	536.5	376.8	43.9	19.9	2889.0	-	-	7.9	21.1	0.2					
		11.0	910.1	17.1	17.3	12.8	7.6	529.1	576.5	44.2	19.9	3307.8	-	-	7.8	0.6	1.4					
Oily-2		-1.0	-	2.4	-	0.0	27.2	524.8	74.1	9.6	0.9	560.6	-	-	8.0	-	-					
carbonate away from hydrate		1.0	17.3	2.3	17.2	0.0	27.7	527.9	138.5	147.0	2.7	1832.1	2.28	0.24	7.4	20.3	2.8	4150	3712.9	5.3	0.1	44
		3.0	34.7	3.4	13.0	0.0	23.8	467.7	209.4	77.6	4.4	1652.9	1.87	0.20	7.6	37.7	1.5					
		5.0	17.0	5.5	5.2	0.4	24.5	527.5	254.4	47.1	6.1	1713.4	1.56	0.10	8.2	24.7	0.6					
		7.0	72.1	6.3	3.3	3.8	20.4	555.5	326.3	35.1	8.4	2009.7	1.06	0.06	8.0	10.2	1.3					
Oily-3		-1.0	280.3	1.9	-	0.7	28.7	556.2	74.1	1.4	2.1	230.8	-	-	7.2	-	-					
oily gassy sediments		1.0	29.8	4.2	-	0.5	25.8	528.1	222.2	89.9	18.5	1887.3	4.36	0.37	7.8	7024.3	1.5	1.2	66930.7	1429.2	0.2	7146
		3.0	75.9	5.7	48.3	2.3	20.4	489.2	254.4	36.5	17.1	1658.2	5.25	0.31	7.9	179278	0.6					
		5.0	1163.6	9.4	-	3.6	22.0	559.8	248.0	37.9	17.9	2774.8	4.60	0.32	8.0	215427	2.3					
		7.0	452.1	24.2	16.7	18.9	2.8	544.5	583.0	20.3	14.5	-	3.35	0.15	7.8	2184.2	0.3					
		11.0	656.7	23.7	9.7	15.6	1.9	510.9	595.9	19.4	11.6	1928.4	1.82	0.07	7.7	754.7	0.5					
Oily-4		-1.0	103.8	2.3	-	0.2	28.3	560.0	119.2	3.8	1.2	264.7	-	-	7.5	-	-					
oily gassy sediments hosting white Beggiatoa spp.		1.0	84.3	6.4	15.1	2.4	23.4	546.0	331.7	280.5	15.6	1416.3	2.96	0.32	7.7	1080.5	9.1	1.2	7278.5	1205.3	0.3	4018
		3.0	181.8	7.9	15.7	5.1	21.3	545.1	331.7	42.2	14.8	1024.4	2.90	0.29	7.8	14088.3	6.7					
		5.0	134.4	8.3	13.9	7.0	19.6	527.9	357.5	14.5	13.3	1174.5	2.48	0.25	7.8	19037.5	2.8					
		7.0	442.4	10.0	11.3	9.2	17.4	550.5	488.3	24.8	10.7	1777.6	2.49	0.24	7.7	13310.3	1.5					
		9.0	879.6	9.9	17.5	11.0	14.9	515.1	602.3	22.7	10.2	1870.1	-	-	7.7	-	-					
		11.0	686.0	12.3	45.6	9.6	16.0	548.9	512.1	26.1	10.7	2491.2	-	-	8.0	-	-					
		13.0	695.8	11.9	19.0	10.7	14.7	521.4	531.4	36.2	7.6	2159.8	-	-	7.7	-	-					
		15.0	1324.7	17.1	17.3	17.0	11.4	554.0	821.3	47.5	11.9	2054.5	-	-	7.7	-	-					

Table 2.2. Aliphatic Hydrocarbon Fraction (AHF) from select depth horizons.

Site (depth, cm)	Aliphatic Hydrocarbon Fraction (µg/g wet sediment)
Gassy Seep	
Gassy-1 (1)	127
Gassy-1 (11)	87
Gassy-2 (4.5)	87
Oily Seep	
Oily-1 (1)	477
Oily-1 (7)	1541
Oily-2 (1)	310
Oily-2 (11)	2027
Oily-3 (1)	7428
Oily-3 (13)	6680
Oily-4 (1)	2294
Oily-4 (7)	1048

Table 2.3. Relevant environmental concentrations used for ΔG calculations, and ΔG_f for respective compounds.

Compound	ΔG_f (kJ mol^{-1})	Concentration (mM)
SO_4^{2-}	-744.6	28
H_2S	-27.87	5
CH_4	-34.33	1
C_3H_8	-23.49	0.1
$C_{16}H_{34}$	52.2[a]	0.0025
HCO_3^-	-586.8	10
CH_3COO^-	-369.4	0.01
H^+	0	10^{-4}
H_2O	-237.1	
H_2	17.55	2, 14, 20 (nM)[b]

[a] is estimated as described in Zengler et al., 1999, [b] three H_2 concentrations were considered, but 14 nM is the generalized concentration at MC118 seep sites.

Table 2.4. Balanced equations used for ΔG calculations, ΔG^{o} for reaction, and calculated ΔG at described conditions.

Process	Equation	ΔG° (kJ mol^{-1})	ΔG (kJ mol^{-1})[a]
Sulfate Reduction/ Methane Oxidation	$CH_4 + SO_4^{2-} + H^+ \rightarrow HCO_3^- + H_2S + H_2O$	-72.84	-34.4
Sulfate Reduction/ Propane Oxidation	$2C_3H_8 + 5SO_4^{2-} + 4H^+ \rightarrow 6HCO_3^- + 5H_2S + 2H_2O$	-364.37	-51.4
Sulfate Reduction/ Hexadecane Oxidation	$C_{16}H_{34} + 12.25SO_4^{2-} + 8.5H^+ \rightarrow 16HCO_3^- + 12.25H_2S + H_2O$	-898.2	-62.9
Methanogenesis/ Bicarbonate	$4H_2 + HCO_3^- + H^+ \rightarrow CH_4 + 3H_2O$	-229.03	-27.6
Methanogenesis/ Acetate	$H_2O + CH_3COO^- \rightarrow CH_4 + HCO_3^-$	-14.63	-14.63

[a]ΔG expressed as kJ mol^{-1} S reduced for sulfate reduction reactions.

Table 2.5. Frequency and distribution of bacterial phylogenies from MC118 clones based on 16S bacterial sequences. Phylogeny inferred based on Silva's *SINA* alignment with manual edits and subsequent phylogenetic tree generated from this alignment. Includes all clones analyzed from *E. coli* positions 27 through 627, and 892 through 1492.

Bacterial Division	Gassy Seep		Oily Seep	
	n	%	n	%
Proteobacteria				
alpha	0	0	3	4
delta	10	20	12	17
gamma	3	6	3	4
epsilon	23	46	22	32
Bacteroidetes	4	8	9	13
Firmicutes	2	4	1	1
Spirocheates	1	2	3	4
Chloriflexi	0	0	3	4
Actinobacteria	3	6	0	0
Planctomycetes	2	4	0	0
Aquificae/Acidobacteria	0	0	4	6
OD1	1	2	4	6
JS1	1	2	3	4
Unclassified	0	0	2	3
	# of clones		# of clones	
	50		69	

Table 2.6. Frequency and distribution of archaeal phylogenies from MC118 clones based on 16S archaeal sequences. Phylogeny inferred based on Silva's *SINA* alignment with manual edits and subsequent phylogenetic tree generated from this alignment. Includes all clones analyzed from *E.coli* positions 20 through 620, and 792 through 1392.

Archaeal Division	Gassy Seep		Oily Seep	
	n	%	n	%
Euryarchaeota				
ANME-1	27	53	14	18
Methanosarcinales				
ANME-2a	7	14	0	0
ANME-2b	1	2	2	3
ANME-2c	11	22	38	50
GoM Arc 1	0	0	2	3
GoM Arc 2	0	0	3	4
Methanococci	0	0	0	0
Thermoplasmata	0	0	0	0
Unclassified Eury.	3	6	4	5
Crenarchaeota				
Thermoprotei	1	2	3	4
Unclassified Cren.	1	2	10	13
	# of clones		**# of clones**	
	51		**76**	

Table 2.7. Frequency and distribution of *dsrAB* phylogenies from MC118. Phylogeny inferred based on alignment of clones to pure culture sulfate reducing microorganisms and the subsequent phylogenetic tree generated from this alignment.

***dsrAB* affiliation**	**Gassy Seep**		**Oily Seep**	
	n	%	n	%
Desulfovibrionaceae	12	48	10	38
Desulfobacteraceae	9	36	10	38
D. anilini	(3)	(12)	(3)	(12)
Syntrophobacteraceae	1	4	1	4
Desulfobulbaceae	1	4	2	8
Guaymas Group IV	2	8	2	8
Archaeal S-reducer	0	0	1	4
	# of clones		**# of clones**	
	25		**26**	

Table 2.8. Global summary of integrated rates of sulfate reduction and anaerobic oxidation of methane and the presence of brine (Cl^-), gaseous alkanes (C_2-C_5), and liquid hydrocarbons. Depth over which integration was made corresponds to the maximum depth and depth to sulfate depletion (<2mM) are noted. For all categories (+) represents the presence of the variable and (-) the absence. *NA* means the data were *not available.* Only sulfate reduction and anaerobic oxidation of methane rates determined *ex situ* with radiotracers are included. The median SR and AOM rates and the ΣSRR/ΣAOM are given. Inclusion in multiple groups (e.g. presence of oil and Cl^- >580 mM) for some sites occurs for determinations of median SR and AOM rates, as well as for ΣSRR/ΣAOM. All sites without UCM/visible oil, gaseous alkanes (C_2-C_5), or Cl^->550 mM are considered high CH_4 flux. *Estimated from salinity data. ***Sources*****:** 1) Niemann et al., 2006a; 2) Hensen et al., 2007; 3) Omoregie et al., 2009; 4) Dupre et al., 2007; 5) Omoregie et al., 2008; 6) Treude et al., 2003; 7) Treude et al., 2005; 8) Treude et al., 2005b; 9) Niemann et al., 2006b; 10) Joye et al., 2004; 11) Orcutt et al., 2010; 12) Orcutt et al., 2005; 13) Joye et al., 2010.

Site		Water Depth (m)	Cl^- (mM)	C_2-C_5	UCM/ Visible Oil	Depth of SO_4^{2-} Depletion (cm)	Max. Depth (cm)	Σ SRR (mmol m^{-2} day^{-1})	Σ AOM (mmol m^{-2} day^{-1})	Σ SRR/ Σ AOM	Source
Gulf of Cadiz	Captain Arutyunov	1315	565-600[a]	+	+	75	180	1.8	1.0	1.8	1, 2[a]
Mud Volcanoes	Bomjardim	3090	510-570[a]	+	+	75	180	1.9	0.1	19.2	1, 2[a]
Mediterranean	Amon (NL11PO1)	1121	NA	+[b]	NA	*No Depletion*	20	10.5	3.1	3.0	3, 4[b]
Sea Mud	Amon (NL12PO2)	1120	NA	+[b]	NA	*No Depletion*	20	16.7	5.8	3.0	3, 4[b]
Volcanoes	Isis (NL8PO1)	992	NA	+[b]	NA	*No Depletion*	20	3.8	0.3	12.0	3, 4[b]
	Isis (NL8PO3)	992	NA	+[b]	NA	*No Depletion*	20	8.6	0.3	26.0	3, 4[b]
	Isis (NL13PO4)	991	NA	+[b]	NA	*No Depletion*	20	44	3.6	12.0	3, 4[b]
	Chefren (NL4PO1)	3023	brine flows	NA	NA	NA	20	66.5	0.9	75.0	3
	Chefren (NL18PO4)	3024	863-1573[c]	NA	NA	*No Depletion*	20	4.4	0.2	26.0	3, 5[c]
	Chefren (NL18PO2)	3022	657-1388[c]	NA	NA	*No Depletion*	20	5.3	0.5	11.0	3, 5[c]
	Chefren (NL19PO3)	2968	brine flows	NA	NA	NA	20	0.2	0.3	1.0	3
	Napoli (NL21PO5)	1946	brine flows	NA	NA	NA	20	8	0.1	87.0	3
Hydrate Ridge	S. Summit Beggiatoa	777	NA	NA	NA	8.5	8	32	5.1	6.3	6
Chilean	GeoB No. 7165	880	NA	NA	NA	350	70	165	734	0.2	7
Continental	GeoB No. 7166	1160	NA	NA	NA	180	120	208	80	2.6	7
Margin	GeoB No. 7155	1750	NA	NA	NA	210	90	95	3	31.7	7
Eckernförde	Sta. A Early Sep.	25	~250-350~	NA	NA	23	25	7.3	0.9	8.1	8
Bay	Sta. A Late Sep.	25	~250-350~	NA	NA	22	25	4.1	0.8	5.1	8
	Sta. A Early Mar.	25	~250-350~	NA	NA	28	25	4.2	0.4	10.5	8
	Sta. B Early Sep.	28	~250-350~	NA	NA	25	25	10.5	0.9	11.7	8
	Sta. B Late Sep.	28	~250-350~	NA	NA	21	25	7.8	1.5	5.2	8
	Sta. B Early Mar.	28	~250-350~	NA	NA	26	25	5.6	0.51	11.0	8
Haakon Mosby	Centre	~1260	NA	-[d]	-[d]	8	10	0.3	2.3	0.1	9
Mud Volcano	*Beggiatoa*	~1260	NA	-[d]	-[d]	4	10	14.9	12.3	1.2	9
Gulf of Mexico	GC185-4309	560	511	-	-	*No Depletion*	15	18.9	0.3	63.0	10
Green Canyon	GC185-4324	560	535	+	+	*No Depletion*	12	244.3	11.6	21.1	10
	GC185-Sta.156	546	549	-	+	8	10	5.6	16.2	0.3	11
	GC234-4313	540	510	-	-	*No Depletion*	14	13.4	0.3	44.7	10
	GC234-4316	540	540	-	-	*No Depletion*	20	49.1	0.3	163.7	10
	GC234-4315	540	515	+	+	5	14	12.6	4.6	2.7	10
	GC234-Sta. 87	552	557	-	+	*No Depletion*	10	22.2	0.2	111.0	11
	GC232-4463	504	530	+	+	*No Depletion*	10	10.1	4.2	2.4	11
	GC232-4459	504	441-556	+	+	*No Depletion*	11	13	6.4	4.7	12
	GC233-4458	650	551-571	-	-	*No Depletion*	10	154	0.1	1540.0	12
	GC600-4174Y	1170	623	+	+	*No Depletion*	12	0.48	1.2	0.4	13
	GC852-4169R	1435	565	-	-	*No Depletion*	12	0.25	0.32	0.8	13
	GC852-4169Y	1435	569	-	-	*No Depletion*	12	3.8	0.3	12.7	13
Garden Banks	GB415-Sta. 161	950	713	+	+	*No Depletion*	10	27.9	10.8	2.6	11
Chapopote	Sta. 140	2902	640	+	+	1	10	0.2	0.1	2.0	11
Atwater Valley	AT340-4173Y	2200	1558	-	-	15	12	3.2	1.4	2.3	13
	AT340-4173R	2200	586	-	-	*No Depletion*	12	10.6	0.01	1060.0	13
	AT340-4183R	2200	610	-	-	*No Depletion*	12	0.2	0.01	20.0	13
Miss. Canyon	MC640-4182R	1420	861	-	-	*No Depletion*	12	1.2	0.3	4.0	13
	MC853-4178Y	1070	1299	+	+	5	12	5.3	0.9	5.9	13
	MC853-4178R	1070	778	-	-	*No Depletion*	12	8.7	0.1	87.0	13
Alaminos Canyon	AC818-Y5	2740	579	-	-	*No Depletion*	12	0.4	2	0.2	13

MEDIAN	Σ SRR/Σ AOM	SRR	AOM	n Σ SRR/ Σ AOM
UCM/Oil/C_2-C_5	5.9	10.1	1	23
Cl^- > 580 mM	4.9	2.5	0.4	12
High CH_4 flux	9.3	9.2	0.8	21
Total	10.7	7.8	0.5	52

Figure 2.1. Mississippi Canyon lease block 118 (MC118) in the Gulf of Mexico (USA) denoted by circle marker. Bathymetric contours are at 500 meter intervals (Ryan et al., 2009).

Figure 2.2. Geochemical and microbial activity profiles over depth (cm) for gassy seep core gassy-1 (**A-E**) and oily seep core oily-4 (**F-J**). **(A,F)** profiles of SO_4^{2-} (mM), H_2S (mM), and DIC (mM); **(B,G)** $\delta^{13}CH_4$ (‰), CH_4 (μM), ΣC as C_2-C_5 (μM), and Cl^- (mM); **(C,H)** NO_x^- (μM), NH_4^+ (μM), PO_4^{3-} (μM), and H_2 (nM); **(D,I)** pH and DOC (μM); and **(E,J)** AOM and SR rate (nmol cm^{-3} day^{-1}).

Figure 2.3. Gas chromatographs of the aliphatic hydrocarbon fraction (AHF) from oily seep [**(A)** oily-4, 1cm; **(B)** oily-4 at 7 cm; **(C)** oily-3 at 1 cm; **(D)** oily-3 at 13 cm] and gassy seep [**(E)** gassy-1 at 1 cm; **(F)** gassy-1 at 11 cm. Oily seep chromatographs are relative intensity x2 while gassy seep are relative intensity. All graphs are plotted against retention time.

Figure 2.4. 16S rDNA bacterial phylogeny of gassy seep (MC118Gassy; red) and oily seep (MC118Oily; blue) environmental clones relative to environmental clones from other sites and pure culture data. Neighbor joining method was used to generate the tree with a Jukes-Cantor correction of evolutionary distance. Bootstrap values for branches occurring for >50% of 1000 iterations are reported. Scaling of the phylogenetic tree is based on an evolutionary distance of 0.03.

Figure 2.5. 16S rDNA archaeal phylogeny of gassy seep (MC118Gassy; red) and oily seep (MC118Oily; blue) environmental clones relative to environmental clones from other sites and pure culture data. Neighbor joining method was used to generate the tree with a

Jukes-Cantor correction of evolutionary distance. Bootstrap values for branches occurring for >50% of 1000 iterations are reported. Scaling of the phylogenetic tree is based on an evolutionary distance of 0.03.

Figure 2.6. *dsrAB* phylogeny of gassy seep (MC118Gassy; red) and oily seep (MC118Oily; blue) environmental clones relative to environmental clones from other sites and pure culture data. Minimum evolution method was used to generate the phylogeny, with a poisson correction of evolutionary distance. Bootstrap values for branches occurring for >50% of 1000 iterations are reported. Scaling of the phylogenetic tree is based on an evolutionary distance of 0.05.

Figure 2.7. ΔG (kJ mol^{-1}) of the respective reaction versus methane (mM) for AOM, MOGbicarbonate (at $[H_2]$ = 2, 14, 20 nM), and MOG-acetate. The ΔG of AOM is divided by 2 to represent the energy gain by bacteria and archaea in the purported synthrophic process. Region considered energy limited (> -20 kJ mol^{-1}) is highlighted by shading.

Figure 2.1.

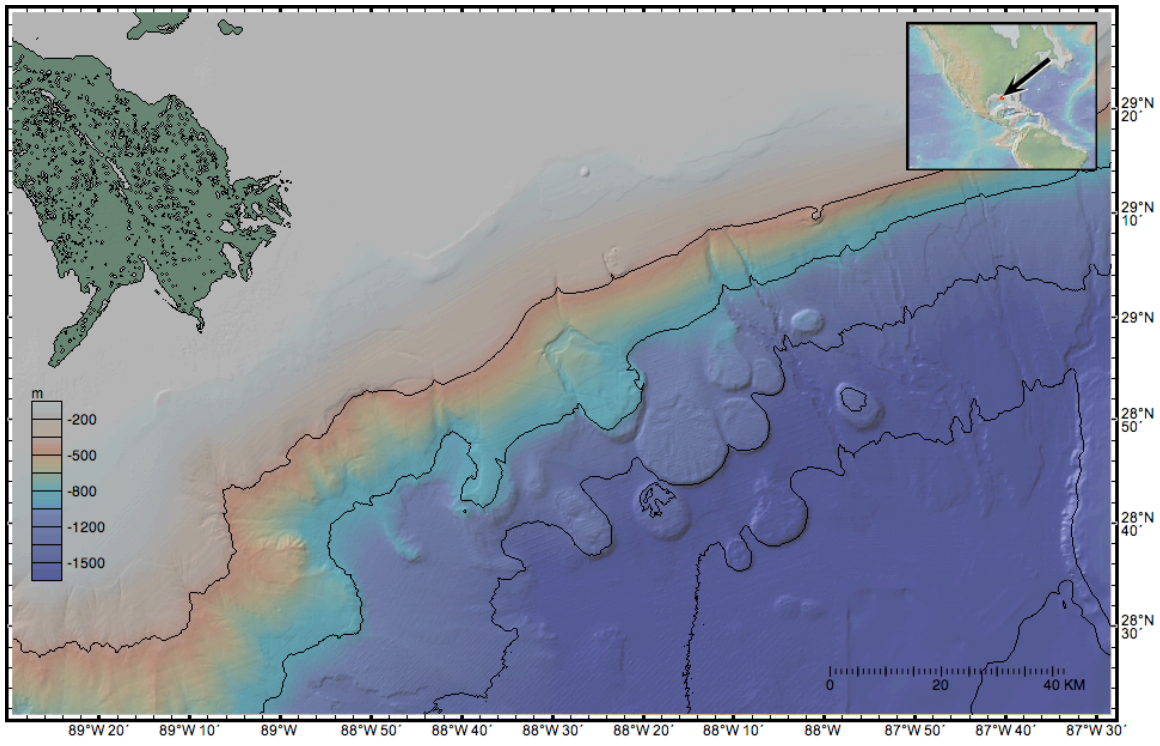
m
-200
-500
-800
-1200
-1500
0
20
40 KM
29°N 20´
29°N 10´
29°N
28°N 50´
28°N 40´
28°N 30´
89°W 20´
89°W 10´
89°W
88°W 50´
88°W 40´
88°W 30´
88°W 20´
88°W 10´
88°W
87°W 50´
87°W 40´
87°W 30´

Figure 2.2.

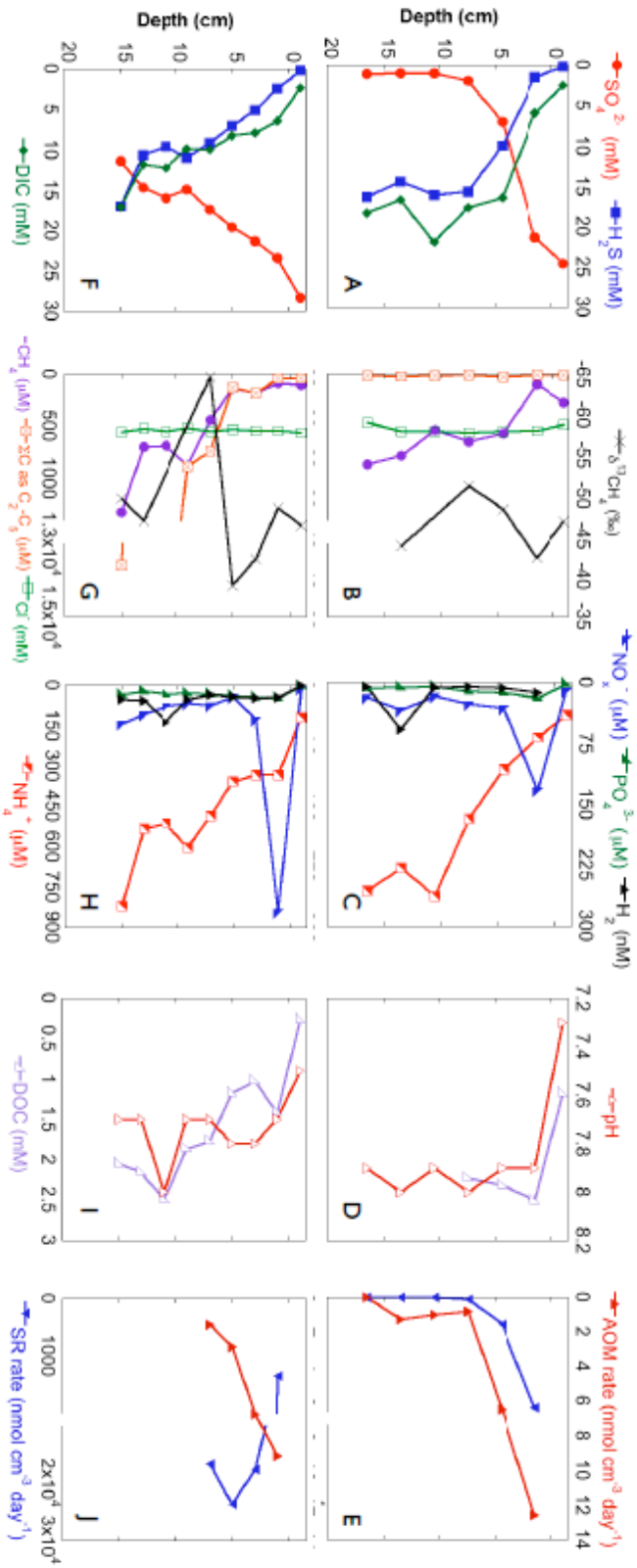
Depth (cm)
Depth (cm)
SO_4^{2-} (mM)
H_2S (mM)
DIC (mM)
$\delta^{13}CH_4$ (‰)
NO_x^- (μM)
PO_4^{3-} (μM)
H_2 (nM)
CH_4 (μM)
ΣC as C_2-C_3 (μM)
Cl^- (mM)
NH_4^+ (μM)
pH
DOC (mM)
AOM rate (nmol cm^{-3} day^{-1})
SR rate (nmol cm^{-3} day^{-1})
A
B
C
D
E
F
G
H
I
J

Figure 2.3.

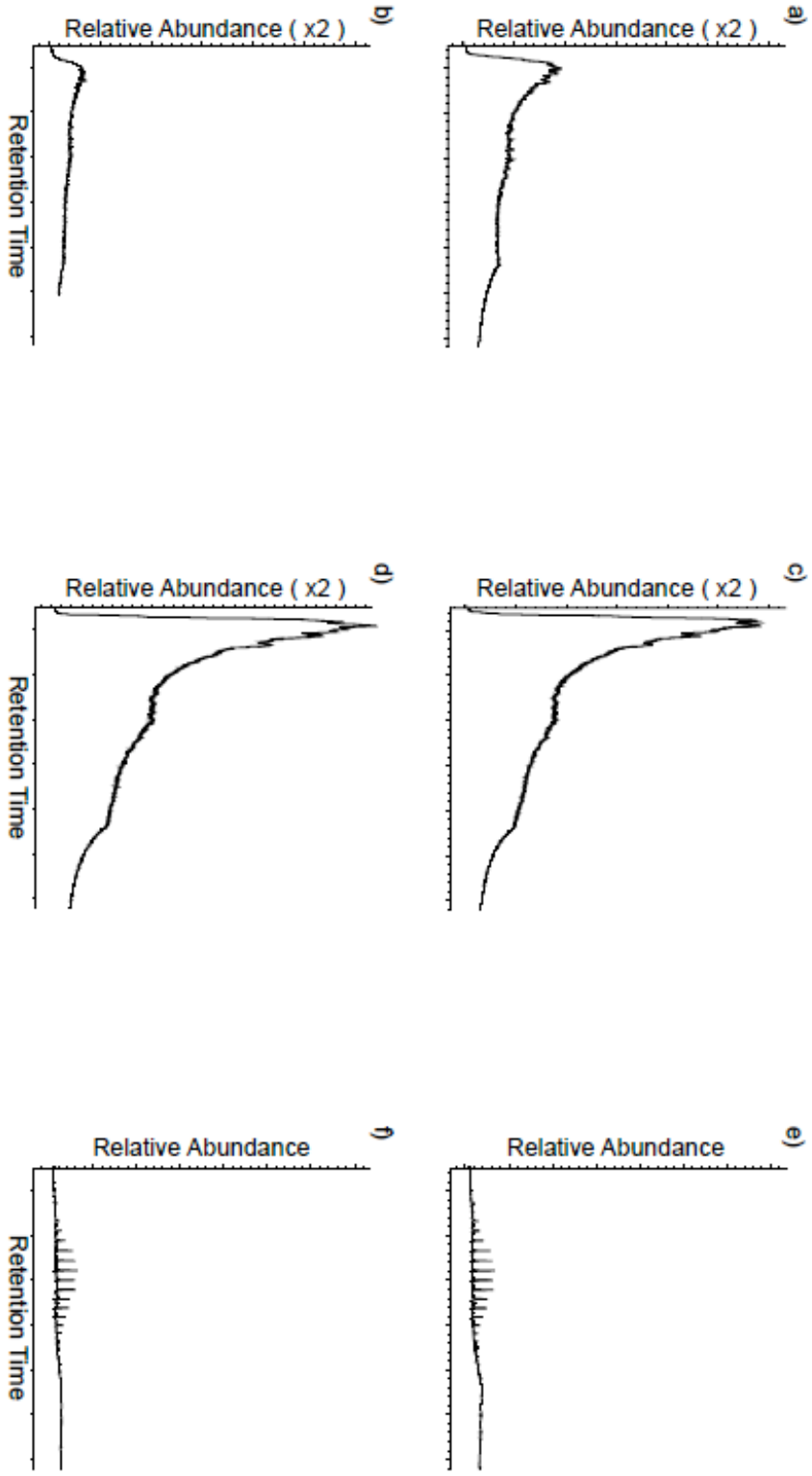
b)
Relative Abundance (x2)
Retention Time
a)
Relative Abundance (x2)
d)
Relative Abundance (x2)
Retention Time
c)
Relative Abundance (x2)
f)
Relative Abundance
Retention Time
e)
Relative Abundance

Figure 2.4.

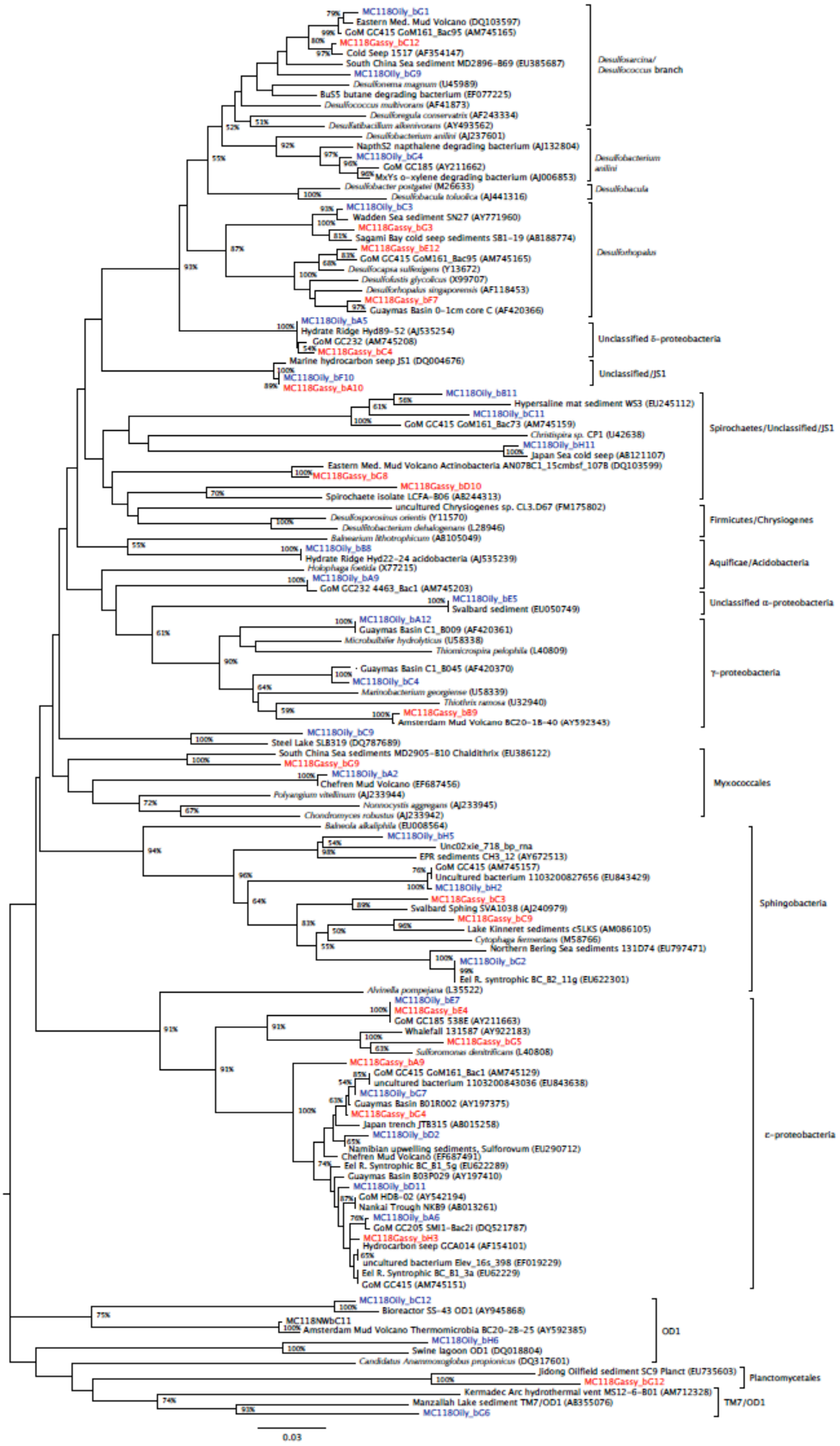
MC118Oily_bG1
Eastern Med. Mud Volcano (DQ103597)
GoM GC415 GoM161_Bac95 (AM745165)
MC118Gassy_bC12
Cold Seep 1517 (AF354147)
South China Sea sediment MD2896-869 (EU385687)
MC118Oily_bG9
Desulfonema magnum (U45989)
Bu55 butane degrading bacterium (EF077225)
Desulfococcus multivorans (AF41873)
Desulforegula conservatrix (AF243334)
Desulfotalea psychrophila (AY493562)
Desulfobacterium anilini (AJ237601)
NaphS2 napthalene degrading bacterium (AJ132804)
MC118Oily_bC4
GoM GC185 (AY211662)
MxYs o-xylene degrading bacterium (AJ006853)
Desulfobacter postgatei (M26633)
Desulfobacula toluolica (AJ441316)
MC118Oily_bC3
Wadden Sea sediment SN27 (AY771960)
MC118Gassy_bG3
Sagami Bay cold seep sediments S81-19 (AB188774)
MC118Gassy_bE12
GoM GC415 GoM161_Bac95 (AM745165)
Desulfocapsa sulfexigens (Y13672)
Desulfofustis glycolicus (X99707)
Desulforhopalus singaporensis (AF118453)
MC118Gassy_bF7
Guaymas Basin 0-1cm core C (AF420366)
MC118Oily_bA5
Hydrate Ridge Hyd89-52 (AJ535254)
GoM GC232 (AM745208)
MC118Gassy_bC4
Marine hydrocarbon seep JS1 (DQ004676)
MC118Oily_bF10
MC118Gassy_bA10
MC118Oily_bB11
Hypersaline mat sediment WS3 (EU245112)
MC118Oily_bC11
GoM GC415 GoM161_Bac73 (AM745159)
Christiopira sp. CP1 (U42638)
MC118Oily_bH11
Japan Sea cold seep (AB121107)
Eastern Med. Mud Volcano Actinobacteria AN07BC1_15cmbsf_107B (DQ103599)
MC118Gassy_bG8
MC118Gassy_bD10
Spirochaete isolate LCFA-B06 (AB244313)
uncultured Chrysiogenes sp. CL3.D67 (FM175802)
Desulfosporosinus orientis (Y11570)
Desulfitobacterium dehalogenans (L28946)
Balneatrix alkaliphila (AB105049)
MC118Oily_bB8
Hydrate Ridge Hyd22-24 acidobacteria (AJ535239)
Holophaga foetida (X77215)
MC118Oily_bA9
GoM GC232 4463_Bac1 (AM745203)
MC118Oily_bE5
Svalbard sediment (EU050749)
MC118Oily_bA12
Guaymas Basin C1_B009 (AF420361)
Microbulbifer hydrolyticus (U58338)
Thiomicrospira pelophila (L40809)
Guaymas Basin C1_B045 (AF420370)
MC118Oily_bC4
Marinobacterium georgiense (U58339)
Thiothrix ramosa (U32940)
MC118Gassy_bB9
Amsterdam Mud Volcano BC20-18-40 (AY592343)
MC118Oily_bC9
Steel Lake SLB319 (DQ787689)
South China Sea sediments MD2905-B10 Chaldithrix (EU386122)
MC118Gassy_bG9
MC118Oily_bA2
Chefren Mud Volcano (EF687456)
Polyangium vitellinum (AJ233944)
Nannocystis aggregata (AJ233945)
Chondromyces robustus (AJ233942)
Balneola alkaliphila (EU008564)
MC118Oily_bH5
Unc02xie_718_bp_rna
EPR sediments CH3_12 (AY672513)
GoM GC415 (AM745157)
Uncultured bacterium 1103200827656 (EU843429)
MC118Oily_bH2
MC118Gassy_bC3
Svalbard Sphing SVA1038 (AJ240979)
MC118Gassy_bC9
Lake Kinneret sediments c5LKS (AM086105)
Cytophaga fermentans (M58766)
Northern Bering Sea sediments 131D74 (EU797471)
MC118Oily_bC2
Eel R. syntrophic BC_B2_11g (EU622301)
Alvinella pompejana (L35522)
MC118Oily_bE7
MC118Gassy_bE4
GoM GC185 538E (AY211663)
Whalefall 131587 (AY922183)
MC118Gassy_bG5
Sulfuromonas dienitrificans (L40808)
MC118Gassy_bA9
GoM GC415 GoM161_Bac1 (AM745129)
uncultured bacterium 1103200843036 (EU843638)
MC118Oily_bC7
Guaymas Basin B01R002 (AY197375)
MC118Gassy_bC4
Japan trench JTB315 (AB015258)
MC118Oily_bD2
Namibian upwelling sediments, Sulforovum (EU290712)
Chefren Mud Volcano (EF687491)
Eel R. Syntrophic BC_B1_5g (EU622289)
Guaymas Basin B03P029 (AY197410)
MC118Oily_bD11
GoM HD8-02 (AY542194)
Nankai Trough NKB9 (AB013261)
MC118Oily_bA6
GoM GC205 SMI1-Bac2i (DQ521787)
MC118Gassy_bH3
Hydrocarbon seep GCA014 (AF154101)
uncultured bacterium Elev_16s_398 (EF019229)
Eel R. Syntrophic BC_B1_3a (EU622291)
GoM GC415 (AM745151)
MC118Oily_bC12
Bioreactor SS-43 OD1 (AY945868)
MC118NWbC11
Amsterdam Mud Volcano Thermomicrobia BC20-2B-25 (AY592385)
MC118Oily_bH6
Swine lagoon OD1 (DQ018804)
Candidatus Anammoxoglobus propionicus (DQ317601)
Jidong Oilfield sediment SC9 Planct (EU735603)
MC118Gassy_bG12
Kermadec Arc hydrothermal vent MS12-6-B01 (AM712328)
Manzallah Lake sediment TM7/OD1 (AB355076)
MC118Oily_bG6
Desulfosarcina/
Desulfococcus branch
Desulfobacterium
anilini
Desulfobacula
Desulforhopalus
Unclassified δ-proteobacteria
Unclassified/JS1
Spirochaetes/Unclassified/JS1
Firmicutes/Chrysiogenes
Aquificae/Acidobacteria
Unclassified α-proteobacteria
γ-proteobacteria
Myxococcales
Sphingobacteria
ε-proteobacteria
OD1
Planctomycetales
TM7/OD1
0.03

Figure 2.5.

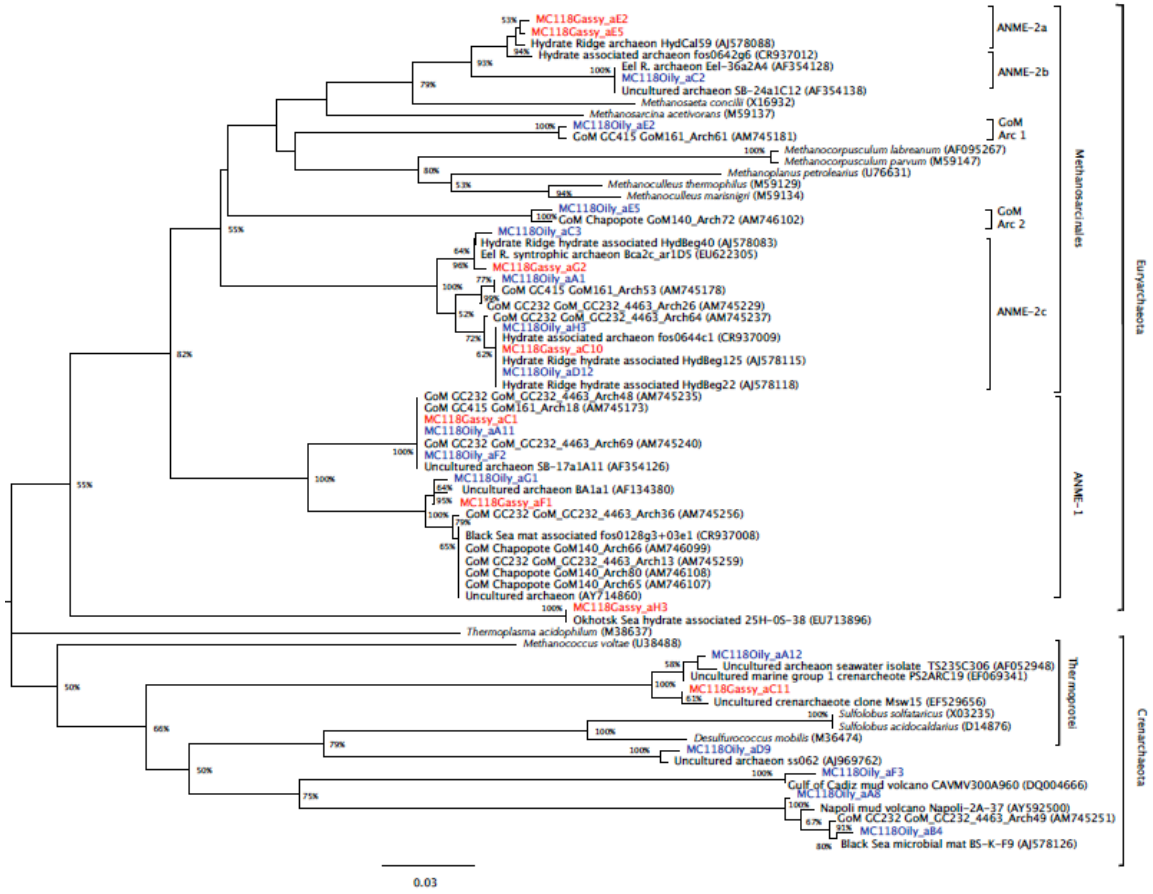
MC118Gassy_aE2
MC118Gassy_aE5
Hydrate Ridge archaeon HydCal59 (AJ578088)
Hydrate associated archaeon fos0642g6 (CR937012)
Eel R. archaeon Eel-36a2A4 (AF354128)
MC118Oily_aC2
Uncultured archaeon SB-24a1C12 (AF354138)
Methanosaeta concilii (X16932)
Methanosarcina acetivorans (M59137)
MC118Oily_aE2
GoM GC415 GoM161_Arch61 (AM745181)
Methanocorpusculum labreanum (AF095267)
Methanocorpusculum parvum (M59147)
Methanoplanus petrolearius (U76631)
Methanoculleus thermophilus (M59129)
Methanoculleus marisnigri (M59134)
MC118Oily_aE5
GoM Chapopote GoM140_Arch72 (AM746102)
MC118Oily_aC3
Hydrate Ridge hydrate associated HydBeg40 (AJ578083)
Eel R. syntrophic archaeon Bca2c_ar1D5 (EU622305)
MC118Gassy_aG2
MC118Oily_aA1
GoM GC415 GoM161_Arch53 (AM745178)
GoM GC232 GoM_GC232_4463_Arch26 (AM745229)
GoM GC232 GoM_GC232_4463_Arch64 (AM745237)
MC118Oily_aH3
Hydrate associated archaeon fos0644c1 (CR937009)
MC118Gassy_aC10
Hydrate Ridge hydrate associated HydBeg125 (AJ578115)
MC118Oily_aD12
Hydrate Ridge hydrate associated HydBeg22 (AJ578118)
GoM GC232 GoM_GC232_4463_Arch48 (AM745235)
GoM GC415 GoM161_Arch18 (AM745173)
MC118Gassy_aC1
MC118Oily_aA11
GoM GC232 GoM_GC232_4463_Arch69 (AM745240)
MC118Oily_aF2
Uncultured archaeon SB-17a1A11 (AF354126)
MC118Oily_aG1
Uncultured archaeon BA1a1 (AF134380)
MC118Gassy_aF1
GoM GC232 GoM_GC232_4463_Arch36 (AM745256)
Black Sea mat associated fos0128g3+03e1 (CR937008)
GoM Chapopote GoM140_Arch66 (AM746099)
GoM GC232 GoM_GC232_4463_Arch13 (AM745259)
GoM Chapopote GoM140_Arch80 (AM746108)
GoM Chapopote GoM140_Arch65 (AM746107)
Uncultured archaeon (AY714860)
MC118Gassy_aH3
Okhotsk Sea hydrate associated 25H-0S-38 (EU713896)
Thermoplasma acidophilum (M38637)
Methanococcus voltae (U38488)
MC118Oily_aA12
Uncultured archeaon seawater isolate_TS235C306 (AF052948)
Uncultured marine group 1 crenarcheote PS2ARC19 (EF069341)
MC118Gassy_aC11
Uncultured crenarchaeote clone Msw15 (EF529656)
Sulfolobus solfataricus (X03235)
Sulfolobus acidocaldarius (D14876)
Desulfurococcus mobilis (M36474)
MC118Oily_aD9
Uncultured archaeon ss062 (AJ969762)
MC118Oily_aF3
Gulf of Cadiz mud volcano CAVMV300A960 (DQ004666)
MC118Oily_aA8
Napoli mud volcano Napoli-2A-37 (AY592500)
GoM GC232 GoM_GC232_4463_Arch49 (AM745251)
MC118Oily_aB4
Black Sea microbial mat BS-K-F9 (AJ578126)
0.03
ANME-2a
ANME-2b
GoM Arc 1
GoM Arc 2
ANME-2c
Methanosarcinales
ANME-1
Euryarchaeota
Thermoprotei
Crenarchaeota

Figure 2.6.

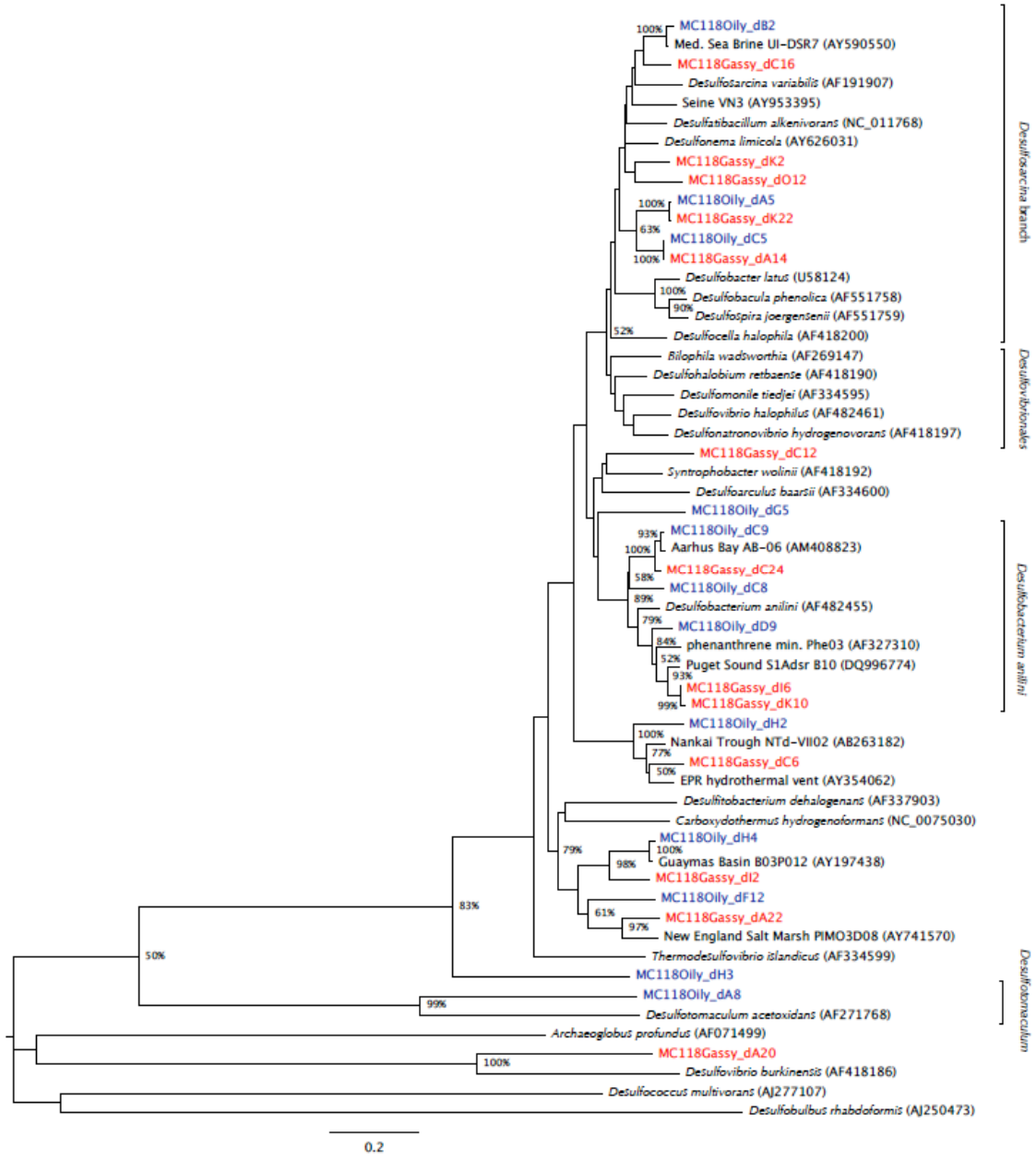
MC118Oily_dB2
Med. Sea Brine UI-DSR7 (AY590550)
MC118Gassy_dC16
Desulfosarcina variabilis (AF191907)
Seine VN3 (AY953395)
Desulfatibacillum alkenivorans (NC_011768)
Desulfonema limicola (AY626031)
MC118Gassy_dK2
MC118Gassy_dO12
MC118Oily_dA5
MC118Gassy_dK22
MC118Oily_dC5
MC118Gassy_dA14
Desulfobacter latus (U58124)
Desulfobacula phenolica (AF551758)
Desulfospira joergensenii (AF551759)
Desulfocella halophila (AF418200)
Bilophila wadsworthia (AF269147)
Desulfohalobium retbaense (AF418190)
Desulfomonile tiedjei (AF334595)
Desulfovibrio halophilus (AF482461)
Desulfonatronovibrio hydrogenovorans (AF418197)
MC118Gassy_dC12
Syntrophobacter wolinii (AF418192)
Desulfoarculus baarsii (AF334600)
MC118Oily_dG5
MC118Oily_dC9
Aarhus Bay AB-06 (AM408823)
MC118Gassy_dC24
MC118Oily_dC8
Desulfobacterium anilini (AF482455)
MC118Oily_dD9
phenanthrene min. Phe03 (AF327310)
Puget Sound S1Adsr B10 (DQ996774)
MC118Gassy_dI6
MC118Gassy_dK10
MC118Oily_dH2
Nankai Trough NTd-VII02 (AB263182)
MC118Gassy_dC6
EPR hydrothermal vent (AY354062)
Desulfitobacterium dehalogenans (AF337903)
Carboxydothermus hydrogenoformans (NC_0075030)
MC118Oily_dH4
Guaymas Basin B03P012 (AY197438)
MC118Gassy_dI2
MC118Oily_dF12
MC118Gassy_dA22
New England Salt Marsh PIMO3D08 (AY741570)
Thermodesulfovibrio islandicus (AF334599)
MC118Oily_dH3
MC118Oily_dA8
Desulfotomaculum acetoxidans (AF271768)
Archaeoglobus profundus (AF071499)
MC118Gassy_dA20
Desulfovibrio burkinensis (AF418186)
Desulfococcus multivorans (AJ277107)
Desulfobulbus rhabdoformis (AJ250473)
0.2
Desulfosarcina branch
Desulfovibrionales
Desulfobacterium anilini
Desulfotomaculum

Figure 2.7.

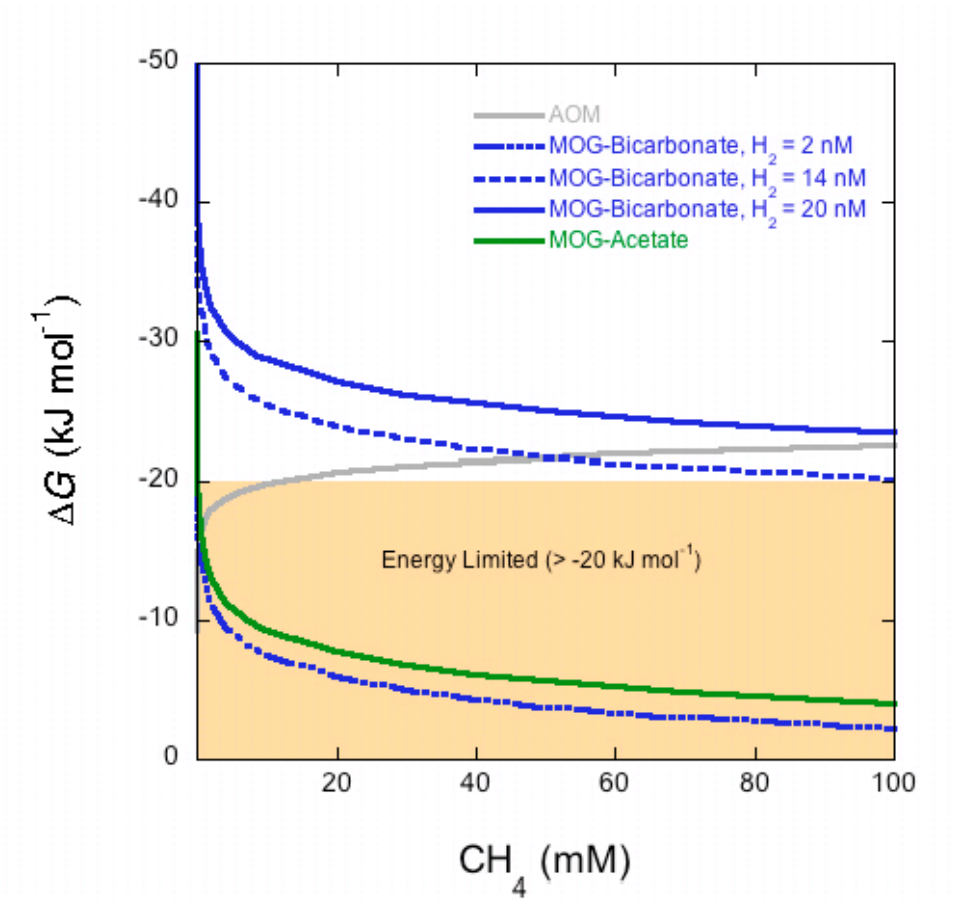
-50
-40
-30
-20
-10
0
20
40
60
80
100
ΔG (kJ mol-1)
CH4 (mM)
AOM
MOG-Bicarbonate, H2 = 2 nM
MOG-Bicarbonate, H2 = 14 nM
MOG-Bicarbonate, H2 = 20 nM
MOG-Acetate
Energy Limited (> -20 kJ mol-1)

References

Aharon, P. and Fu, B., 2000. Microbial sulfate reduction rates and sulfur and oxygen isotope fractionations at oil and gas seeps in deepwater Gulf of Mexico. *Geochimica et Cosmochimica Acta* **64**, 233-246.

Aharon, P. and Fu, B., 2003. Sulfur and oxygen isotopes of coeval sulfate-sulfide in pore fluids of cold seep sediments with sharp redox gradients. *Chemical Geology* **195**, 201-218.

Alperin, M. J., Reeburgh, W. S., and Whiticar, M. J., 1988. Carbon And Hydrogen Isotope Fractionation Resulting From Anaerobic Methane Oxidation. *Global Biogeochem. Cycles* **2**, 279-288.

Alperin, M.J. and Hoehler, T.M., 2009. Bioenergetics in archaea/sulfate-reducing bacteria aggregates. *Geochimica et Cosmochimica Acta* **73**, 13, Supplement 1, A32.

Alperin, M. J., Reeburgh, W. S., and Whiticar, M. J., 1988. Carbon And Hydrogen Isotope Fractionation Resulting From Anaerobic Methane Oxidation. *Global Biogeochemical Cycles* **2**, 279-288.

Arvidson, R. S., Morse, J. W., and Joye, S. B., 2004. The sulfur biogeochemistry of chemosynthetic cold seep communities, gulf of Mexico, USA. *Marine Chemistry* **87**, 97-119.

Berner, R. A., 1980. *Early Diagenesis: A theoretical approach.* Princeton University Press, Princeton, New Jersey.

Blazejak, A. and Schippers, A., 2010. High abundance of JS-1 and Chloroflexi-related Bacteria in deeply buried marine sediments revealed by quantitive, real-time PCR. *FEMS Microbiology Ecology*, **72**, 2, 198-207.

Boudreau, B. P. and Westrich, J. T., 1984. The dependence of bacterial sulfate reduction on sulfate concentration in marine sediments. *Geochimica et Cosmochimica Acta* **48**, 2503-2516.

Boudreau, B.P., Algar, C., Johnson, B.D., Croudace, I., Reed, A., Furukawa, Y., Dorgan, K.M., Jumars, P.A., Grader, A.S., and Gardiner, B.S, 2005. Bubble growth and rise in soft sediments. *Geology* **33**, 6, 517-520.

Bowles, M.W. and Joye, S.B., 2010. High rates of denitrification and nitrate removal in cold seep sediments. *ISME Journal*, **in press**.

Canfield, D. E., 1991. Sulfate reduction in deep-sea sediments. *Am J Sci* **291**, 177-188.

Canfield, D. E., R. Raiswell, J.T. Westrich, C.M. Reaves, and Berner, R.A., 1986. The Use of Chromium Reduction in the Analysis of Reduced Inorganic Sulfur in Sediments and Shales. *Chemical Geology* **54**, 149-155.

Canfield, D. E., Thamdrup, B., Kristensen, E., 2005. *Aquatic Geomicrobiology*. Elsevier, San Diego, CA.

Cline, J. D., 1969. Spectrophotometric Determination of Hydrogen Sulfide in Natural Waters. *Limnology and Oceanography* **14**, 454-458.

Dale, A. W., Brüchert, V., Alperin, M., and Regnier, P., 2009. An integrated sulfur isotope model for Namibian shelf sediments. *Geochimica et Cosmochimica Acta* **73**, 1924-1944.

Dhillon, A., Teske, A., Dillon, J., Stahl, D. A., and Sogin, M. L., 2003. Molecular Characterization of Sulfate-Reducing Bacteria in the Guaymas Basin. *Appl. Environ. Microbiol.* **69**, 2765-2772.

Dupré, S., Woodside, J., Foucher, J.-P., de Lange, G., Mascle, J., Boetius, A., Mastalerz, V., Stadnitskaia, A., Ondréas, H., Huguen, C., Harmégnies, F., Gontharet, S., Loncke, L., Deville, E., Niemann, H., Omoregie, E., Olu-Le Roy, K., Fiala-Medioni, A., Dählmann, A., Caprais, J.-C., Prinzhofer, A., Sibuet, M., Pierre, C., and Damsté, J. S., 2007. Seafloor geological studies above active gas chimneys off Egypt (Central Nile Deep Sea Fan). *Deep Sea Research Part I: Oceanographic Research Papers* **54**, 1146-1172.

Elvert, M., Suess, E., Greinert, J., and Whiticar, M. J., 2000. Archaea mediating anaerobic methane oxidation in deep-sea sediments at cold seeps of the eastern Aleutian subduction zone. *Organic Geochemistry* **31**, 1175-1187.

Evans, P. J., Mang, D. T., and Young, L. Y., 1991. Degradation of toluene and m-xylene and transformation of o-xylene by denitrifying enrichment cultures. *Appl. Environ. Microbiol.* **57**, 450-454.

Fossing, H. and Jørgensen, B. B., 1989. Measurement of bacterial sulfate reduction in sediments: Evaluation of a single-step chromium reduction method. *Biogeochemistry* **8**, 205-222.

Gordon, E. S. and Goñi, M. A., 2004. Controls on the distribution and accumulation of terrigenous organic matter in sediments from the Mississippi and Atchafalaya river margin. *Marine Chemistry* **92**, 331-352.

Gouch, M. A., Rhead, M. M., and Rowland, S. J., 1992. Biodegradation studies of unresolved complex mixtures of hydrocarbons: model UCM hydrocarbons and the aliphatic UCM. *Organic Geochemistry* **18**, 17-22.

Hallam, S. J., Putnam, N., Preston, C. M., Detter, J. C., Rokhsar, D., Richardson, P. M., and DeLong, E. F., 2004. Reverse Methanogenesis: Testing the Hypothesis with Environmental Genomics. *Science* **305**, 1457-1462.

Hansen, T. A., 1994. Metabolism of sulfate-reducing prokaryotes. *Antonie van Leeuwenhoek* **66**, 165-185.

Harris, J.K., Kelley, S.T., and Pace, N.R., 2004. New Perspective on Uncultured Bacterial Phylogenetic Division OP11. *Applied and Environmental Microbiology* **70**, 845-849.

Hensen, C., Nuzzo, M., Hornibrook, E., Pinheiro, L. M., Bock, B., Magalhães, V. H., and Brückmann, W., 2007. Sources of mud volcano fluids in the Gulf of Cadiz--indications for hydrothermal imprint. *Geochimica et Cosmochimica Acta* **71**, 1232-1248.

Hinrichs, K.-U., Hayes, J. M., Sylva, S. P., Brewer, P. G., and DeLong, E. F., 1999. Methane-consuming archaebacteria in marine sediments. *Nature* **398**, 802-805.

Hinrichs, K.-U., Summons, R. E., Orphan, V., Sylva, S. P., and Hayes, J. M., 2000. Molecular and isotopic analysis of anaerobic methane-oxidizing communities in marine sediments. *Organic Geochemistry* **31**, 1685-1701.

Hinrichs, K.-U. and Boetius, A., 2002. *The anaerobic oxidation of methane: new insights in microbial ecology and biogeochemistry*. Springer-Verlag, Berlin, Germany.

Hoehler, T. M., Alperin, M. J., Albert, D. B., and Martens, C. S., 1994. Field and Laboratory Studies of Methane Oxidation in an Anoxic Marine Sediment: Evidence for a Methanogen-Sulfate Reducer Consortium. *Global Biogeochem. Cycles*.

Høgslund, S., Revsbech, N. P., Kuenen, J. G., Jørgensen, B. B., Gallardo, V. A., Vossenberg, J. v. d., Nielsen, J. L., Holmkvist, L., Arning, E. T., and Nielsen, L. P., 2009. Physiology and behaviour of marine Thioploca. *ISME J* **3**, 647-657.

House, C. H., Orphan, V. J., Turk, K. A., Thomas, B., Pernthaler, A., Vrentas, J. M., and Joye, S. B., 2009. Extensive carbon isotopic heterogeneity among methane seep microbiota. *Environmental Microbiology* **11**, 2207-2215.

Huber, T., Faulkner, G., and Hugenholtz, P., 2004. Bellerophon: a program to detect chimeric sequences in multiple sequence alignments. *Bioinformatics* **20**, 2317-2319.

Iversen, N. and Jørgensen, B.B., 1993. Diffusion-coefficients of sulfate and methane in marine sediments – Influence of porosity. *Geochimica et Cosmochimica Acta* **57**, 3, 571-578.

Janzen, M. P., Nicholson, R. V., and Scharer, J. M., 2000. Pyrrhotite reaction kinetics: reaction rates for oxidation by oxygen, ferric iron, and for nonoxidative dissolution. *Geochimica et Cosmochimica Acta* **64**, 1511-1522.

Jetten, M. S. M., Strous, M., Pas-Schoonen, K. T., Schalk, J., Dongen, U. G. J. M., Graaf, A. A., Logemann, S., Muyzer, G., Loosdrecht, M. C. M., and Kuenen, J. G., 1998. The anaerobic oxidation of ammonium. *FEMS Microbiology Reviews* **22**, 421-437.

Jørgensen, B.B., 1978. Comparison of methods for the quantification of bacterial sulfate reduction in coastal marine sediments 1. Measurement with radiotracer techniques. *Geomicrobiology Journal* **1**, 1, 11-27.

Jørgensen, B. B. and Bak, F., 1991. Pathways and Microbiology of Thiosulfate Transformations and Sulfate Reduction in a Marine Sediment (Kattegat, Denmark). *Appl. Environ. Microbiol.* **57**, 847-856.

Joye, S. B., Boetius, A., Orcutt, B. N., Montoya, J. P., Schulz, H. N., Erickson, M. J., and Lugo, S. K., 2004. The anaerobic oxidation of methane and sulfate reduction in sediments from Gulf of Mexico cold seeps. *Chemical Geology* **205**, 219-238.

Joye, S. B., Samarkin, V. A., Orcutt, B. N., MacDonald, I. R., Hinrichs, K.-U., Elvert, M., Teske, A. P., Lloyd, K. G., Lever, M. A., Montoya, J. P., and Meile, C. D., 2009a. Metabolic variability in seafloor brines revealed by carbon and sulphur dynamics. *Nature Geosci* **2**, 349-354.

Joye, S. B., Bowles, M.W., Samarkin, V.A., Hunter, K.S., Niemann, H., 2010. Biogeochemical signatures and microbial activity of different cold seep habitats along the Gulf of Mexico lower slope. *Deep Sea Research Part II: Topical Studies in Oceanography* ***in press***.

Judd, A. G., 2004. Natural seabed gas seeps as sources of atmospheric methane. *Environmental Geology* **46**, 988-996.

Knab, N. J., Cragg, B.A., Hornibrook, E.R.C., Holmkvist, L., Pancost, R.D., Borowski, C., Parkes, R.J., and Jørgensen, B.B., 2009. Regulation of anaerobic methane oxidation in sediments of the Black Sea. *Biogeosciences* **6**, 1505-1518.

Kniemeyer, O., Musat, F., Sievert, S. M., Knittel, K., Wilkes, H., Blumenberg, M., Michaelis, W., Classen, A., Bolm, C., Joye, S. B., and Widdel, F., 2007. Anaerobic oxidation of short-chain hydrocarbons by marine sulphate-reducing bacteria. *Nature* **449**, 898-901.

Knittel, K., Boetius, A., Lemke, A., Eilers, H., Lochte, K., Pfannkuche, O., Linke, P., and Amann, R., 2003. Activity, Distribution, and Diversity of Sulfate Reducers and Other Bacteria in Sediments above Gas Hydrate (Cascadia Margin, Oregon). *Geomicrobiology Journal* **20**, 269-269.

Knittel, K., Lösekann, T., Boetius, A., Kort, R., and Amann, R., 2005. Diversity and Distribution of Methanotrophic Archaea at Cold Seeps. *Appl. Environ. Microbiol.* **71**, 467-479.

Lanoil, B. D., Sassen, R., La Duc, M. T., Sweet, S. T., and Nealson, K. H., 2001. Bacteria and Archaea Physically Associated with Gulf of Mexico Gas Hydrates. *Appl. Environ. Microbiol.* **67**, 5143-5153.

Lapham, L.L., Chanton, J.P., Martens, C.S., Higley, P.D., Jannasch, H.W., and Woolsey, J.R., 2008. Measuring Temporal Variability in Pore-Fluid Chemistry to Assess Gas Hydrate Stability: Development of a Continuous Pore-Fluid Array. *Environmental Science and Technology* **42**, 19, 7368–7373.

Larkin, M. A., Blackshields, G., Brown, N. P., Chenna, R., McGettigan, P. A., McWilliam, H., Valentin, F., Wallace, I. M., Wilm, A., Lopez, R., Thompson, J. D., Gibson, T. J., and Higgins, D. G., 2007. Clustal W and Clustal X version 2.0. *Bioinformatics* **23**, 2947-2948.

Levin, L.A., 2005. Ecology of Cold Seep Sediments: Interactions of Fauna with Flow, Chemistry and Microbes. Eds. Gibson, R.N., Atkinson, R.J.A., and Gordon, J.D.M. in *Oceanography and Marine Biology: An Annual Review*. **43**, 1-46.

Lloyd, K. G., Lapham, L., and Teske, A., 2006. An Anaerobic Methane-Oxidizing Community of ANME-1b Archaea in Hypersaline Gulf of Mexico Sediments. *Appl. Environ. Microbiol.* **72**, 7218-7230.

Londry, K. L., Dawson, K. G., Grover, H. D., Summons, R. E., and Bradley, A. S., 2008. Stable carbon isotope fractionation between substrates and products of Methanosarcina barkeri. *Organic Geochemistry* **39**, 608-621.

Lösekann, T., Knittel, K., Nadalig, T., Fuchs, B., Niemann, H., Boetius, A., and Amann, R., 2007. Diversity and abundance of aerobic and anaerobic methane oxidizers at the Haakon Mosby Mud Volcano, Barents Sea. *Appl. Environ. Microbiol.*, AEM.00016-07-AEM.00016-07.

Ludwig, W., Strunk, O., Westram, R., Richter, L., Meier, H., Yadhukumar, Buchner, A., Lai, T., Steppi, S., Jobb, G., Forster, W., Brettske, I., Gerber, S., Ginhart, A. W., Gross, O., Grumann, S., Hermann, S., Jost, R., Konig, A., Liss, T., Lussmann, R., May, M., Nonhoff, B., Reichel, B., Strehlow, R., Stamatakis, A., Stuckmann, N., Vilbig, A., Lenke, M., Ludwig, T., Bode, A., and Schleifer, K.-H., 2004. ARB: a software environment for sequence data. *Nucl. Acids Res.* **32**, 1363-1371.

MacDonald, I. R., Leifer, I., Sassen, R., Stine, P., Mitchell, R., and Jr, N. G., 2002. Transfer of hydrocarbons from natural seeps to the water column and atmosphere. *Geofluids* **2**, 95-107.

McGee, T., Woolsey, J.R., Lapham, L., Kleinberg, R., Macelloni, L., Battista, B., Knapp, C., Caruso, S., Goebel, V., Chapman, R., Gerstoft., P., 2008. Structure of a carbonate/hydrate mound in the Northern Gulf of Mexico. *International Conference on Gas Hydrate Papers.* Vancouver, Canada.

Milkov, A. V., 2005. Molecular and stable isotope compositions of natural gas hydrates: A revised global dataset and basic interpretations in the context of geological settings. *Organic Geochemistry* **36**, 681-702.

Miralles, G., Nérini, D., Manté, C., Acquaviva, M., Doumenq, P., Michotey, V., Nazaret, S., Bertrand, J., and Cuny, P., 2007. Effects of Spilled Oil on Bacterial Communities of Mediterranean Coastal Anoxic Sediments Chronically Subjected to Oil Hydrocarbon Contamination. *Microbial Ecology* **54**, 646-661.

Niemann, H., Elvert, M., Hovland, M., Orcutt, B., Judd, A., Suck, I., Gutt, J., Joye, S., Damm, E., Finster, K., and Boetius, A., 2005. Methane emission and consumption at a North Sea gas seep (Tommeliten area). *Biogeosciences Discussions* **2**, 1197-1241.

Niemann, H., Duarte, J., Hensen, C., Omoregie, E., Magalhães, V. H., Elvert, M., Pinheiro, L. M., Kopf, A., and Boetius, A., 2006a. Microbial methane turnover at mud volcanoes of the Gulf of Cadiz. *Geochimica et Cosmochimica Acta* **70**, 5336-5355.

Niemann, H., Lösekann, T., de Beer, D., Elvert, M., Nadalig, T., Knittel, K., Amann, R., Sauter, E. J., Schlüter, M., Klages, M., Foucher, J. P., and Boetius, A., 2006b. Novel microbial communities of the Haakon Mosby mud volcano and their role as a methane sink. *Nature* **443**, 854-858.

Niemann, H. and Elvert, M., 2008. Diagnostic lipid biomarker and stable carbon isotope signatures of microbial communities mediating the anaerobic oxidation of methane with sulphate. *Organic Geochemistry* **39**, 1668-1677.

O'Hara, S. C. M., Dando, P. R., Schuster, U., Bennis, A., Boyle, J. D., Chui, F. T. W., Hatherell, T. V. J., Niven, S. J., and Taylor, L. J., 1995. Gas seep induced interstitial water circulation: observations and environmental implications. *Continental Shelf Research* **15**, 931-948.

Omoregie, E. O., Mastalerz, V., de Lange, G., Straub, K. L., Kappler, A., Roy, H., Stadnitskaia, A., Foucher, J.-P., and Boetius, A., 2008. Biogeochemistry and Community Composition of Iron- and Sulfur-Precipitating Microbial Mats at the Chefren Mud Volcano (Nile Deep Sea Fan, Eastern Mediterranean). *Appl. Environ. Microbiol.* **74**, 3198-3215.

Omoregie, E. O., Niemann, H., Mastalerz, V., de Lange, G. J., Stadnitskaia, A., Mascle, J., Foucher, J.-P., and Boetius, A., 2009. Microbial methane oxidation and sulfate reduction at cold seeps of the deep Eastern Mediterranean Sea. *Marine Geology* **261**, 114-127.

Orcutt, B., Boetius, A., Elvert, M., Samarkin, V., and Joye, S. B., 2005. Molecular biogeochemistry of sulfate reduction, methanogenesis and the anaerobic oxidation of methane at Gulf of Mexico cold seeps. *Geochimica et Cosmochimica Acta* **69**, 4267-4281.

Orcutt, B. and Meile, C., 2008. Constraints on mechanisms and rates of anaerobic oxidation of methane by microbial consortia: process-based modeling of ANME-2 archaea and sulfate reducing bacteria interactions. *Biogeosciences Discussions* **5**, 1933-1967.

Orcutt, B., Joye, S.B., Kleindienst, S., Knittel, K., Ramette, A., Reitz, A., Samarkin, V., Treude, T., Boetius, A., 2009. Impact of natural oil and higher hydrocarbons on microbial diversity, distribution and activity in Gulf of Mexico cold seep sediments. *Deep Sea Research Part II: Topical Studies in Oceanography* ***in press***.

Orphan, V. J., Hinrichs, K. U., Ussler, W., Paull, C. K., Taylor, L. T., Sylva, S. P., Hayes, J. M., and Delong, E. F., 2001a. Comparative Analysis of Methane-Oxidizing Archaea and Sulfate-Reducing Bacteria in Anoxic Marine Sediments. *Appl. Environ. Microbiol.* **67**, 1922-1934.

Orphan, V. J., House, C. H., Hinrichs, K.-U., McKeegan, K. D., and DeLong, E. F., 2001b. Methane-Consuming Archaea Revealed by Directly Coupled Isotopic and Phylogenetic Analysis. *Science* **293**, 484-487.

Orphan, V. J., House, C.H., Hinrichs, K.-U., McKeegan, K.D., DeLong, E.F., 2002. Multiple archaeal groups mediate methane oxidation in anoxic cold seep

sediments. *Proceedings of the National Academy of Sciences of the United States of America* **99**, 7663-7668.

Otte, S., Kuenen, J. G., Nielsen, L. P., Paerl, H. W., Zopfi, J., Schulz, H. N., Teske, A., Strotmann, B., Gallardo, V. A., and Jørgensen, B. B., 1999. Nitrogen, Carbon, and Sulfur Metabolism in Natural Thioploca Samples. *Appl. Environ. Microbiol.* **65**, 3148-3157.

Preisler, A., de Beer, D., Lichtschlag, A., Lavik, G., Boetius, A., and Jørgensen, B. B., 2007. Biological and chemical sulfide oxidation in a Beggiatoa inhabited marine sediment. *ISME J* **1**, 341-353.

Pruesse, E., Quast, C., Knittel, K., Fuchs, B. M., Ludwig, W., Peplies, J., and Glockner, F. O., 2007. SILVA: a comprehensive online resource for quality checked and aligned ribosomal RNA sequence data compatible with ARB. *Nucl. Acids Res.* **35**, 7188-7196.

Reeburgh, W. S., 1967. An improved interstitial water sampler. *Limnology and Oceanography* **12**, 163-165.

Reeburgh, W.S., 1980. Anaerobic methane oxidation: Rate depth distributions in Skan Bay sediments. *Earth Planetary Science Letters* **47**, 345-352.

Reeburgh, W. S., 2007. Oceanic Methane Biogeochemistry. *Chemical Reviews* **107**, 486-513.

Ryan, W. B. F., S.M. Carbotte, J. Coplan, S. O'Hara, A. Melkonian, R. Arko, R.A. Weissel, V. Ferrini, A. Goodwillie, F. Nitsche, J. Bonczkowski, and R. Zemsky (2009), Global Multi-Resolution Topography (GMRT) synthesis data set, *Geochem. Geophys. Geosyst.*, 10, Q03014.

Sahling, H., Bohrmann, G., Artemov, Y. G., Bahr, A., Brüning, M., Klapp, S. A., Klaucke, I., Kozlova, E., Nikolovska, A., Pape, T., Reitz, A., and Wallmann, K., 2009. Vodyanitskii mud volcano, Sorokin trough, Black Sea: Geological characterization and quantification of gas bubble streams. *Marine and Petroleum Geology* **26**, 1799-1811.

Sayama, M., Risgaard-Petersen, N., Nielsen, L. P., Fossing, H., and Christensen, P. B., 2005. Impact of Bacterial NO3- Transport on Sediment Biogeochemistry. *Appl. Environ. Microbiol.* **71**, 7575-7577.

Schippers, A. and Jørgensen, B. B., 2001. Oxidation of pyrite and iron sulfide by manganese dioxide in marine sediments. *Geochimica et Cosmochimica Acta* **65**, 915-922.

Schulz, H.D., 2000. Quantification of early diagenesis: Dissolved constituents in marine pore water, in: *Marine Geochemistry* (eds.) Schulz, H.D. and Zabel, M., Springer Verlag, Berlin, Germany, 85-128.

Sørensen, J., Christensen, D., and Jørgensen, B. B., 1981. Volatile Fatty Acids and Hydrogen as Substrates for Sulfate-Reducing Bacteria in Anaerobic Marine Sediment. *Appl. Environ. Microbiol.* **42**, 5-11.

Summons, R. E., Franzmann, P. D., and Nichols, P. D., 1998. Carbon isotopic fractionation associated with methylotrophic methanogenesis. *Organic Geochemistry* **28**, 465-475.

Sweerts, J-P.R.A., Beer, D.d., Nielsen, L.P., Verdouw, H., Heuvel, J.C.V. d., Cohen, Y., and Cappenberg, T. E., 1990. Denitrification by sulphur oxidizing Beggiatoa spp. mats on freshwater sediments. *Nature* **344**, 762-763.

Tamura, K., Dudley, J., Nei, M., and Kumar, S., 2007. MEGA4: Molecular Evolutionary Genetics Analysis (MEGA) Software Version 4.0. *Mol Biol Evol* **24**, 1596-1599.

Teske, A., Brinkhoff, T., Muyzer, G., Moser, D. P., Rethmeier, J., and Jannasch, H. W., 2000. Diversity of Thiosulfate-Oxidizing Bacteria from Marine Sediments and Hydrothermal Vents. *Appl. Environ. Microbiol.* **66**, 3125-3133.

Teske, A. and Sørensen, K. B., 2007. Uncultured archaea in deep marine subsurface sediments: have we caught them all? *ISME J* **2**, 3-18.

Treude, T., Boetius, A., Knittel, K., Wallmann, K., Jørgensen, B., 2003. Anaerobic oxidation of methane above gas hydrates at Hydrate Ridge, NE Pacific Ocean. *Marine Ecology Progress Series* **264**, 1-14.

Treude, T., Krüger, M., Boetius, A., and Jørgensen, B. B., 2005a. Environmental Control on Anaerobic Oxidation of Methane in the Gassy Sediments of Eckernförde Bay (German Baltic). *Limnology and Oceanography* **50**, 1771-1786.

Treude, T., Niggemann, J., Kallmeyer, J., Wintersteller, P., Schubert, C. J., Boetius, A., and Jørgensen, B. B., 2005b. Anaerobic oxidation of methane and sulfate

reduction along the Chilean continental margin. *Geochimica et Cosmochimica Acta* **69**, 2767-2779.

Valentine, D. L. and Reeburgh, W. S., 2000. New perspectives on anaerobic methane oxidation. *Environmental Microbiology* **2**, 477-484.

Wagner, M., Roger, A. J., Flax, J. L., Brusseau, G. A., and Stahl, D. A., 1998. Phylogeny of Dissimilatory Sulfite Reductases Supports an Early Origin of Sulfate Respiration. *J. Bacteriol.* **180**, 2975-2982.

Wegener, G., Niemann, H., Elvert, M., Hinrichs, K.-U., and Boetius, A., 2008. Assimilation of methane and inorganic carbon by microbial communities mediating the anaerobic oxidation of methane. *Environmental Microbiology* **10**, 2287-2298.

Weston, N., Porubsky, W., Samarkin, V., Erickson, M., Macavoy, S., and Joye, S., 2006. Porewater Stoichiometry of Terminal Metabolic Products, Sulfate, and Dissolved Organic Carbon and Nitrogen in Estuarine Intertidal Creek-bank Sediments. *Biogeochemistry* **77**, 375-408.

Weston, N. B. and Joye, S. B., 2005. Temperature-driven decoupling of key phases of organic matter degradation in marine sediments. *Proceedings of the National Academy of Sciences of the United States of America* **102**, 17036-17040.

Whitman, W., Bowen, T., and Boone, D., 2006. The Methanogenic Bacteria. *The Prokaryotes*, Springer, New York.

Widdel, F., Boetius, A., and Rabus, R., 2006. Anaerobic Biodegradation of Hydrocarbons Including Methane.

Widdel, F. and Pfennig, N., 1981. Sporulation and further nutritional characteristics of Desulfotomaculum acetoxidans. *Archives of Microbiology* **129**, 401-402.

Widdel, F. and Rabus, R., 2001. Anaerobic biodegradation of saturated and aromatic hydrocarbons. *Current Opinion in Biotechnology* **12**, 259-276.

Zehnder, A. J. and Brock, T. D., 1979. Methane formation and methane oxidation by methanogenic bacteria. *J. Bacteriol.* **137**, 420-432.

CHAPTER 3

IMPROVED MEASUREMENT OF MICROBIAL ACTIVITY IN DEEP-SEA SEDIMENTS AT *IN SITU* PRESSURE AND METHANE CONCENTRATION[1]

[1] Bowles, M.W., Samarkin, V.A., and S.B. Joye, submitted to *Limnology and Oceanography: Methods*, 2011.

Abstract

A robust and convenient method was developed to evaluate rates of microbial activity in gas-charged deep-sea sediments at *in situ* pressure, temperature, and gas concentration. The method utilized a hydrostatic chamber to maintain high pressures, and a modified hungate tube and plunger to contain samples. This technique can be easily applied to quantifying rates of microbial processes sensitive to dissolved gas concentration (e.g. sulfate reduction, anaerobic methane oxidation, and methanogenesis) in high pressure, gas-rich environments. Here, the method was used to determine rates of microbial activity in cold seep sediments from the Gulf of Mexico and the California coast. We measured rates of sulfate reduction (SR), anaerobic oxidation of methane (AOM), and methanogenesis (MOG) with radiotracers. We compared *in situ* pressure and elevated methane concentration assays to traditional *ex situ* incubations at 1 bar in degassed sediment. Methane concentrations were elevated in *ex situ* incubations to assess a substrate level affect. Upon the application of pressure, rates of AOM, SR, and MOG rates increased. AOM and MOG rates were more influenced by the addition of methane. Measuring rates of deep-sea microbial activity at *in situ* pressure and gas concentrations is essential to quantify carbon flow in these environments.

1. Introduction

Seventy one percent of the Earth's surface area is covered by the ocean. Pressure increases rapidly, 1 bar for every 10 m of water depth, below the sea surface, yet little is known about rates of microbial processes in deep sea sediments under *in situ* conditions. As water depth increases, the chemistry of sediment pore fluids changes because high pressure increases the solubility of biologically important gases, such as methane, ethane, propane, butane, and hydrogen. For example, methane solubility at atmospheric pressure is ~1-2 mM, depending on temperature and salinity. At 10 bar or 100 m water depth, up to 17 mM methane can be dissolved in the pore fluids, while at 100 bar or 1000 m, models suggest that excluding hydrate formation methane concentrations can reach >120 mM (Duan and Mao, 2006). However, higher pressures (200 bars or 2000 m water depth) are required to impart what is traditionally considered a pressure-specific signature on microbial distributions/activity (Overmann, 2000 *and references therein*), i.e. barophilism. Because lesser depth induces pressure-related changes in gas solubility, pressure could therefore significantly influence microbial activity at depths less than 2000m (Bowles et al. submitted). While microbial dynamics at elevated pressure have been studied using an array of methods and techniques (see Jannasch and Taylor, 1984, Kim and Kato, 2010 *and references therein*), the influence of *in situ* gas concentration has not been considered thus far.

Methane is cycled rapidly by a number of microbial pathways in the marine environment, and methane cycling links the carbon cycle to other biogeochemical cycles, such as the sulfur cycle through sulfate reduction (Hoehler et al., 1994). Tight coupling

between biogeochemical cycles is particularly important in methane-rich cold seep environments (Lapham et al., 2008, Wankel et al., 2010). Upon recovery of gas-rich sediment cores from the seafloor to the ship, extensive degassing occurs which decreases dissolved gas concentrations. Here we outline a method by which *in situ* gas concentrations can be restored to more accurately estimate rates of microbial processes in deep-sea sediments. This work focused on the processes of sulfate reduction (SR), anaerobic methane oxidation (AOM), and methanogenesis (MOG) but could easily be applied to other processes.

No prior study has used intact deep sea sediment sub-samples to determine rates of microbial processes at *in situ* pressure and elevated methane concentration. To date sulfate reduction (Nauhaus et al., 2002, Weber et al., 2001) is the only process measured at near potential *in situ* methane concentrations and pressure. Weber and coworkers (2001) used radiotracers to directly quantify SR at *in situ* pressure, while Nauhaus and coworkers (2002) used sulfide accumulation to estimate rates. No previous method has allowed direct measurement of multiple processes on intact deep-sea sediments while maintaining *in situ* pressure or restoring potential *in situ* methane concentration.

Methodologically, prior attempts to evaluate processes at elevated or *in situ* methane concentrations either involved recovery of sediment to surface pressure and then restoration of *in situ* gas concentration using a syringe system to add methane as samples were pressurized (Nauhaus et al., 2002), or *in situ* radioisotope injection (of ^{35}S-labeled sulfate) and incubation at the seafloor (Weber et al., 2001). The disadvantages of the syringe system includes 1) limited number of samples because of the restricted space

available in a hydrostatic pressure vessel, 2) fragile connections that could lead to breakage and isotope contamination, and 3) inability to measure processes such as MOG due to the potential for degassing. The *in situ* sulfate reduction rate determination used by Weber and colleagues (2001) is impractical for use with processes that involve gaseous tracer (AOM) or gaseous products (MOG) that may be present at supersaturated concentration due the inability to add sufficient tracer (former) or degassing of materials upon recovery (latter). Thus, this approach disturbs surficial sediments and introduces a substantial artifact.

Here, we present an improved technique for quantifying rates of microbial activity using a modified hungate tube and plunger assembly. We used a hydrostatic pressure vessel to achieve *in situ* pressure. Using the modified hungate tube permitted addition of methane gas and radioactive methane tracer. Once pressurized the tube plunger compressed the sample and headspace, equalizing pressure within the the tube. The impact of changes in methane concentration and pressure were evaluated in incubations of cold seep sediments by comparing rates under 1) *ex situ* conditions (no methane addition, 1 bar pressure), 2) low methane (1.4 mM) addition, 1 bar pressure, 3) *in situ* pressure, low (1.4 mM) methane, and 4) *in situ* pressure, increased (5 mM) methane.

2. Materials and Procedures

2.1. Hydrostatic Pressure System

The pressure vessel was a 5 cm thick stainless steel hallowed chamber and accompanying lid designed by Fluitron® and rated to 470 bar (Fig. 1). The vessel has two entry points, one for pressure monitoring, and the other a one-way valve for water

addition to the chamber. The lid of the chamber was sealed with a butyl rubber gasket and secured by stainless steel bolts.

The chamber was pressurized hydrostatically using pumps designed and manufactured by Richard Dudgeon, Inc. Once the desired pressure was reached, the valve was closed and the pump disconnected. The hoses used in the connection, and all fittings, were designed for high pressure use.

2.2. Modified Sample Tube and Assembly

A modified hungate tube and stopper were used to contain the sample (Fig. 2A). The round end of the hungate tube (20 mL; Bellco Glass, Inc.) was cut off. After adding sediment to the tube, a retractable butyl rubber stopper (13 x 20 mm; Geo-Microbial Technologies, Inc.) was inserted into the tube. The stoppers were pre-treated (boiled in 2N NaOH and then soaked in milliQ water for a day and then rinsed copiously in milliQ water) to remove potential microbial toxins. The stopper had a monofilament polyethylene line passed through its center (hereafter the modified stopper is termed a plunger; Fig. 2A). A screw lid and septa (Bellco Glass, Inc.) sealed the top of the vial.

2.3. Sample collection and incubation procedure

Intact sediment samples were introduced into the modified hungate tube through the cut-end and then the plunger was added (Fig. 2). Next the plunger was used to move the sediment so that it was flush with the end of the tube. Then, the septa was placed onto the sediment, without a headspace, and the screw cap was tightened. The end result was a sediment plug with no headspace in a glass tube sealed by a butyl rubber seal (plunger or septa) on each end (see complete assembly in Fig. 2A). Next, methane (ultra

high purity 100% methane, Airgas®) was added in a precise volume to achieve the desired dissolved concentration at *in situ* pressure. We used the ideal gas law to determine the amount of gas to add considering the salinity of the particular sample and incubation temperature. Addition of the gas was made by piercing the septa with a gas filled syringe, and simultaneously pulling the polyethylene loop to gently draw the gas from the syringe into the tube, thereby forming a headspace (see Fig. 2B). Radiotracer additions are described in the following section.

2.4. Rate Measurement

We used this method to quantify rates of key microbial processes in gassy cold seep sediments from Mississippi Canyon (MC) Gulf of Mexico, USA, and Monterey Bay (MB) California coast, USA, and in brine-influenced sediments from the Garden Banks (GB), Gulf of Mexico, USA. MC and MB sediments were obtained via push-coring using remotely operated vehicles; GB sediment was collected by piston coring. For GB samples, limited sample volume required a 1:1 slurry of brine sediments to perform AOM and SR rate measurements.

Radiotracer assays were used to measure the rate of AOM, SR, and bicarbonate based MOG. For rate assays, sediment was introduced to the tubes as described above and methane was added prior to radiotracer addition. In MC and MB, the upper 6 cm of sediment was used, while deeper methane-rich sediments (~1 m) were used in the GB piston core. Approximately 2 cm^{-3} of sediment was placed into each sample tube, and the incubation time was 24 hours at *in situ* temperature (6°C). Sediments from MC and MB were retrieved at approximately 1000 m depth, so a pressure of 100 bar was applied

during these incubations. Sediment from GB was collected at a water depth of 500 m, so these samples were pressurized to 50 bar.

For sulfate reduction, 100 µL of high specific activity $Na_2{}^{35}SO_4$ dissolved in slightly alkaline deionized H_2O (pH ~ 9.4; 400 kBq) was added to samples following the addition of the methane headspace. Controls consisted of samples where microbial activity was halted prior to radioisotope addition by injecting 3 mL of 20% (w/v) zinc acetate into the sample tube. Anaerobic oxidation of methane samples and killed controls were injected with 100 µL of purified gaseous $^{14}CH_4$ (133 kBq). The CH_4 tracer was purified using Hopcalite and activated carbon (Harder, 1997). The activity of the gaseous methane tracer was determined by dissolving an aliquot of gas into scintillation cocktail in a sealed scintillation vial. Methane concentration used in these incubations were below saturation for the respective pressures, assuring that all the methane was dissolved after application of *in situ* pressure. For incubations at 1 bar, 100 µL of dissolved $^{14}CH_4$ (8.3 kBq) tracer was used to avoid inconsistencies related to gaseous tracer dissolution. The activity of the tracer was verified as described above. For AOM controls, 2 mL of 2N NaOH was injected to the sample prior to isotope addition. Bicarbonate reduction to methane was assessed in sediments by adding 100 µL of $NaH^{14}CO_3$ dissolved in slightly alkaline deionized H_2O (pH ~ 9.4; 350 kBq). For MOG controls, 2 mL of 2N NaOH was injected to the sample prior to isotope addition. For all analyses, triplicate live samples and a dead control were run for each treatment.

At the termination of the incubation, samples were depressurized, and microbial activity was halted immediately by injecting either 20% (w/v) zinc acetate or 2N NaOH,

as described for control samples. Within 1-hour of terminating the experiment, the sample was transferred into a 50 mL centrifuge tube containing 5 or 10 mL of NaOH or zinc acetate for AOM and SR samples, respectively. The SR samples were stored at -20ºC to prevent oxidation of radioactive reduced sulfide species. Samples for MOG were stored (<1 week) in modified hungate tubes under a slight negative pressure to prevent the loss of radioactive methane.

2.5. Sample Processing and Rate Calculation

2.5.1. Sulfate Reduction

Ejecting the sample into 50 mL centrifuge tubes containing zinc acetate served to arrest microbial activity and convert $H_2{}^{35}S$ to $Zn^{35}S$. To recover the radioactive sulfide, samples were thawed, and then radioactive sulfate was removed by adding anoxic seawater, centrifuging, removing the anoxic seawater; this rinse was repeated a total of three times. After each centrifugation step the supernatant was collected and after the final collection, the supernatant was sub-sampled to determine the $^{35}SO_4{}^{2-}$ activity. Ethanol (10 mL) was added to the sample and it was temporarily stored at -20ºC. Samples were distilled via a one-step wet-acid reduction and evolved $H_2{}^{35}S$ was trapped in 5% (w/v) zinc acetate (Canfield et al., 1986; Fossing and Jørgensen, 1989). Activities of sulfate and sulfide samples were measured using Scintisafe Gel (Fisher®) scintillation cocktail. Rates of sulfate reduction (SR) were determined from equation (1).

$$\text{SR Rate}=[SO_4{}^{2-}]\times \alpha_{SO4}/t \times(\text{DPM-}H_2{}^{35}S/(\text{DPM-}{}^{35}SO_4+\text{DPM-}H_2{}^{35}S)) \quad (1)$$

Here, the SR rate (nmol cm^{-3} day^{-1}) is the rate of sulfate reduction, $[SO_4{}^{2-}]$ is the concentration of sulfate (nmol cm^{-3} wet sediment; obtained by multiplying the porewater

sulfate concentration times the sediment porosity), α is the fractionation factor (1.06; Jørgensen, 1978), *t* is the time of incubation (days), DPM-$H_2{}^{35}S$ is the activity of sulfide generated (minus activity in killed controls specific to the treatment), and DPM-$^{35}SO_4$+DPM-$H_2{}^{35}S$ reflects the total tracer activity injected.

2.5.2. Anaerobic oxidation of methane

Samples were stored until processing via a passive acid distillation (Joye et al., 2004). Briefly, samples were transferred into a 250 mL Erlenmeyer flasks along with 1 mL of saturated cupric sulfate. The cupric sulfate served to trap sulfide, which can reduce the efficiency of carbon dioxide capture using CarboSorb E®. A scintillation vial containing CarboSorb E® and filter paper was suspended from the butyl rubber stopper that sealed each flask. Phosphoric acid (final concentration of≈10%) was added and samples were immediately sealed with the butyl stopper holding the CO_2 trap; the evolved $^{14}CO_2$ was trapped directly into the CarboSorb E®. Samples were shaken gently during distillation (at least 4-hr) and afterwards, Scintisafe Gel (Fisher®) was added and radioactivity was quantified using liquid scintillation counting. The recovery efficiency was determined from distillation of $NaH^{14}CO_3$ standards and averaged 99%. Rates of the anaerobic oxidation of methane (AOM) were calculated from equation (2)

$$\text{AOM Rate}=[CH_4]\times \alpha_{CH4}/t \times(\text{DPM-}^{14}CO_2/\text{DPM-}^{14}CH_4) \qquad (2)$$

Here, the AOM rate (nmol cm^{-3} day^{-1}) is the rate of methane oxidation, $[CH_4]$ is the concentration of methane (nmol cm^{-3} of wet sediment), α is the fractionation factor (1.018; Alperin et al., 1988), *t* is the time of incubation (days), DPM-$^{14}CO_2$ is the activity

of carbon dioxide generated minus activity from the control, and DPM-$^{14}CH_4$ is the total tracer activity injected.

2.5.3. Methanogenesis

The rate of methane production from bicarbonate was determined by quantitatively converting $^{14}CH_4$ to $^{14}CO_2$ and trapping the $^{14}CO_2$. Briefly, vessels were shaken vigorously then purged with a gentle flow of CO_2 free compressed air. The gas stream was passed through an 800°C titanium-nickel alloy column packed with copper oxide used to catalyze the oxidation of $^{14}CH_4$ to $^{14}CO_2$. The resulting $^{14}CO_2$ was trapped in a mixture of Carbosorb E® (Perkin Elmer®) and the scintillation cocktail Permafluor E® (Perkin Elmer®). Immediately following purging and trapping the cocktail was counted on a liquid scintillation counter. Rates were calculated using substrate concentrations measured in separate samples, and activities recovered in $^{14}CH_4$ pool (equation 3):

$$MOG_{DIC}\ \text{rate} = [\text{DIC}] \times \alpha_{DIC} / t \times (\text{a-}^{14}CH_4/\text{a-}^{14}\text{C-DIC}) \qquad (3)$$

where MOG_{DIC} is the rate of methanogenesis from dissolved inorganic carbon (DIC) in (nmol substrate reduced cm^{-3} day^{-1}), [DIC] is the concentration of DIC (nmol cm^{-3}), α_{DIC} is the isotopic fractionation factor (1.06; Krzycki et al., 1987), t is the period of incubation (days), a-$^{14}CH_4$ is the activity recovered in the products pool (DPM), and ^{14}C-DIC is the activity of the substrate injected into sample (DPM).

2.6. Geochemistry

To calculate rates of processes, we measured sulfate, dissolved inorganic carbon, and methane concentration in the sediment cores (detailed by Joye et al., 2004). Briefly, sulfate was measured using a Dionex® Ion Chromatograph and methane on a Shimadzu

Gas Chromatograph using Flame Ionization Detector (GC-FID). Porewater for DIC quantification was injected into a sealed headspace vial and acidified (pH = 1); a headspace subsample was injected into the methanizer equipped GC-FID, where CO_2 was quantitatively reduced to CH_4 over the nickel catalyst in the methanizer column. DIC measurements were standardized using certified gas standards (1% CO_2).

3. Assessment

The rates of AOM and SR measured in gassy cold seep sediments using the standard *ex situ* approach were similar to previous measurements (Joye et al., 2004, Orcutt et al., 2005, Omoregie et al., 2009, Joye et al., 2010). Rates of AOM in gassy sediments are usually <1 to a few 100 nmol cm^{-3} d^{-1} (Orcutt et al., 2005), while AOM rates in brine-rich sediments are typically <1 nmol cm^{-3} d^{-1} (Joye et al., 2010). The *ex situ* AOM rates in MC and MB gassy sediments, 1.42 (±0.33) and 0.06 (±0.01) nmol cm^{-3} d^{-1}, were comparable to published rates (Orcutt et al., 2005). The GB AOM rate was lower, 0.05 (± 0.009) pmol cm^{-3} d^{-1}, but was also comparable with previous rates obtained at brine sites (Orcutt et al., 2005, Joye et al., 2010). Volumetric rates of SR at cold seeps can be extremely high, up to 10s of μmol cm^{-3} d^{-1} (Arvidson et al., 2004, Bowles et al., 2011); rates generally range from 100 to 1000 nmol cm^{-3} d^{-1} in gassy seep sediments (Boetius et al., 2000; Joye et al., 2004; Orcutt et al., 2005), while rates in brine are lower (Joye et al., 2010). The *ex situ* SR rates in gassy sediments were 45.8 (± 8.9) and 16.5 (± 1.7) nmol cm^{-3} d^{-1} for MC and MB, respectively. The SR rates from the GB brine sediments were lower, 0.04 (± 0.002) nmol cm^{-3} d^{-1}.

MOG is not frequently measured in cold seep sediments (Orcutt et al., 2005, Knab et al., 2009, Joye et al., 2009), but rates range from 10-100 pmol cm^{-3} d^{-1}. Higher rates of MOG, up to 100s of nmol cm^{-3} d^{-1} have been measured in some gassy sediments (Orcutt et al., 2005). In mat sediment from MC and MB, *ex situ* MOG rates were 0.11 (± 0.06) and 0.36 (± 0.03) nmol cm^{-3} d^{-1}. The MOG rates are comparable to rates from low activity sediments measured previously (Orcutt et al., 2005).

All of the processes evaluated in this study could be sensitive to methane concentration. AOM and SR are linked through the purported reaction stoichiometry of the anaerobic oxidation of methane (Hoehler et al., 1994) and therefore would become more thermodynamically favorable as methane concentration increased. Virtually all processes analyzed showed pressure and methane related increase in rates, and AOM rates were most influenced by methane concentration (Fig. 3). A pressure affect on AOM at MC and MB was apparent, as the AOM rate at 1.4 mM methane and *in situ* pressure was 2-3 times the rate at 1.4 mM and 1 bar (Fig. 3). Pressure did not stimulate AOM activity in GB sediments, which may reflect a separate mechanism for methane oxidation in brine-rich sediments or variability of the extremely low AOM activity measured. A pressure affect on SR was apparent, at all sites, where the 1.4 mM methane treatment without pressure ranged from 19 to 57% of the rate at *in situ* pressure and 1.4 mM methane. AOM and MOG were both influenced by further increases in methane concentration, rates at 1.4 mM and *in situ* pressure were approximately 20 to 52% of the rate at 5 mM methane.

MOG rates were expected to decrease with methane addition, as MOG becomes less energetically favorable at higher methane concentration. However, at MC and MB, rates of MOG were stimulated under pressure relative to *ex situ* conditions; rates without pressure were 13 and 7% of the rate at *in situ* pressure, respectively. MOG rates at 1.4 mM methane and *in situ* pressure were 28 and 52% of rates at 5 mM methane and *in situ* pressure.

4. Discussion

Evaluating rates of methane-sensitive microbial processes under quasi-*in situ* conditions provides more accurate and realistic estimates of microbial activity in the deep sea. The differences in process rates at elevated methane concentration underscore this point. The procedure we developed allowed measurement of rates in intact sediments retrieved from methane rich environments. The method was advantageous in comparison to previously used methods. Each tube was conveniently isolated from other samples, and the minimal size requirement for each sample tube allowed numerous samples and processes to be analyzed. In addition the method allowed for quantification of process rates for gaseous reactants and products, which was previously not possible. Though we targeted only three processes, this method can be applied to other processes that could be sensitive to gas concentration.

All three processes assessed were influenced by pressure and methane concentration. There is some basis for comparing the SR rates presented here to prior data (Weber et al., 2001, Nauhaus et al., 2002). Weber and coworkers (2001) focused on SR rates in slope sediments (50 to 2000m) from the Black Sea. In these sediments, *ex situ* SR

rates were typically higher than *in situ* rates. The discrepancy could be explained by two mechanisms: 1) lower methane concentrations or 2) sampling artifacts related to disturbance introduced by the lander. Methane concentrations were not measured in that study, but subsequent work (Reidinger et al., 2010) showed methane concentrations were typically low in these sediments. Lower methane concentrations might not support thriving communities of sulfate reducing bacteria and methanotrophs, relative to the high methane flux cold seep sites assayed here. The *in situ* sampler used by Weber and coworkers (2001) disturbed the surface layer of the sediment as it was removed from the seafloor. Thus, another advantage of the method presented here is that surface horizons, which remain intact when collected with multicores and pushcores, can be analyzed easily. The work by Nauhaus et al. (2002) used sulfide production to estimate SR rates and used SR rates as a proxy for AOM rates, but rates were not measured directly using radiotracers.

Rates of AOM were very responsive to pressure and methane increases. This increase is best explained by energetics, as methane concentration increases the energy yield of AOM (Bowles et al., 2011). While the increased energy yield favors AOM it should make MOG less favorable (Bowles et al., 2011).

In addition to illustrating that specific processes respond strongly to increased methane concentration, we show that generalizations about microbial metabolism at pressure are not accurate unless they also account for the influence of dissolved gas concentration. Barophiles are traditionally classified as microorganisms thriving at extreme pressures (>200 bar). Processes at relatively lower pressures have been previously

measured, but those measurements did not account for degassing (e.g. deAngelis et al., 1991, Parkes et al., 1995). Here, we show that maintaining substrate levels at *in situ* conditions is required to describe rates accurately.

5. Comments and Recommendations

The data presented here represent two types of sediment, gassy and brine-influenced, that are common in the deep sea. The approach presented here could be applied easily to oily, gassy deep sea sediments (Bowles et al. in preparation), deep biosphere sediments, or to hydrothermal sediments (Joye et al. in preparation). In addition although only three processes were analyzed here, the method could be applied to any process (e.g. measuring rates of Fe and Mn reduction) or to different dissolved gases (CO_2 or H_2 as well as CH_4). The data clearly show that without restoring pressure and *in situ* gas concentrations, microbial processes are not accurately assessed. The procedure used and materials required for *in situ* pressure and gas concentrations are portable and can be used at sea, as well as in the laboratory. If these techniques were to be applied at sea, and in combination with an *in situ* mass spectrometer (Wankel et al., 2010) or raman spectrometer (Zhang et al., 2009), then microbial processes would be assessed even more precisely.

Acknowledgements. We thank Peter Girguis, Scott Wankel, and Bernie Bernard for assistance with sample collection. This research was supported by the NOAA National Institute for Undersea Science and Technology (award numbers 06-09-018, 07-10-028 and 08-10-031).

Figure 3.1. A) Pressure vessel with valve and pressure gauge on cap. **B)** Water pump for applying water at high pressures to the pressure chamber.

Figure 3.2. A) Modified hungate tube and plunger assembly used for high pressure incubations with septa and cap, sediment, plunger (modified butyl rubber stopper), and polyethylene line designated. **B)** Modified hungate tube after the addition of the desired gaseous addition, and prior to pressurization.

Figure 3.3. Rates of **A)** AOM, **C)** SR, and **E)** MOG at various sites with the ordinate axis in log scale. Treatments displayed are *ex situ* or no methane or pressure addition, 1.4 mM CH_4 with *in situ* pressure (P) and at 1 bar, and 5 mM CH_4 at *in situ* P are displayed. Comparisons of **B)** AOM, **D)** SR, and **F)** MOG rates expressed as percentages (%) of 1 bar at 1.4 mM and *in situ* P at 1.4 mM, and also *in situ* P at 1.4 mM and *in situ* P at 5 mM CH_4. *NM* represents *N*ot *M*easured.

Figure 3.1.

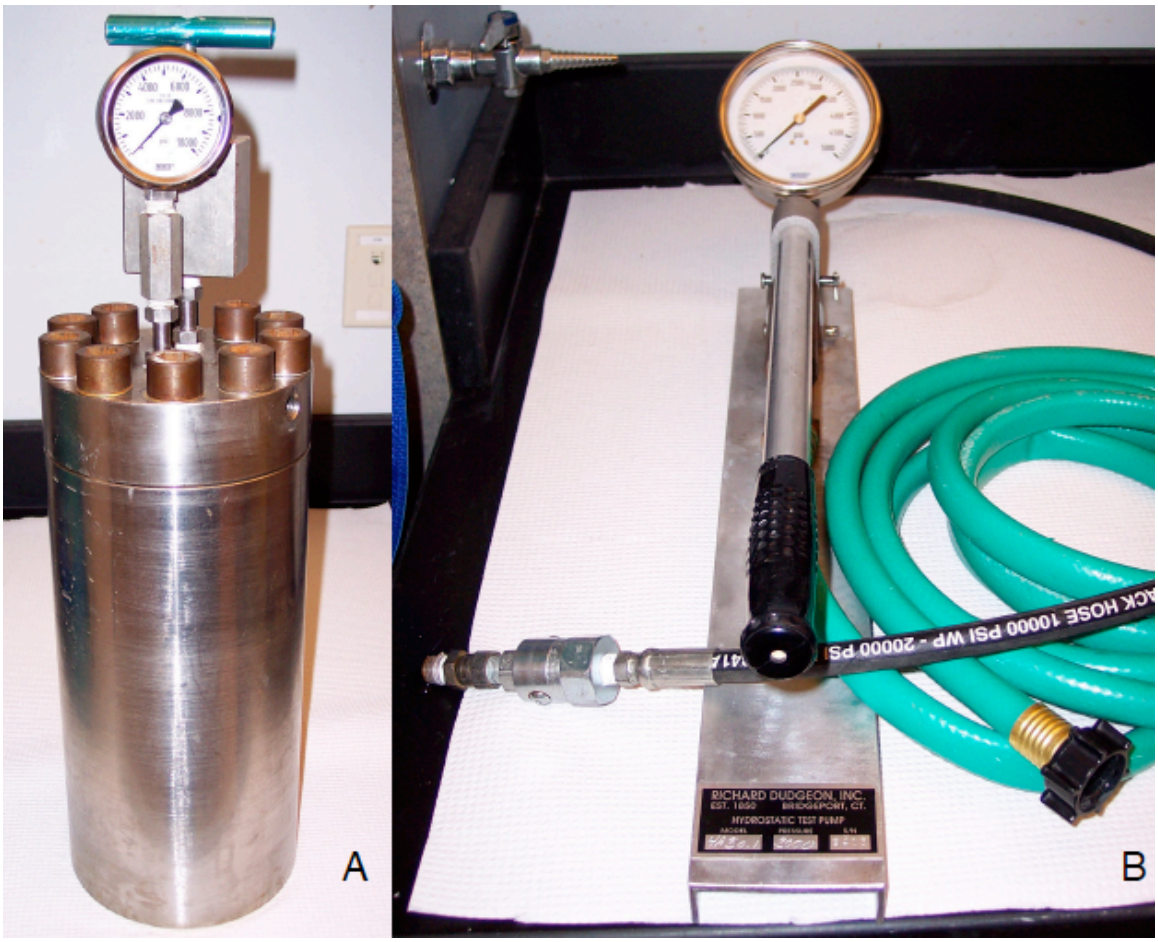
A
RICHARD DUDGEON, INC.
EST. 1850 BRIDGEPORT, CT.
HYDROSTATIC TEST PUMP
B

Figure 3.2.

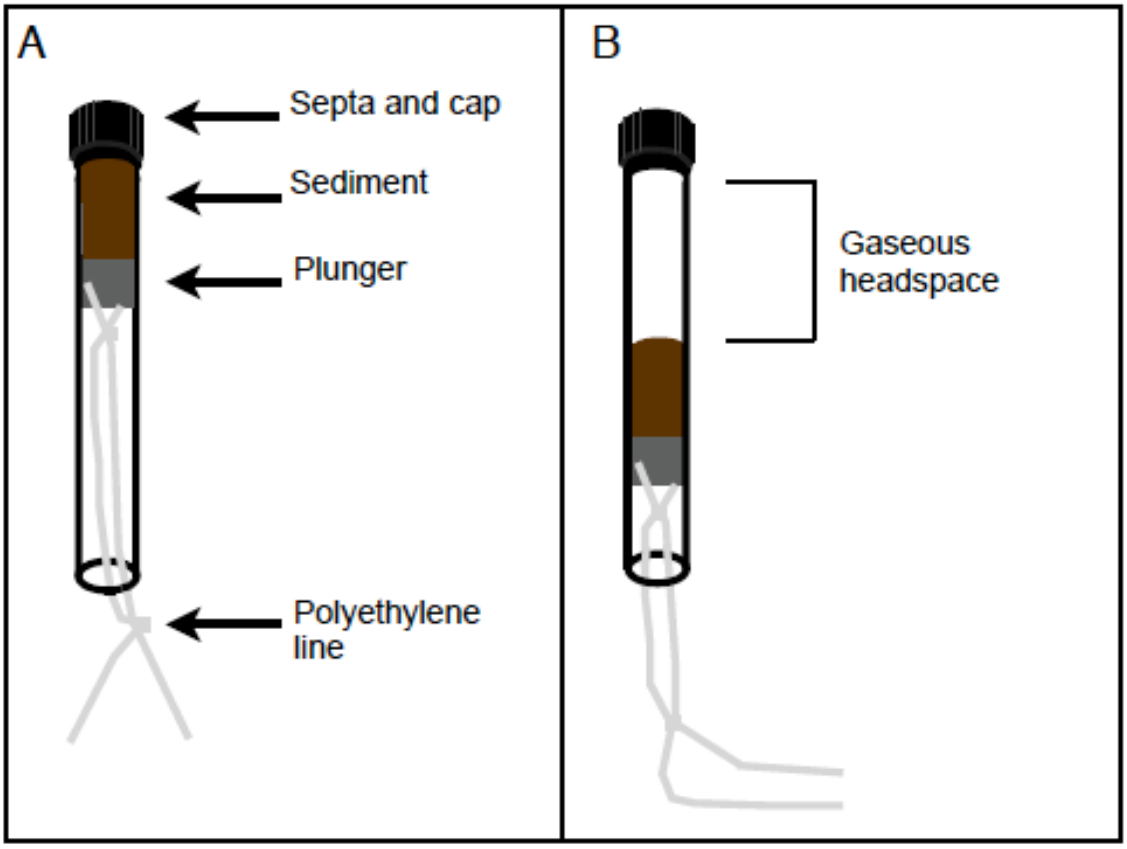
A
Septa and cap
Sediment
Plunger
Polyethylene line
B
Gaseous headspace

Figure 3.3.

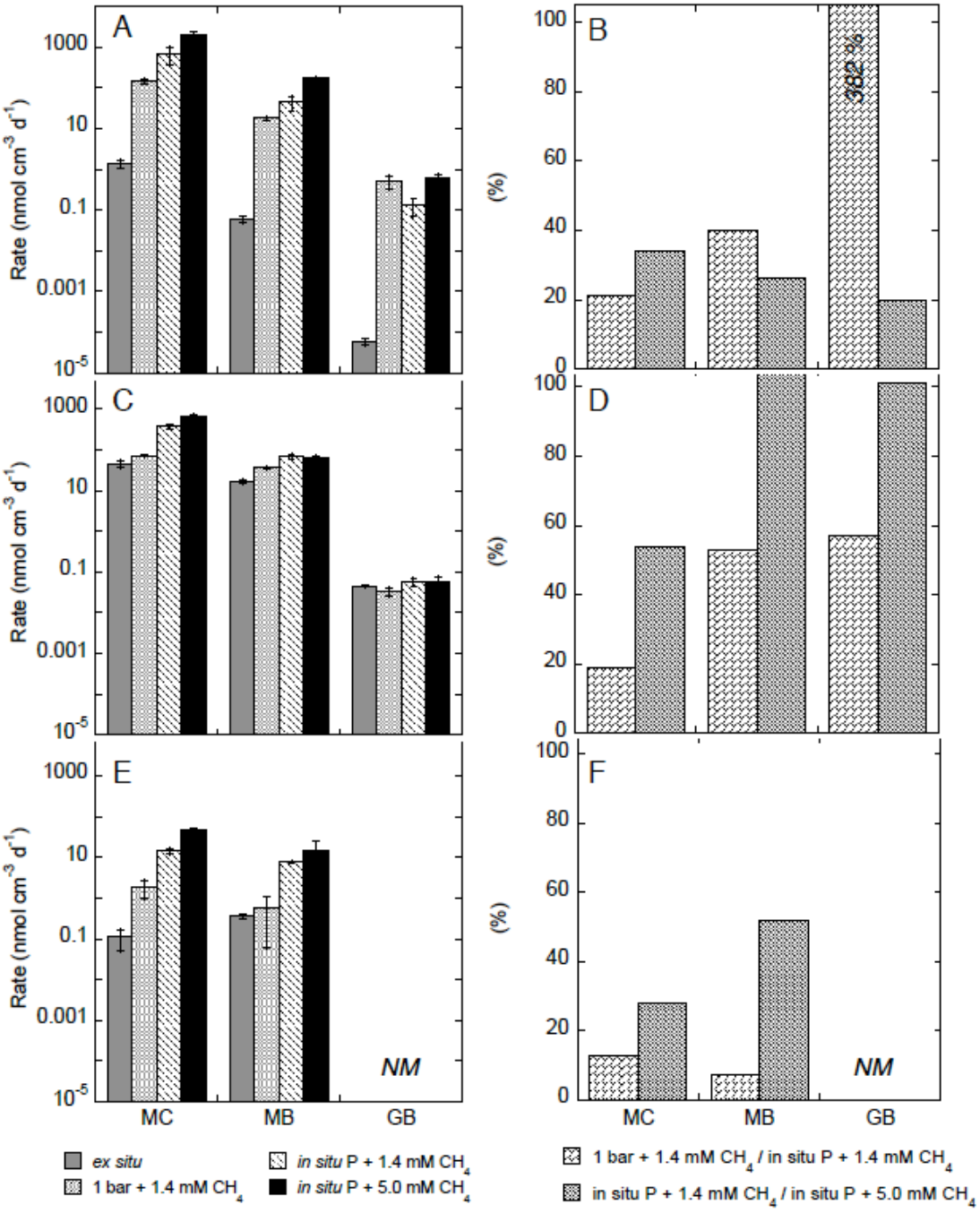
A
B
C
D
E
F
Rate (nmol cm-3 d-1)
(%)
1000
10
0.1
0.001
10-5
100
80
60
40
20
0
382 %
NM
MC
MB
GB
ex situ
1 bar + 1.4 mM CH4
in situ P + 1.4 mM CH4
in situ P + 5.0 mM CH4
1 bar + 1.4 mM CH4 / in situ P + 1.4 mM CH4
in situ P + 1.4 mM CH4 / in situ P + 5.0 mM CH4

References

Alperin, M. J., W.S. Reeburgh, and M.J. Whiticar, 1988. Carbon And Hydrogen Isotope Fractionation Resulting From Anaerobic Methane Oxidation. *Global Biogeochem. Cycles* **2**, 279-288.

Arvidson, R. S., J.W. Morse, and S.B. Joye. 2004. The sulfur biogeochemistry of chemosynthetic cold seep communities, Gulf of Mexico, USA. *Mar. Chem.* **87**, 97-119.

Boetius, A., K. Ravenschlag, C.J. Schubert, D. Rickert, F. Widdel, and A. Gieseke, 2000. A marine microbial consortium apparently mediating anaerobic oxidation of methane. *Nature* **407**, 623-626.

Bowles, M.W., Samarkin, V.A., Bowles, K.M., and Joye, S.B., 2011. Weak coupling between sulfate reduction and the anaerobic oxidation of methane in methane-rich seafloor sediments in *ex situ* incubations. *Geochim. Cosmochim. Acta.* **75**, 500-519, doi:10.1016/j.gca.2010.09.043.

Bowles, M.W., V.A. Samarkin, Teske, A., Girguis, P.R., Joye, S.B. (submitted) Dissolved methane - not sulfate - governs methane cycling in deep-ocean sediments.

Canfield, D. E., R. Raiswell, J.T. Westrich, C.M. Reaves, and R.A. Berner, 1986. The Use of Chromium Reduction in the Analysis of Reduced Inorganic Sulfur in Sediments and Shales. *Chem. Geol.* **54**, 149-155.

Duan Z.H. and S.D. Mao, 2006. A thermodynamic model for calculating methane solubility, density and gas phase composition of methane-bearing aqueous fluids from 273 to 523 K and from 1 to 2000 bar. *Geochim. Cosmochim. Acta.* **70**(13), 3369-3386.

Fossing, H. and B.B. Jørgensen, 1989. Measurement of bacterial sulfate reduction in sediments: Evaluation of a single-step chromium reduction method. *Biogeochem*. **8**, 205-222.

Jannasch, H.W. and C.D. Taylor, 1984. Deep-sea Microbiology. *Ann. Rev. Microbiol.* **38**, 487-513.

Jørgensen, B. B. 1989. A comparison of methods for the quantification of bacterial sulfate reduction in coastal marine sediments: II. Calculation from mathematical models. *Geomicrobiol. J.* **1**(1), 29-47.

Joye, S. B., A. Boetius, B.N. Orcutt, J.P. Montoya, H.N. Schulz, M.J. Erickson, and S.K. Lugo, 2004. The anaerobic oxidation of methane and sulfate reduction in sediments from Gulf of Mexico cold seeps. *Chem. Geol.* **205**, 219-238.

Joye, S.B., V.A. Samarkin, B.N. Orcutt, I.R. MacDonald, K.-U. Hinrichs, M. Elvert, A.P. Teske, K.G. Lloyd, M.A. Lever, J.P. Montoya, and C.D. Meile, 2009. Metabolic variability in seafloor brines revealed by carbon and sulphur dynamics. *Nat. Geosci.* **2**, 349-354.

Joye, S.B., M.W. Bowles, V.A. Samarkin, K.S. Hunter and H. Niemann, 2010. Biogeochemical signatures and microbial activity of different cold seep habitats along the Gulf of Mexico lower slope. *Deep Sea Research I, in press*.

Kim, S.-J. and C. Kato, 2010. 40 Sampling, Isolation, Cultivation, and Characterization of Piezophilic Microbes. *In* K.N. Timmis ed., Handbook of Hydrocarbon and Lipid Microbiology. Berlin: Springer-Verlag, p. 3869-3881.

Knab, N.J., B.A. Cragg, E.R.C. Hornibrook, L. Holmkvist, R.D. Pancost, C. Borowski, R.J. Parkes, and B.B. Jørgensen, 2009. Regulation of anaerobic methane oxidation in sediments of the Black Sea. *Biogeosci.* **6**, 1505-1518.

Krzycki, J.A., W.R. Kenealy, M.J. DeNiro, and J.G. Zeikus. 1987. Stable Carbon Isotope Fractionation by *Methanosarcina barkeri* during methanogenesis from Acetate, Methanol, or Carbon Dioxide-Hydrogen. *Appl. Environ. Microbiol.* **53**(10), 2597-2599.

Harder, J., 1997. Anaerobic methane oxidation by bacteria employing ^{14}C-methane uncontaminated with ^{14}C-carbon monoxide. Mar. Geol. **137**(1-2), 13-23.

Hoehler, T.M., M.J. Alperin, D.B. Albert, and C.S. Martens. 1994. Field and laboratory studies of methane oxidation in an anoxic marine sediment: evidence for a methanogen-sulfate reducer consortium. *Global Biogeochem. Cycles* **8**, 451-463.

Lapham, L. L., J.P. Chanton, C.S. Martens, P.D. Higley, H.W. Jannasch, and J.R. Woolsey, 2008. Measuring Temporal Variability in Pore-Fluid Chemistry To Assess Gas Hydrate Stability: Development of a Continuous Pore-Fluid Array. *Environ. Sci. Technol.* **42**(19), 7368-7373.

Meulepas, R.J.W., C.G. Jagersma, Y. Zhang, M. Petrillo, H. Cai, C.J.N. Buisman, A.J.M. Stams, and P.N.L. Lens, 2010. Trace methane oxidation and the methane dependency of sulfate reduction in anaerobic granular sludge. *FEMS Microbial Ecol.* **72**, 261-271.

Nauhaus, K., A. Boetius, M. Kruger, and F. Widdel, 2002. *In vitro* demonstration anaerobic oxidation of methane oxidation coupled to sulfate reduction in sediment from a marine gas hydrate area. *Environ. Microbiol.* **4**(5), 296-305.

Omoregie, E.O., H. Niemann, V. Mastalerz, G.J. de Lange, A. Stadnitskaia, J. Mascle, J-P., Foucher, and A. Boetius, 2009. Microbial methane oxidation and sulfate reduction in cold seeps of the deep Eastern Mediterranean Sea. *Mar. Geol.* 261(1-4), 114-127.

Orcutt, B., M. Elvert, V.A. Samarkin, and S.B. Joye, 2005. Molecular biogeochemistry of sulfate reduction, methanogenesis, and the anaerobic oxidation of methane at Gulf of Mexico cold seeps. *Geochim. Cosmochim. Acta.* **69**(17), 4267-4281.

Reidinger, N., B. Brunner, Y.-S. Lin, A. Vossmeyer, T.G. Ferdelman, and B.B. Jørgensen, 2010. Methane at the sediment-water transition in Black Sea sediments. *Chem. Geol.* 274(1-2), 29-37.

Wankel, S.D., S.B. Joye, V.A. Samarkin, S. Shah, G. Friderich, J. Melas-Kryiazi, and P.R. Girguis, 2010. New constraints of diffusive methane fluxes and rates of anaerobic methane oxidation in a Gulf of Mexico brine pool through the use of a deep sea *in situ* mass spectrometer. *Deep Sea Research I, in press.*

Weber, A., W. Riess, F. Wenzhoefer, and B.B. Jørgensen, 2001. Sulfate reduction in Black Sea sediments: in situ and laboratory radiotracer measurements from the shelf to 2000m depth. *Deep-Sea Research I* **48**, 2073-2096.

Welhan, J.A., 1988. Origins of methane in hydrothermal systems. *Chem. Geol.* **71**, 183-198.

Zhang, X., P.M. Walz, W.J. Kirkwood, K.C. Hester, W. Ussler, E.T. Peltzer, and P.G. Brewer, 2009. Development and deployment of a deep-sea Raman probe for measurement of pore water geochemistry. *Deep Sea Research I* **57**, 297-306.

CHAPTER 4

DISSOLVED METHANE-NOT SULFATE-GOVERNS METHANE CYCLING IN DEEP OCEAN SEDIMENTS[1]

[1] Bowles, M.W., Samarkin, V.A., Teske, A., Girguis, P., and S.B. Joye, in preparation, 2011.

Abstract

We measured rates of anaerobic oxidation of methane (AOM), sulfate reduction (SR), and bicarbonate-based methanogenesis (MOG) at various elevated methane concentrations in cold seep and hydrothermally altered sediments at *in situ* pressures. In addition we measured particulate organic carbon (POC) formation rates as a proxy for methane and separately bicarbonate assimilation, termed mPOC and bPOC for methane and bicarbonate derived POC. In general, rates of AOM, SR, and MOG all increased as additional methane was added to sediments. In all sediments analyzed AOM was decoupled from SR as methane concentrations increased, at times becoming 10 times greater than SR. Rates of bPOC typically exceeded mPOC formation, and bPOC typically occurred on the same magnitude as MOG. Together these findings suggest that anaerobic methanotrophs are predominantly supported by carbon assimilated from bicarbonate. The broader impacts of these findings suggest that novel mechanisms, or pathways, for methane oxidation exist in marine sediments. To clarify these mechanisms we measured the formation of volatile organics (e.g. acetate) and additionally postulate the release of hydrogen during AOM to support such elevated rates and stimulation of multiple processes like SR and MOG. In the contemporary ocean, AOM rates exceeding SR rates and high rates of POC formation suggest significant oversights in carbon budgeting at cold seeps and hydrothermal vents. During low sulfate ancient oceans (i.e. Proterozoic) methane oxidation might have been more pronounced than originally thought.

1. Introduction

Biogeochemists have long attempted to relate microbial activity to geochemical parameters, and likewise link the products of microbial activity to environmental signatures (Vernadsky, 1926). Sophisticated analytical methods permit microbial activity assessments in a range of environments; however, quantifying microbial activity in deep-sea sediments, one of the planet's largest ecosystems, and gas-rich continental margin sediments, remains a challenge (Jorgensen, 2006).

To evaluate rates of elemental cycling in these habitats, cores of sediment are collected at the seafloor, returned to the research vessel, and manipulated and most often subjected to rate assay experiments, at surface pressure (~1 bar). Depressurization and incubation at surface pressure imparts a significant potential artifact as pressure can exert a positive (de Angelis et al., 1991, Kallmeyer and Boetius, 2004) or negative (Parkes et al., 1995) affect on microbial activity. Furthermore, the energetics of processes involving dissolved gases as substrates or products change due to the impact of pressure on gas solubility. For example, methane concentrations at surface pressure (~1 mM) are 10 to 100's of times lower than potential *in situ* concentrations, depending on the depth and habitat (Duan and Mao, 2006). Realistic constraints on methane sources and sinks in nature, a potent greenhouse gas that is increasing in concentration in the atmosphere (Whitman et al., 2006), are paramount for determining or predicting climate models of the past and of the future. No previous studies have examined the impact of methane concentration on the suite of microbial processes that are potentially sensitive to this variable.

To evaluate the impact of pressure versus methane concentration on rates of sulfate reduction (SR) and anaerobic oxidation of methane (AOM), we measured rates at a low methane concentration (1.4 mM) and atmospheric (1 bar) pressure, low methane concentration and *in situ* (100 bar) pressure, and over a range of pressures (10-100 bar) at a constant high methane concentration (10 mM) in Gulf of Mexico (GoM) cold seep sediments (see Supplemental Methods). SR and AOM rates were significantly higher at 100 bar compared to 1 bar (ANOVA, $\alpha = 0.05$: SR $p = 0.0002$, AOM $p = 0.04$; Fig. 1A). At pressures greater than 25 bar SR and AOM rates did not increase significantly (ANOVA, $\alpha = 0.05$: SR $p = 0.51$, AOM $p = 0.26$; Fig. 1B) at a constant methane concentration.

2. Methane Concentration Affects a Multitude of Processes

At three sites, the Gulf of Mexico (GoM), Guaymas Basin (GB), and Monterey Bay (MB) (see Supplemental Information for details), we measured rates of SR, AOM, bicarbonate based methanogenesis (MOG) (Fig. 2), and microbial assimilation of carbon derived from methane (hereafter mPOC for methane derived particulate organic carbon) or bicarbonate (hereafter bPOC for bicarbonate derived particulate organic carbon) at *in situ* pressure and over a range of methane concentrations (Figs. 2,3). All sediments analyzed were anoxic within millimeters of the sediment water interface, and the experiments reported here were carried out under anoxic conditions. GoM and GB sediments were gaseous and contained visible oil, while MB sediment was only gaseous. Sediment from GoM and MB was collected at 1000 m depth, while GB sediment was collected at 2000 m. At elevated methane concentrations, rates and patterns of microbial

metabolism and carbon assimilation into biomass differed dramatically from those observed at the low methane concentrations (~1 mM) typical of incubations at 1 bar.

The rate of AOM has not been assayed directly in marine sediments at elevated methane concentration and *in situ* pressure; previously SR rates were used as a proxy for AOM rates at high pressure (Nauhaus et al., 2002). Increased methane concentrations should increase AOM rates, as higher methane concentrations make the reaction more energetically favorable. Rates of AOM displayed a Michaelis-Menten response to methane concentration. *In situ* incubations at GOM and GB generated the highest absolute rates at 4.8 (±0.4) and 3.6 (±0.3) μmol cm^{-3} d^{-1} and estimated V_{max} at 5.7 (S.E. = 0.1) and 5.0 (S.E. = 0.7) μmol cm^{-3} d^{-1}, respectively (Fig. 2A). Rate observations at GOM and GB were similar in magnitude. The V_{max} at MB, 280 nmol cm^{-3} d^{-1} (S.E. = 23 nmol cm^{-3} d^{-1}) was significantly lower than observations at GOM and GB. The estimated K_s, or half-saturation constant of anaerobic methanotrophs, ranged from 4 to 18 mM CH_4, which exceeds by far the saturated methane concentration at 1 bar (~1 mM). The range of K_s observed across these sites is comparable to a previous estimate of 10 mM, where AOM rates were estimated from SR rates (Nauhaus et al., 2002, 9 Scheller et al., 2010).

Rates of both SR and MOG exhibited a strong kinetic response to methane concentration in GoM and GB sediments, suggesting a dependency on methane concentration, possibly through AOM via either direct reaction coupling or consumption of a metabolic by-product. SR rates increased up to 1305 (±53) and 681 (±37) nmol cm^{-3} d^{-1} at GoM and GB with respective V_{max} values of 1414 and 850 nmol cm^{-3} d^{-1} (SE = 77 and 81 nmol cm^{-3} d^{-1}), respectively. Surprisingly, SR rates were significantly lower than AOM rates (Fig. 2A,B). At MB, in contrast, SR rates were much lower (16 to 96 nmol

cm^{-3} d^{-1}) and were insensitive to methane concentration. For methane production, MOG rates increased with increasing methane concentration in GoM and GB, with maximum rates of 265 (±35) and 108 (±32) nmol cm^{-3} d^{-1}, respectively (Fig. 2C). At MB, MOG rates did not increase with methane concentration and were much lower, ranging between 0.3 and 14 nmol cm^{-3} d^{-1}. Generally rates of SR and MOG at MB were insensitive to increases in methane concentration, which strongly contrasted with the positive correlation of SR and MOG rates observed within GB and GoM sediments.

Previous quantification of SR rates at elevated methane concentration in sediment slurries showed stimulation of SR (Scheller et al., 2010, Meulepas et al., 2010). In cold seep sediments (Scheller et al., 2010), SR rates increased by a factor of five as methane concentration increased from 1.4 to 15.8 mM. Over a similar range (1.4 to 10 mM), we observed a 2 and 3 times increase in SR rates at GoM and GB, respectively. However we observed a 3.5 and 4 times increase when methane concentrations were 50 mM, relative to rates at concentrations of 1.4 mM methane at GoM and GB, respectively.

In addition to the stimulation of dissimilatory and/or fermentative processes, methane concentration increased the formation of mPOC at all sites. In GoM sediments the maximum mPOC formation rate was 28.5 nmol cm^{-3} d^{-1} (at 50 mM methane; Fig. 3A). Slightly more mPOC was formed in sediments from GB and MB, at an average maximum rate of 44 nmol cm^{-3} d^{-1} (50 mM methane). The fraction of mPOC formed relative to the AOM rate was lower at GoM and GB, relative to MB. In GoM sediment, mPOC was typically less than 0.6% of AOM rates, and in general did not increase with methane concentration (Supplementary Fig. 1). At GB mPOC reached as much as 1.2% of the AOM rate, and increased slightly with respect to methane concentration. In MB

sediments, a much larger fraction (up to 17%) of mPOC relative to AOM rate was observed. The lower proportion of mPOC formation relative to AOM at GoM and GB relative to MB might indicate different methane oxidation pathways or communities of methanotrophs.

The formation rate of bPOC was almost always higher than that of mPOC (Fig. 3B). The bPOC formation rate was positively related to methane concentration in GoM and GB sediments, but negatively correlated at MB, again suggesting fundamental differences in regulation of carbon flow at these sites. At GoM and GB, the rates of bPOC increased to 125 (±14) and 80.5 (±4) nmol cm^{-3} d^{-1}, respectively. The maximum bPOC rate determined at MB was 40 (±5) nmol cm^{-3} d^{-1}, and decreased to a constant rate of ~12 nmol cm^{-3} d^{-1} at >5 mM methane. The rate of bPOC formation exceeded the MOG rate by a factor of two at low (1.4 mM) methane concentrations at all sites (Supplementary Fig. 2).

Trends in sources and rates of biomass carbon incorporation along with process rate data can be used to tease apart the relative importance of carbon assimilation pathways in high methane concentration environments. Bicarbonate was by far the most important source of carbon assimilated into microbial biomass (Fig.3C). The rate of bPOC production at GoM and GB exceeded mPOC production at all methane concentrations. Bicarbonate assimilation can be attributed to a number of microorganisms, including autotrophic sulfate reducers (Rabus et al., 2006) and also anaerobic methanotrophs, through DIC-reducing enzymes shared with methanogens (Wegener et al., 2008). We doubt this represents DIC assimilation by methanogens because bPOC rates are comparable to or exceed those of Bi-MOG. Positive correlations

between mPOC formation and AOM rates in GoM and GB sediments could suggest methane assimilation by methanotrophic communities. Much higher relative proportions of mPOC and AOM at MB indicate either a different methanotrophic community with different physiology or one in another growth phase.

Putative anaerobic methanotrophs are theorized to assimilate methane into their biomass, i.e. form mPOC (Wegener et al., 2008, Hinrichs et al., 1999, Orphan et al., 2001). To date methane assimilation into biomass has been examined through stable-isotopic studies of lipids (Wegener et al., 2008, Hinrichs et al., 1999, Orphan et al., 2001), but not typically quantified as mPOC. Stable isotope tracer studies have indicated that anaerobic methanotrophs assimilate CO_2 (Wegener et al., 2008). Those data - along with the data shown here - suggest that anaerobic methanotrophs control carbon assimilation observed as mPOC and bPOC. The most comparable data are from Black Sea mat samples where methane assimilation was about 1.6 ± 0.6 % of the AOM rate (Treude et al., 2007), percentages that are similar to our observations in GoM and GB. In the same experiments, assimilation of DIC corresponds to approximately 10% of the AOM rate (Treude et al., 2007), congruent with our results supporting higher C assimilation rates with DIC than with CH_4.

3. AOM and biogeochemical teleconnections

In marine sediments, AOM has been linked to a syntrophic partnership of sulfate reducing bacteria and methane oxidizing archaea (Hinrichs et al., 1999, Orphan et al., 2001, Hoehler et al., 1994, Boetius et al., 2000). This reaction should generate a 1:1 stoichiometry between sulfate reduced and methane oxidized (Eq. 1).

$$CH_4 + SO_4^{2-} \rightarrow HCO_3^- + HS^- + H_2O \qquad \text{(Eq. 1)}$$

While some studies have documented the predicted 1:1 ratio, others have documented elevated rates of SR relative to AOM (Joye et al., 2004, Orcutt et al., 2005). Such elevation of SR in the absence of AOM has been attributed to SR fueled by endogenous hydrocarbons and/or organic matter. In this study, we scarcely observed a 1:1 stoichiometry of SR and AOM. Only at the low methane concentrations typical of degassed cores were SR and AOM rates observed to be coupled 1:1. At high methane concentration (50 mM), AOM rates were significantly (paired Student's t-test; $\alpha = 0.05$, $p = 0.002$) higher than SR rates, exceeding SR by as much as 5.5 times (Fig. 4). (To match the text, Figure 4 could be plotted AOM:SR, instead of SR:AOM) Yes, that should be done.

The AOM rates increased consistently with methane concentrations in the absence of a concomitant increase in SR (Figs. 2, 4). The independence of AOM from SR has fundamental implications for our understanding of AOM physiology in marine sediments. In sediments from GoM and GB, rates of AOM, SR, MOG, and POC formation responded positively to increased methane concentration (Figs. 2, 3). At GoM and GB, rates of SR were 10 to 40% of AOM rates, at methane concentrations equal to or greater than 1.4 mM. Thus, consumption of an AOM intermediate by sulfate reducing bacteria could only support a fraction of the observed AOM activity. This suggests an opportunistic relationship, rather than strict coupling of AOM and sulfate reducing bacteria, and multiple pathways of AOM.

The observed patterns of SR and MOG suggest simultaneous occurrence of these processes, which has been documented previously in the absence of substrate competition (Oremland et al., 1982). However, the pronounced increase in MOG rates as a function of

methane concentration was not anticipated, as higher methane concentration reduces the energy yield of MOG. One option is that increases in MOG rates are simply the result of a back reaction of AOM. In GoM and GB sediments MOG rates on average were 1 and 4% of AOM rates, respectively. The extent of AOM back reaction is unknown, but trace methane oxidation by methanogens was found to at most reach approximately 0.4% of the methane produced (Zehnder and Brock, 1979, Moran et al., 2005). Alternatively, increases in SR and MOG with elevated methane concentrations could result from consumption of a by-product(s) of AOM that stimulates both SR and MOG. The release of H_2, which has been implicated in the process of methane oxidation, could fuel SR and/or MOG or release of a labile carbon substrate could stimulate SR.

4. Potential intermediates of anaerobic methane cycling

The potential and necessity for release of multiple AOM intermediate(s) was not apparent in previous 1 bar rate assays, because AOM rates were typically equal to or much less than SR rates (Bowles et al., 2011). Through incubation at *in situ* pressure, elevated methane concentrations, and non-limiting sulfate concentration, we discovered an additional mechanism of AOM, most likely a simple carbon shuttle, such as acetate. The labile carbon shuttle can be oxidized to bicarbonate by numerous microorganisms. In a mixed microbial community, acetate production can be a function of methane concentration, suggesting such a link between methane and acetate formation (Schilov et al, 1999).

We measured production of volatile organics as a proxy for acetate production to investigate the potential for organic intermediate from methane in GoM sediments at *in situ* pressure and 10 mM methane (see Supplemental Methods for details). We measured

homoacetogenesis, MOG, AOM, and acetate production from methane. The net production of volatile organics from methane was low, 0.79 (±0.19) nmol cm^{-3} d^{-1}, but accumulation shows that radiolabeled carbon intermediates are produced during AOM and such substrates could support processes such as SR or acetoclastic MOG for example.

5. Implications for carbon cycling in contemporary and ancient sediments

Most previous analyses of microbial processes in deep-ocean sediments were not reflective of *in situ* pressure or methane concentration (Joye et al., 2004, Orcutt et al., 2005, Bowles et al., 2011, Omoregie et al, 2009). The classic studies that established a relationship between SR and AOM (Reeburgh and Heggie, 1977, Iversen and Blackburn, 1981, Devol, 1983, Iversen and Jorgensen, 1985), and later work reporting a 1:1 stoichiometry (Boetius et al., 2000) between these processes did not explicitly evaluate the potential impacts of methane concentration on AOM rates or coupling of AOM to other processes. At high methane concentration rates of microbial activity and microbial carbon cycling were dramatically different. The discovery of higher AOM rates than can be predicted by SR, the potential for multiple by-products of AOM, and rapid POC production rates have implications for carbon cycling in the contemporary and ancient ocean. In particular, the methane concentration and pressure effects and the absence of a 1:1 stoichiometry between CH_4 and SO_4 consumption makes it impossible to use sulfate profiles as proxy for CH_4 cycling, and means that prior studies that estimated AOM rates relying on SR profiles or SR rates (Hinrichs and Boetius, 2002), or *ex situ* incubations (Bowles et al., 2011, and references therein), have grossly underestimated AOM rates.

The sulfate-free mechanism of AOM reported here provides a pathway for AOM in ancient low sulfate oceans. In the anoxic Proterozoic ocean, sulfate concentrations were much lower than in the contemporary ocean (Shen et al., 2003) and atmospheric methane concentrations were higher (Kasting, 2005). The pathway outlined here (Fig. 5) would supply the water column and sediments with energy-rich intermediate, supporting a dynamic and metabolically diverse microbial community in the ancient ocean. In the Proterozoic substantial hydrogen release is thought to have occurred, but was thought to be dominated by photolysis (Catling et al., 2001) and production in bacterial mats (Hoehler et al., 2001). Since hydrogen generation and subsequent conversion of methane to bicarbonate would lower the apparent greenhouse effect during the Proterozoic, sulfate-free AOM could play a role as a microbial trigger impacting Proterozoic climate-atmosphere feedbacks.

6. Conclusion

We document a strong impact of pressure on rates of anaerobic methane oxidation, which challenges past assessments of methane dynamics in marine sediments at potentially shallow water depths (<500m). The observed effect can largely be attributed to the effect of pressure on substrate concentration, and to lesser extent on impact of pressure on microbial metabolic function. The observed impact of in situ conditions on methane oxidation rates has significant implications on C dynamics in the seabed, and will require a systematic evaluation of the in-situ biological and biogeochemical consequences of highly concentrated methane sources.

Our data shows a clear decoupling between C and S cycling during AOM. Hence, not only does it affect our estimates of the contemporary carbon cycle, but it provides a pathway of SR independent AOM that would have been important in the Geologic past as it could have affected ancient microbial carbon cycling, and could have lowered the greenhouse gas warming potential of the atmosphere. Finally, biomass production from bicarbonate and methane in methanotrophic communities are substantial, suggesting that *in situ* measurements are critical to understanding the success of microbes in the deep subsurface, the planet's largest ecosystem.

7. Supplementary Methods

7.1. Sample Description, Treatment, and Collection

The sample suite was collected on separate cruises by remote operated vehicles (ROVs) and a manned deep submergence vehicle (DSV), with sample collections occurring through the Spring and Fall of 2009. Samples were stored at *in situ* temperature until sample manipulation. All samples were collected in sediments containing bacterial mats, as they represent signs of abundant methane flux, or active seepage. Sediments were maintained intact in the core liners with core caps securely fitted on the top and bottom. Sediments from Gulf of Mexico Mississippi Canyon and Monterey Bay were collected during ROV operations, and transported back to UGA, where the experiments were carried out. Samples collected from the Gulf of California at Guaymas Basin and Gulf of Mexico at Green Canyon were collected by the DSV Alvin in the Falls of 2009 and 2010, respectively.

At the laboratory the upper 9 cm of sediment was sampled, and placed in a bottle sealed with a butyl rubber stopper. Next the headspace was purged with Ar, and sediment was homogenized. After homogenization the sediment was sampled under a gentle stream of Ar, by filling modified hungate tubes. For a detailed description of the sampling vessel and outline of the procedure see Bowles and coauthors (submitted). Briefly, the hungate tubes were modified in that they were cut at the base and have a retractable butyl rubber stopper (hereafter termed plunger) in the bottom allowing for expansion during gas amendment and likewise compression during pressurization. Sample tubes were then sealed with no headspace by a butyl rubber septa.

7.2. Methane and Radiotracer Amendment

After samples were collected in modified hungate tubes the first step was to add methane to the sample. Using the ideal gas law, for the salinity and temperature of the sample, we determined the desired amount of 100% ultra high purity methane to add to the sample as a headspace. The methane was added using a syringe and needle and gently pulling the retractable plunger to evacuate the syringe contents into the modified hungate tube. After amendment with methane the respective radio-isotope was added to each sample. The specific activities and sampling details are described in Bowles et al., *submitted*. Briefly, for individual treatments samples were collected in triplicate plus one control for each type of rate measurement and respective methane concentration treatment. For sulfate reduction 100 µL of high specific activity $Na_2{}^{35}SO_4$ dissolved in slightly alkaline deionized H_2O (pH ~ 9.4; 400 kBq) was added to samples. Anaerobic oxidation of methane samples and controls were injected with 100 µL of purified gaseous

$^{14}CH_4$ (133 kBq). Herder (1997) describe the purification procedure using Hopcalite and activated carbon employed. Gaseous methane tracer was dissolved in scintillation cocktail sealed by a butyl rubber stopper and counted prior to injecting samples to verify the activity injected. Bicarbonate reduction to methane was used to assess methanogenesis in sediment slurries, by adding 100 µL of $NaH^{14}CO_3$ dissolved in slightly alkaline deionized H_2O (pH ~ 9.4; 350 kBq). Prior to addition of radiotracer, control samples were injected with 3 mL of 20% (w/v) zinc acetate or 2 N NaOH, for sulfate reduction and anaerobic oxidation of methane or methanogenesis, respectively.

7.3. Incubation Specifications, Sample Processing, and Rate Calculations

All samples were incubated at *in situ* temperature (~5°C) and pressure (GoM and MB: 100 bar, GB: 200 bar) for 24 hours. Pressure was applied as described previously (Bowles et al., submitted). After the incubation activity was halted by addition of the respective killing solution for each process. SR and AOM samples were immediately transferred into 50 mL centrifuge tubes with 10 mL of additional killing solution. AOM samples were processed within 2 days of the termination of the experiment, while SR samples were frozen and processed within 1 week. MOG samples were stored with a negative pressure in order to avoid the possibility for radioactive methane to escape, and were processed within one week after the termination of the experiment. SR samples were processed in a one-step acidic chromium reduction, with methods and calculations described by Joye et al., 2004. AOM samples were processed in an passive acidic distillation and rates determined as described by Bowles et al., 2011. Radioactive methane

generated during MOG was quantitatively converted to CO_2 within a heated copper catalyst column, as described in Orcutt et al., 2005.

7.4. Particulate Organic Carbon Formation Experiments

To determine particular organic carbon formation rates from bicarbonate and methane (bPOC and mPOC, respectively) subsamples were taken from the MOG and AOM samples, respectively. After radioactive methane was purged from the MOG sample, the samples were emptied into 50 mL centrifuge tubes and acidified (pH~1) by adding 5 mL of 50% (v/v) concentrated phosphoric acid. After adding phosphoric acid the sample was shaken vigorously to remove most $^{14}CO_2$ evolved from $H^{14}CO_3^-$ initially injected into the sample. After initial shaking the sample was purged with compressed air for one hour to ensure all trace $^{14}CO_2$ was removed. Following the purging of the sample a small subsample (200 μL) was taken from the centrifuge tube immediately after it was shaken. The subsample was placed in a 20 mL scintillation vial, and scintillation cocktail was added and the sample counted. The DPM found in this aliquot represents the $bPO^{14}C$ formed during the experiment. The bPOC formation rate was next estimated by the calculation (equation 1):

$$bPOC = [DIC] \text{ X } (a\text{-}bPO^{14}C_{live\ sample} - a\text{-}bPO^{14}C_{control}/a\text{-}H^{14}CO_3^-{}_{injected}) \text{ X } 1/t \qquad \text{(eq. 1)}$$

where bPOC is the bPOC formation rate (nmol cm^{-3} d^{-1}), [DIC] is the concentration of dissolved inorganic carbon (nmol cm^{-3} wet sediment), $a\text{-}bPO^{14}C_{live\ sample}$ is the activity (DPM) of the live sample, $a\text{-}bPO^{14}C_{control}$ is the activity (DPM) of the control sample, $a\text{-}H^{14}CO_3^-{}_{injected}$ is the activity (DPM) of the bicarbonate that was initially injected, and t is

the time of the incubation (d). No isotopic discrimination term was added to the calculation (α), as this is unknown for POC formation from bicarbonate.

The rate of mPOC formation was determined similarly. After AOM samples were transferred to 50 mL centrifuge tubes, they were shaken, and a 1 mL aliquot was removed and dispensed into a 20 mL scintillation vial. Next 100 µL of 50% (v/v) concentrated phosphoric acid was added to the sample and then mixed vigorously. The sample was then left open for 24 hours to allow all $^{14}CO_2$ evolved during AOM to be removed from the sample. Next samples were neutralized by adding 9 N NaOH (typically ~200 µL) until pH was approximately 7. To improve counting efficiency we added 500 µL of methanol to the sample, then immediately added scintillation cocktail. The DPM determined from this subsample represents the $mPO^{14}C$ formed during the experiment. The mPOC formation rate was next estimated by the calculation (equation 2):

$$mPOC = [CH_4] \text{ X } (a\text{-}mPO^{14}C_{live\ sample} - a\text{-}mPO^{14}C_{control}/a\text{-}^{14}CH_{4injected}) \text{ X } 1/t \qquad \text{(eq. 2)}$$

where mPOC is the mPOC formation rate (nmol cm^{-3} d^{-1}), $[CH_4]$ is the concentration of methane (nmol cm^{-3} wet sediment), a- $mPO^{14}C_{live\ sample}$ is the activity (DPM) of the live sample, a- $mPO^{14}C_{control}$ is the activity (DPM) of the control sample, a-$^{14}CH_{4injected}$ is the activity (DPM) of the methane that was initially injected, and t is the time of the incubation (d). No isotopic discrimination term was added to the calculation (α), as this is unknown for POC formation from methane. All POC formation rate measurements were triplicated with one control per treatment, or methane concentration.

7.5 Geochemistry

In order to calculate rates we determined substrate levels for CH_4, SO_4^{2-}, and DIC. Methane concentrations were determined using wet sediment, while a 10 mL sediment sample was centrifuged to collect interstitial water for sulfate and DIC analysis. Sulfate concentrations were determined on an ion chromatograph (IC) as previously described by Joye et al., 2004. Methane and DIC concentrations were determined using a gas chromatograph equipped with a flame ionization detector (GC-FID). Methane sample collection and treatment was carried out as previously described by Joye et al., 2004. Methane concentrations were determined for the sediment prior to the application of additional methane gas, so that the total methane concentration could be better estimated. The concentration of DIC was determined by acidification of porewater to pH~1 in a headspace vial, CO_2 was quantitatively converted into methane by a nickel catalyst and the methane was measured by GC-FID (Bowles et al., submitted). The CO_2 was quantified using a 1% CO_2 standard.

7.6. Pressure Effect Experiment

To determine to what extent pressure impacted rates of microbial processes at an elevated methane concentrations we examined SR and AOM. We used sediment from GoM at a methane concentration of 10 mM, samples were incubated at 5°C for 24 hours, at a range of pressures. At the termination of the experiment SR and AOM rate samples were processed as described above. Sulfate and methane concentrations were determined as described in preceding sections.

7.7. Volatile Organics Formation Experiment

To estimate the rate volatile organic carbon formation we measured rates of AOM, MOG, and volatile organics from bicarbonate and methane we used sediments from GoM at 10 mM methane. Specifically, for volatile organics from methane samples were injected with $^{14}CH_4$ as a gaseous tracer (1,333 kBq) for a period of 4 days at *in situ* pressure and temperature. After incubation samples were transfered to 50 mL centrifuge tubes, 1 mL of 5% (w/v) zinc acetate was added to the sample, and the sample was then acidified and purged to remove $^{14}CO_2$. To determine volatile organic formation from bicarbonate samples were incubated with $NaH^{14}CO_3$ (350 kBq), purged of methane, transfered to 50 mL tubes where 1 mL of 5% (w/v) zinc acetate was added to the sample. Next the sample was acidified and purged to remove $^{14}CO_2$. After purging a soxhlet extraction was performed on each acidified fraction, and the DPM of the liquid phase was used as a proxy for volatile organic formation from methane or bicarbonate.

To calculate rates of volatile organic carbon formation we used equation 3:

$$VOC_{substrate} = [Substrate] \text{ X } (\text{a-VO}^{14}C_{live\ sample} - \text{a-VO}^{14}C_{control}/\text{a-Substrate}_{injected}) \text{ X } 1/t \quad \text{(eq. 3)}$$

where $VOC_{substrate}$ is theVOC formation rate (nmol cm^{-3} d^{-1}) from the substrate methane or bicarbonate, [Substrate] is the concentration of methane or bicarbonate (nmol cm^{-3} wet sediment), a-$VO^{14}C_{live\ sample}$ is the activity (DPM) of the live sample, a-$VO^{14}C_{control}$ is the activity (DPM) of the control sample, a-$Substrate_{injected}$ is the activity (DPM) of the methane or bicarbonate that was initially injected, and t is the time of the incubation (d). No isotopic discrimination term was added to the calculation (α), as this is unknown for

VOC formation from bicarbonate or methane. All VOC formation rate measurements were triplicated with one control. Rates of AOM, MOG, and bicarbonate derived VOC formation were used to more precisely estimate methane derived VOC formation.

7.8. Error Propagation and Statistical Analysis

For ratios of mPOC to bPOC, mPOC to AOM, and bPOC to MOG we propagated error involved in measurement of POC formation and microbial activity rates to calculate the error of the ratios. To determine propagate error we used equation 4:

$$\left(\frac{\sigma_r}{r}\right)^2 = \left(\frac{\sigma_A}{A}\right)^2 + \left(\frac{\sigma_B}{B}\right)^2 - 2\left(\frac{\sigma_A \sigma_B}{AB}\right)\rho_{AB} \qquad \text{(eq. 4)}$$

where A and B are the measurement used to formulate the ratio, r is the calculated ratio (A/B), σ_r is the propagated uncertainty, σ_A is the uncertainty of measurement A, σ_B is the uncertainty of measurement B, and ρ_{AB} is the coefficient of correlation used when A and B are not independent measurements. For determination of the error for GoM and GB sediments there was a relationship between all parameters used to formulate ratios. At MB there was no clear relationship between any parameters used to formulate ratios so ρ_{AB} becomes zero.

For all analysis of variance (ANOVA) measurements the statistics package of Excel was used. To estimate the Michaelis-Menten fit of the methane treatment experiment KaleidaGraph Version 4.0 was used.

Acknowledgements. We thank the 2009 Guaymas Basin Science party, the crew of the R/V *Atlantis* and the ALVIN, S. Wankel, and Carol Lutken for assistance in acquiring samples and the Gulf of Mexico Hydrate Research Consortium for providing logistical support and ship time. This research was supported by the NOAA National Institute for Undersea Science and Technology (award numbers 06-09-018, 07-10-028 and 08-10-031) and the National Science Foundation (OCE-0959337 to SBJ and OCE-0647633 to AT).

Figure 4.1. A) Comparison of rates of AOM and SR at 1.4 mM methane with and without pressure. **B)** Rate of AOM and SR (nmol cm^{-3} d^{-1}) versus pressure (bar) in GoM sediments supplied with 10 mM methane.

Figure 4.2. A) Rate of AOM, **B)** SR, and **C)** MOG (nmol cm^{-3} d^{-1}) versus methane concentration (mM) in GoM, GB, and MB sediments at *in situ* pressure. Michaelis-Menten equation fit is applied to AOM rates for all three sites. The R^2 values were all >0.96 for the respective Michaelis-Menten equation fits.

Figure 4.3. A) Production rate of mPOC, **B)** bPOC (nmol cm^{-3} d^{-1}), and **C)** fraction of mPOC per bPOC production rates versus methane concentration (mM) in GoM, GB, and MB sediments.

Figure 4.4. SR and AOM rate ratios, as SR:AOM, versus methane concentration (mM) compiled from MC, GB, and MB sediments. The gray shaded portion represents low methane concentrations typically experienced at all previous rate analysis.

Figure 4.5. Ratio of the rates of mPOC formation and AOM versus methane concentration (mM). Error bars represent propagated uncertainties for rate measurements.

Figure 4.6. Ratio of the rates of bPOC formation and MOG versus methane concentration (mM). Error bars represent propagated uncertainties for rate measurements.

Figure 4.1.

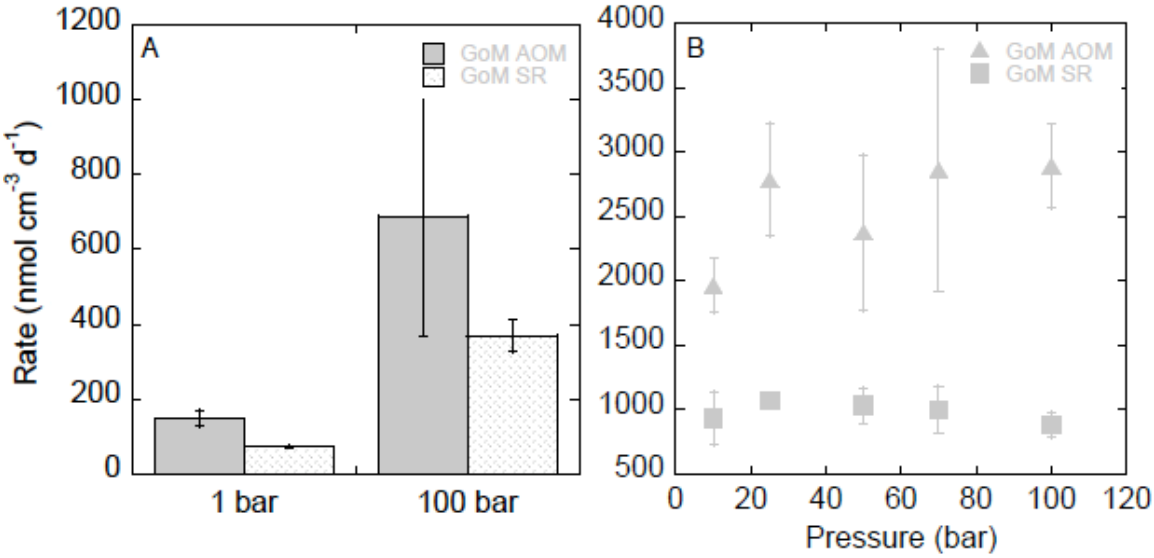
A
GoM AOM
GoM SR
Rate (nmol cm-3 d-1)
1200
1000
800
600
400
200
0
1 bar
100 bar
B
GoM AOM
GoM SR
4000
3500
3000
2500
2000
1500
1000
500
0
20
40
60
80
100
120
Pressure (bar)

Figure 4.2.

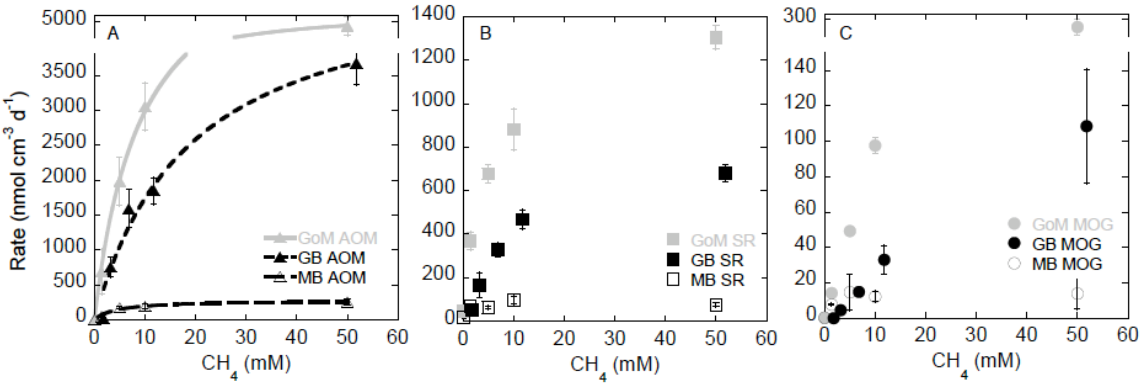
A
B
C
Rate (nmol cm-3 d-1)
CH4 (mM)
GoM AOM
GB AOM
MB AOM
GoM SR
GB SR
MB SR
GoM MOG
GB MOG
MB MOG

Figure 4.3.

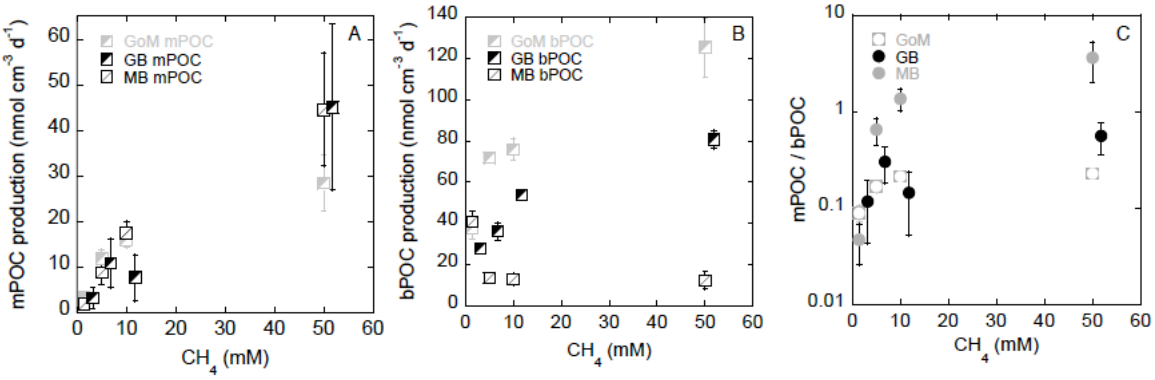
A
GoM mPOC
GB mPOC
MB mPOC
mPOC production (nmol cm-3 d-1)
CH4 (mM)
B
GoM bPOC
GB bPOC
MB bPOC
bPOC production (nmol cm-3 d-1)
CH4 (mM)
C
GoM
GB
MB
mPOC / bPOC
CH4 (mM)

Figure 4.4.

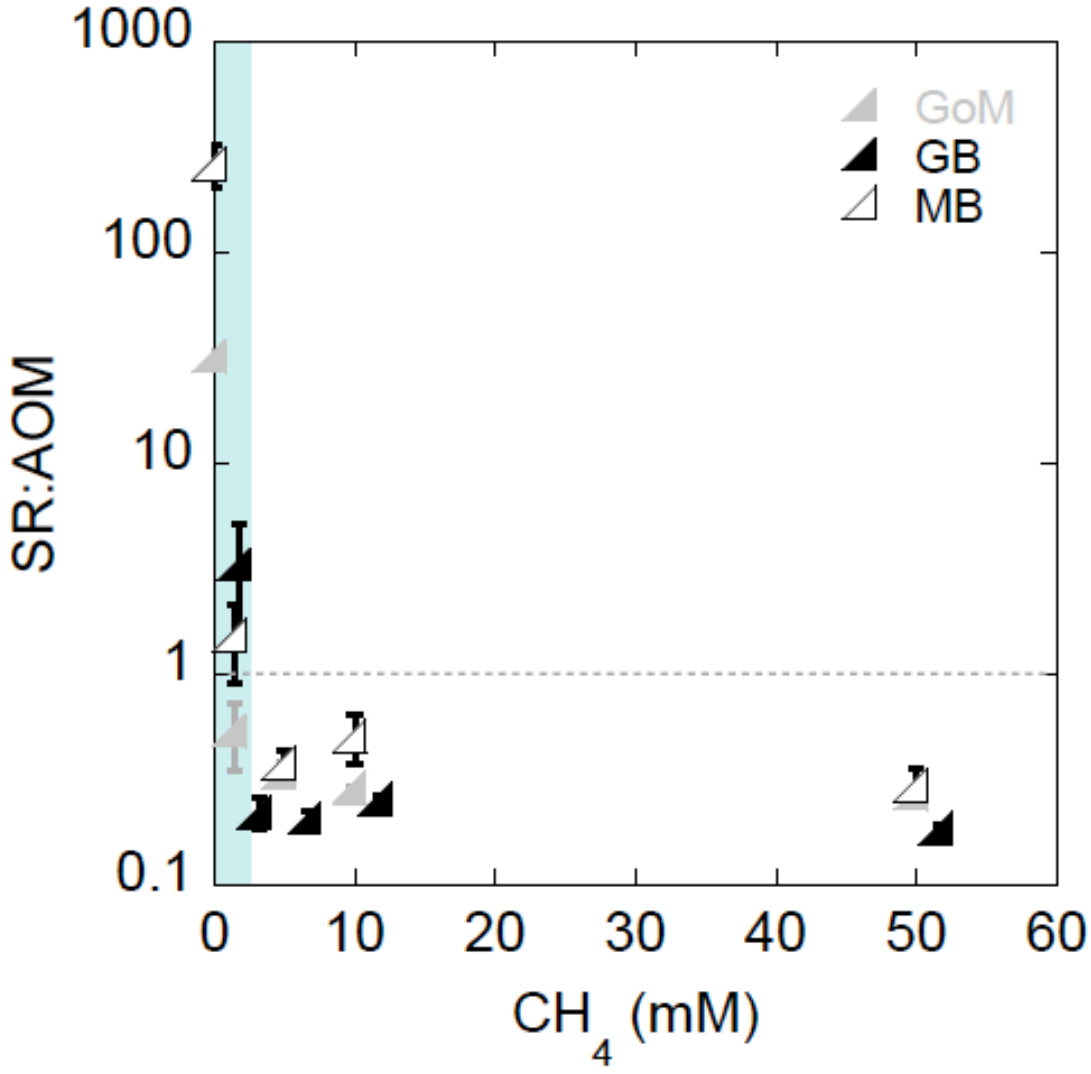

Figure 4.5.

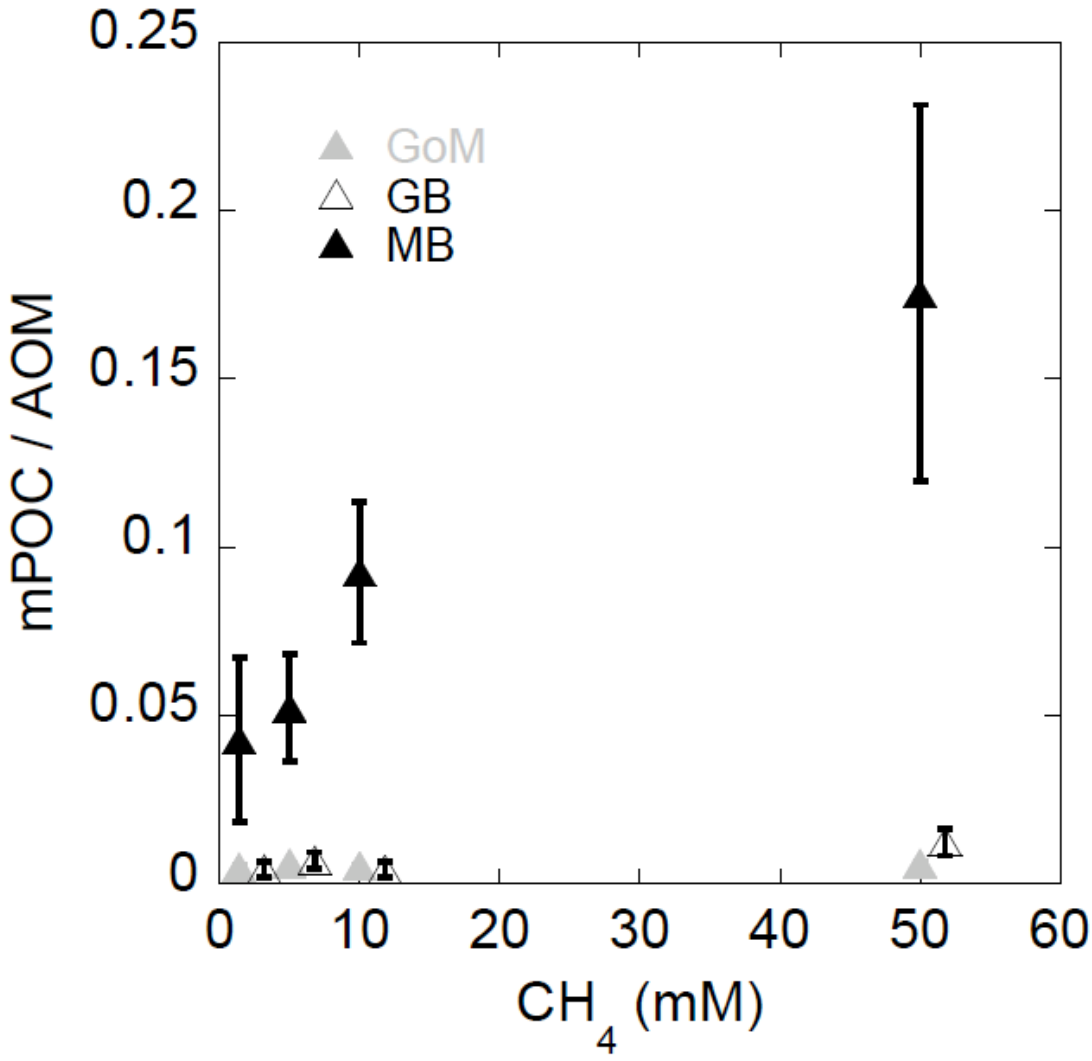

Figure 4.6.

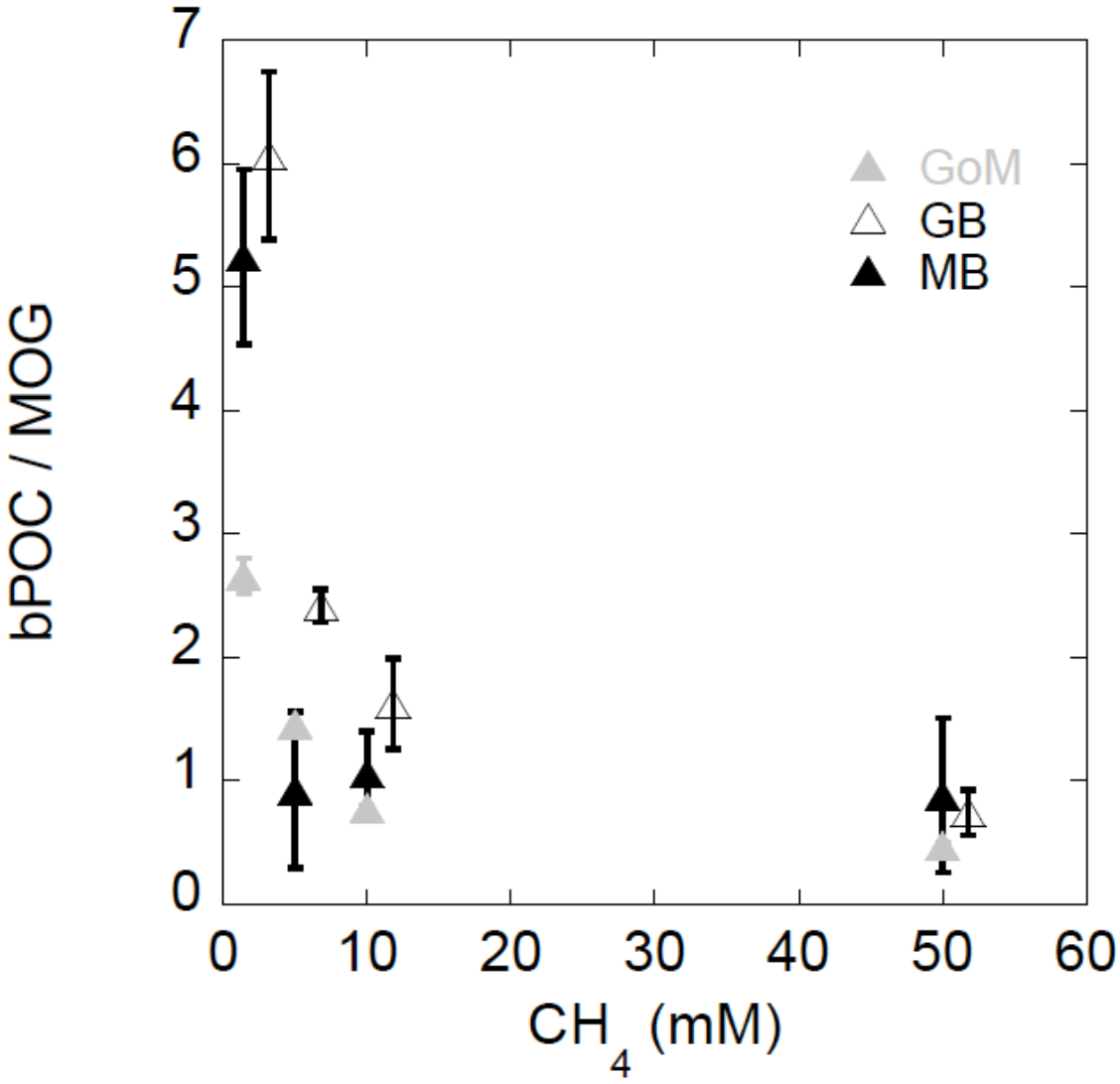

References

Arvidson, R. S., Morse, J. W., and Joye, S. B., 2004. The sulfur biogeochemistry of chemosynthetic cold seep communities, gulf of Mexico, USA. *Marine Chemistry* **87**, 97-119.

Boetius, A., Ravenschlag, K., Schubert, C. J., Rickert, D., Widdel, F., Gieseke, A., Amann, R., Jorgensen, B. B., Witte, U., and Pfannkuche, O., 2000. A marine microbial consortium apparently mediating anaerobic oxidation of methane. *Nature* **407**, 623-626.

Catling, D. C., Zahnle, K. J., and McKay, C., 2001. Biogenic methane, hydrogen escape, and the irreversible oxidation of early Earth. *Science* **293**, 839-839.

Dale, A. W., Aguilera, D. R., Regnier, P., Fossing, H., Knab, N. J., and Jorgensen, B. B., 2008. Seasonal dynamics of the depth and rate of anaerobic oxidation of methane in Aarhus Bay (Denmark) sediments. *Journal of Marine Research* **66**, 127-155.

de Angelis, M. A., Baross, J. A., and Lilley, M. D., 1991. Enhanced microbial methane oxidation in water from a deep-sea hydrothermal vent field at simulated in situ hydrostatic pressures. *Limnology and Oceanography* **36**, 565-570.

Devol, A. H., 1983. Methane oxidation rates in the anaerobic sediments of Saanich Inlet. *Limnology and Oceanography* **28**, 738-742.

Duan, Z. and Mao, S., 2006. A thermodynamic model for calculating methane solubility, density and gas phase composition of methane-bearing aqueous fluids from 273 to

523 ºK and from 1 to 2000 bar. *Geochimica et Cosmochimica Acta* **70**, 3369-3386.

Hinrichs, K.-U., Hayes, J. M., Sylva, S. P., Brewer, P. G., and DeLong, E. F., 1999. Methane-consuming archaebacteria in marine sediments. *Nature* **398**, 802-805.

Hoehler, T. M., Alperin, M. J., Albert, D. B., and Martens, C. S., 1994. Field and Laboratory Studies of Methane Oxidation in an Anoxic Marine Sediment: Evidence for a Methanogen-Sulfate Reducer Consortium. *Global Biogeochem. Cycles* **8**, 451-463.

Iversen, N. and Blackburn, T. H., 1981. Seasonal rates of methane oxidation in anoxic marine sediments. *Applied and Environmental Microbiology* **41**, 1295-1295.

Iversen, N. and Jorgensen, B. B., 1985. Anaerobic methane oxidation rates at the sulfate-methane transition in marine sediments from Kattegat and Skagerrak (Denmark). *Limnology and Oceanography*, 944-955.

Jorgensen, B. B., 2006. *Bacteria and marine biogeochemistry*. Springer, Berlin.

Joye, S. B., Boetius, A., Orcutt, B. N., Montoya, J. P., Schulz, H. N., Erickson, M. J., and Lugo, S. K., 2004. The anaerobic oxidation of methane and sulfate reduction in sediments from Gulf of Mexico cold seeps. *Chemical Geology* **205**, 219-238.

Kallmeyer, J. and Boetius, A., 2004. Effects of temperature and pressure on sulfate reduction and anaerobic oxidation of methane in hydrothermal sediments of Guaymas Basin. *Applied and environmental microbiology* **70**, 1231-1231.

Kasting, J. F., 2005. Methane and climate during the Precambrian era. *Precambrian Research* **137**, 119-129.

Knittel, K., Losekann, T., Boetius, A., Kort, R., and Amann, R., 2005. Diversity and Distribution of Methanotrophic Archaea at Cold Seeps. *Appl. Environ. Microbiol.* **71**, 467-479.

Losekann, T., Knittel, K., Nadalig, T., Fuchs, B., Niemann, H., Boetius, A., and Amann, R., 2007. Diversity and abundance of aerobic and anaerobic methane oxidizers at the Haakon Mosby Mud Volcano, Barents Sea. *Appl. Environ. Microbiol.*, AEM.00016-07-AEM.00016-07.

Lovley, D. R. and Goodwin, S., 1988. Hydrogen concentrations as an indicator of the predominant terminal electron-accepting reactions in aquatic sediments. *Geochimica et Cosmochimica Acta* **52**, 2993-3003.

Meulepas, R. J. W., Jagersma, C. G., Zhang, Y., Petrillo, M., Cai, H., Buisman, C. J. N., Stams, A. J. M., and Lens, P. N. L., 2010. Trace methane oxidation and the methane dependency of sulfate reduction in anaerobic granular sludge. *FEMS Microbiology Ecology* **72**, 261-271.

Moran, J. J., House, C. H., Freeman, K. H., and Ferry, J. G., 2005. Trace methane oxidation studied in several Euryarchaeota under diverse conditions. *Archaea* **1**, 303-303.

Nauhaus, K., Boetius, A., Kr\üger, M., and Widdel, F., 2002. In vitro demonstration of anaerobic oxidation of methane coupled to sulphate reduction in sediment from a marine gas hydrate area. *Environmental Microbiology* **4**, 296-305.

Omoregie, E. O., Niemann, H., Mastalerz, V., de Lange, G. J., Stadnitskaia, A., Mascle, J., Foucher, J.-P., and Boetius, A., 2009. Microbial methane oxidation and sulfate

reduction at cold seeps of the deep Eastern Mediterranean Sea. *Marine Geology* **261**, 114-127.

Orcutt, B., Boetius, A., Elvert, M., Samarkin, V., and Joye, S. B., 2005. Molecular biogeochemistry of sulfate reduction, methanogenesis and the anaerobic oxidation of methane at Gulf of Mexico cold seeps. *Geochimica et Cosmochimica Acta* **69**, 4267-4281.

Orcutt, B., Joye, S.B., Kleindienst, S., Knittel, K., Ramette, A., Reitz, A., Samarkin, V., Treude, T., Boetius, A., 2009. Impact of natural oil and higher hydrocarbons on microbial diversity, distribution and activity in Gulf of Mexico cold seep sediments. *Deep Sea Research Part II: Topical Studies in Oceanography* ***in press***.

Oremland, R. S., Marsh, L. M., and Polcin, S., 1982. Methane production and simultaneous sulphate reduction in anoxic, salt marsh sediments. *Nature* **296**, 143-145.

Orphan, V. J., House, C. H., Hinrichs, K.-U., McKeegan, K. D., and DeLong, E. F., 2001. Methane-Consuming Archaea Revealed by Directly Coupled Isotopic and Phylogenetic Analysis. *Science* **293**, 484-487.

Parkes, R. J., Cragg, B. A., Bale, S. J., Goodman, K., and Fry, J. C., 1995. A combined ecological and physiological approach to studying sulphate reduction within deep marine sediment layers. *Journal of Microbiological Methods* **23**, 235-249.

Reeburgh, W. S., 2007. Oceanic Methane Biogeochemistry. *Chemical Reviews* **107**, 486-513.

Reeburgh, W. S. and Heggie, D. T., 1977. Microbial methane consumption reactions and their effect on methane distributions in freshwater and marine environments. *Limnology and Oceanography* **22**, 1-9.

Scheller, S., Goenrich, M., Boecher, R., Thauer, R. K., and Jaun, B., 2010. The key nickel enzyme of methanogenesis catalyses the anaerobic oxidation of methane. *Nature* **465**, 606-608.

Schilov, A. E., Koldasheva, E.B., Kovalenko, S.V., Akentieva, N.P., Varfolomeyev, S.D., Kalyuzhnyi, S.V., Skylar, V.I., 1999. Methanogenesis is reversible: the formation of acetate in methane carboxylation by bacteria of methanogenic biocenosis. *Dokl RAN* **367**, 557-559.

Shen, Y., Knoll, A. H., and Walter, M. R., 2003. Evidence for low sulphate and anoxia in a mid-Proterozoic marine basin. *Nature* **423**, 632-635.

Treude, T., Orphan, V., Knittel, K., Gieseke, A., House, C. H., and Boetius, A., 2007. Consumption of Methane and CO2 by Methanotrophic Microbial Mats from Gas Seeps of the Anoxic Black Sea. *Appl. Environ. Microbiol.* **73**, 2271-2283.

Tuttle, J. H., Wirsen, C. O., and Jannasch, H. W., 1983. Microbial activities in the emitted hydrothermal waters of the Galapagos Rift vents. *Marine Biology* **73**, 293-299.

Vernadsky, V. I., 1926. *Biosfera*, Leningrad (in Russian).

Weber, A. and J\orgensen, B. B., 2002. Bacterial sulfate reduction in hydrothermal sediments of the Guaymas Basin, Gulf of California, Mexico. *Deep Sea Research Part I: Oceanographic Research Papers* **49**, 827-841.

Wegener, G., Niemann, H., Elvert, M., Hinrichs, K.-U., and Boetius, A., 2008. Assimilation of methane and inorganic carbon by microbial communities mediating the anaerobic oxidation of methane. *Environmental Microbiology* **10**, 2287-2298.

Wirsen, C. O., Tuttle, J. H., and Jannasch, H. W., 1986. Activities of sulfur-oxidizing bacteria at the 21 N East Pacific Rise vent site. *Marine Biology* **92**, 449-456.

Zehnder, A. J. and Brock, T. D., 1979. Methane formation and methane oxidation by methanogenic bacteria. *J. Bacteriol.* **137**, 420-432.

CHAPTER 5

HIGH RATES OF DENITRIFICATION AND NITRATE REMOVAL IN COLD SEEP SEDIMENTS[1]

[1] Bowles, M.W. and S.B. Joye. 2010. *ISME Journal* doi:10.1038/ismej.2010.134. Reprinted here with permission of the publisher.

Abstract

We measured denitrification and nitrate removal rates in cold seep sediments from the Gulf of Mexico. Heterotrophic potential denitrification rates were assayed in time-series incubations. Surficial sediments inhabited by *Beggiatoa* exhibited higher heterotrophic potential denitrification rates (32 μM N reduced d^{-1}) than did deeper sediments (11 μM N reduced d^{-1}). Nitrate removal rates were high in both sediment horizons, respectively. These nitrate removal rates translate into rapid turnover times (<1 d) for the nitrate pool resulting in a faster turnover than for the sulfate pool. Together, these data underscore the rigorous nature of internal nitrogen cycling at cold seeps and a requirement for novel mechanisms providing nitrate to the sediment microbial community.

1. Introduction

Nitrate is abundant (~30-40 μM) in the deep, oxygenated bottom waters that overlie cold seeps but no data describing dissimilatory nitrate reduction (*hereafter* DNF) or total nitrate removal rates in such environments are available. Most studies of nitrate cycling at cold seeps have focused on qualitative descriptions of vacuolate sulfide oxidizing bacteria (VSOB) (Teske and Nelson, 2006 *and references therein*), which concentrate nitrate in their vacuoles and couple nitrate reduction to sulfide oxidation (McHatton et al., 1996, Sayama et al., 2005). GOM cold seeps are characterized by abundant stocks of reduced organic carbon in the form of liquid and gaseous hydrocarbons (Arvidson et al., 2004, Joye et al., 2004). Denitrifying bacteria have a metabolic flexibility similar to that of sulfate reducing bacteria and can degrade liquid hydrocarbons (Widdel and Rabus, 2001). Considering the abundant carbon sources and relatively high concentrations of nitrate in overlying waters (Joye et al., 2004; Joye et al., 2010), heterotrophic DNF is a likely metabolic pathway at cold seeps.

Heterotrophic, or non-sulfide based, DNF has not been measured at cold seeps, which is surprising since cold seeps support extremely high rates of heterotrophic metabolism, mainly sulfate reduction (Arvidson et al. 2004; Bowles et al., submitted). Hexadecane oxidation coupled to DNF, for example, is a highly exergonic process generating -983 kJ per mole N_2 formed (Widdel and Rabus, 2001):

$C_{16}H_{34} + 19.6NO_3^- + 3.6H^+ \rightarrow 16HCO_3^- + 9.8N_2 + 10.8H_2O$ Equation 1

where activities were assumed to be 10^{-2}, pH 7, and liquid *n*-hexadecane was considered. Here we present the first rate assays of heterotrophic potential denitrification from sediments from a northern Gulf of Mexico (GOM) cold seep.

2. Methods

Sediment covered by a *Beggiatoa* mat was collected from an active cold seep in the Northern Gulf of Mexico (lease block Mississippi Canyon 118; see Lapham et al., 2008 for details). Geochemistry (nitrate, nitrite, ammonium, sulfate and sulfide concentration determination) sampling and methods followed Joye et al. (2004). We measured heterotrophic potential denitrification rates in helium-purged, inorganic nitrogen (nitrate, nitrite, and ammonium) and sulfide- and sulfate- free sediment slurries (2:1 artificial porewater (adapted from Weston and Joye, 2005) to sediment ratio) from *Beggiatoa* inhabited surface sediments (0-6 cm) and a deeper layer (6-12 cm) lacking visible filaments. Nitrate removal rates were determined from the linear decrease in nitrate concentration over time while heterotrophic potential denitrification rates were estimated from the evolution of $^{29}N_2$ and $^{30}N_2$ over time (Kana et al., 1998). Briefly, ~75 μM $^{15}NO_3^-$ and 2 mM C (equimolar C from lactate and acetate) was added to headspace free hungate tubes and tubes were sampled for dissolved constituents at multiple time points (Porubsky et al., 2009).

3. Results & Discussion

The concentration of total dissolved inorganic nitrogen species (ammonium, 260 μM; nitrate, 180 μM; and nitrite, 8 μM) was highest just below the sediment surface (1.5 cm, Fig. 1A). Pore water sulfate concentration profiles illustrated significant removal at depth and a concomitant increase in sulfide (Fig. 1B). The observation of low sulfide accumulation and significant concentrations of total dissolved inorganic nitrogen in upper sediments may reflect nitrate storage and sulfide oxidation by *Beggiatoa* (Joye et al., 2004).

Both the upper and lower sediments supported significant rates of heterotrophic potential denitrification. In the surface sediments, nitrate was depleted rapidly and the production of ^{15}N-labeled dinitrogen products (17 μM $^{30}N_2$ and <1 μM $^{29}N_2$) was easily detectable after 4 hours (Fig. 1B). Linear substrate removal and product accumulation over time yielded estimates of nitrate removal and heterotrophic potential denitrification rates of 96 μM N d^{-1} and 32 μM N d^{-1}, respectively. In the deeper sediments, nitrate was also rapidly consumed (Fig. 1C) and at the same time 5 μM of $^{30}N_2$ formed; $^{29}N_2$ generation was low (<1 μM). Rates of nitrate removal and heterotrophic potential denitrification were lower, being 52 μM N reduced d^{-1} and 11 μM N reduced d^{-1}, respectively.

At Gulf of Mexico cold seeps, sulfate reduction is the only terminal metabolic process that has been quantified (Arvidson et al., 2004, Joye et al., 2004). We show that denitrification and nitrate removal are also important processes at these seeps. Denitrification is well documented in numerous other environments (Seitzinger et al., 1988 *and references therein*), and integrated rates typically range from 1 to >1000 μmol N m^{-2} h^{-1} in freshwater and marine systems. The depth integrated potential denitrification rates for GOM seeps are 80 and 27 μmol N m^{-2} h^{-1}, for upper and lower sediment horizons, respectively. These rates are comparable with rates from coastal marine sediments (Seitzinger et al., 1988), and from moderately-eutrophic to eutrophic freshwater environments. Nitrate removal could also reflect additional processes such as assimilation, vacuole storage, reduction to ammonium (DNRA), or nitrite production and removal via anaerobic ammonium oxidation (ANAMMOX). Previously published data

would suggest that DNRA may be more important in sulfidic and carbon-rich cold seep sediments than ANAMMOX (Burgin and Hamilton, 2007).

The integrated heterotrophic potential denitrification rates result in an extremely fast turnover time (on the order of 2 days) for the nitrate pool in these seep sediments (Fig. 2). The sulfate pool turnover time was 11 to 72 days (Bowles et al., submitted; Fig. 2). When factoring in total nitrate removal, the turnover time of the nitrate pool is faster, being 0.7 and 0.4 days, in upper and lower sediment horizons, respectively. These results lead us to postulate that 1) heterotrophic denitrification is a relevant and important component of C and N cycling in cold seeps and 2) dissimilatory nitrate reduction, nitrate storage in vacuoles, and/or assimilation into biomass requires tight coupling of nitrogen cycling processes and raises the potential for internal nitrate sources, such as anaerobic nitrification (Luther et al., 1997) and/or downward advection of bottom water nitrate within these habitats.

Acknowledgements. This research was supported by the NOAA National Institute for Undersea Science and Technology (award numbers 06-09-018, 07-4 10-028 and 08-10-031). The Gulf of Mexico Gas Hydrate Research Consortium provided ship time and at-sea logistical support. We thank W. Porubsky for providing useful suggestions and assistance in the early stages of this research.

Figure 5.1. A) Geochemical constituent NH_4^+ (μM), NO_3^- (μM), NO_2^- (μM), SO_4^{2-} (mM), H_2S (μM) versus depth (cm). **B)** Average concentrations of reactant, NO_3^- (μM), and potential products, NO_2^-, $^{29}N_2$, and $^{30}N_2$ (μM) versus time (hr) for slurried sediments from 0-6 cm, as well as **C)** 6-12 cm horizons.

Figure 5.2. Turnover times (d) of nitrate and sulfate from MC118 (sulfate turnover time calculated from data in Bowles et al., *submitted*) due to total nitrate removal and heterotrophic potential denitrification, and SR, respectively.

Figure 5.1.

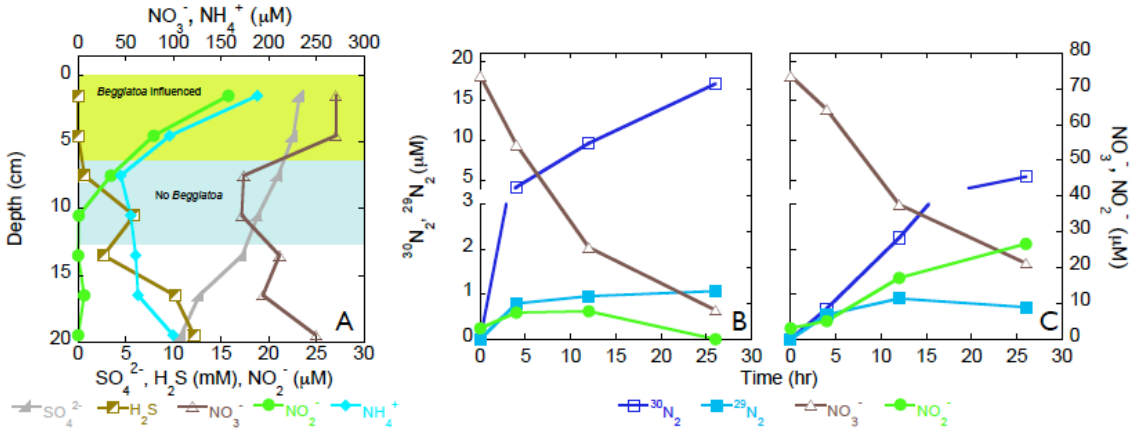
NO3-, NH4+ (μM)
Beggiatoa Influenced
No Beggiatoa
Depth (cm)
A
SO4 2-, H2S (mM), NO2- (μM)
SO4 2-
H2S
NO3-
NO2-
NH4+
30N2, 29N2 (μM)
B
Time (hr)
30N2
29N2
C
NO3-, NO2- (μM)

Figure 5.2.

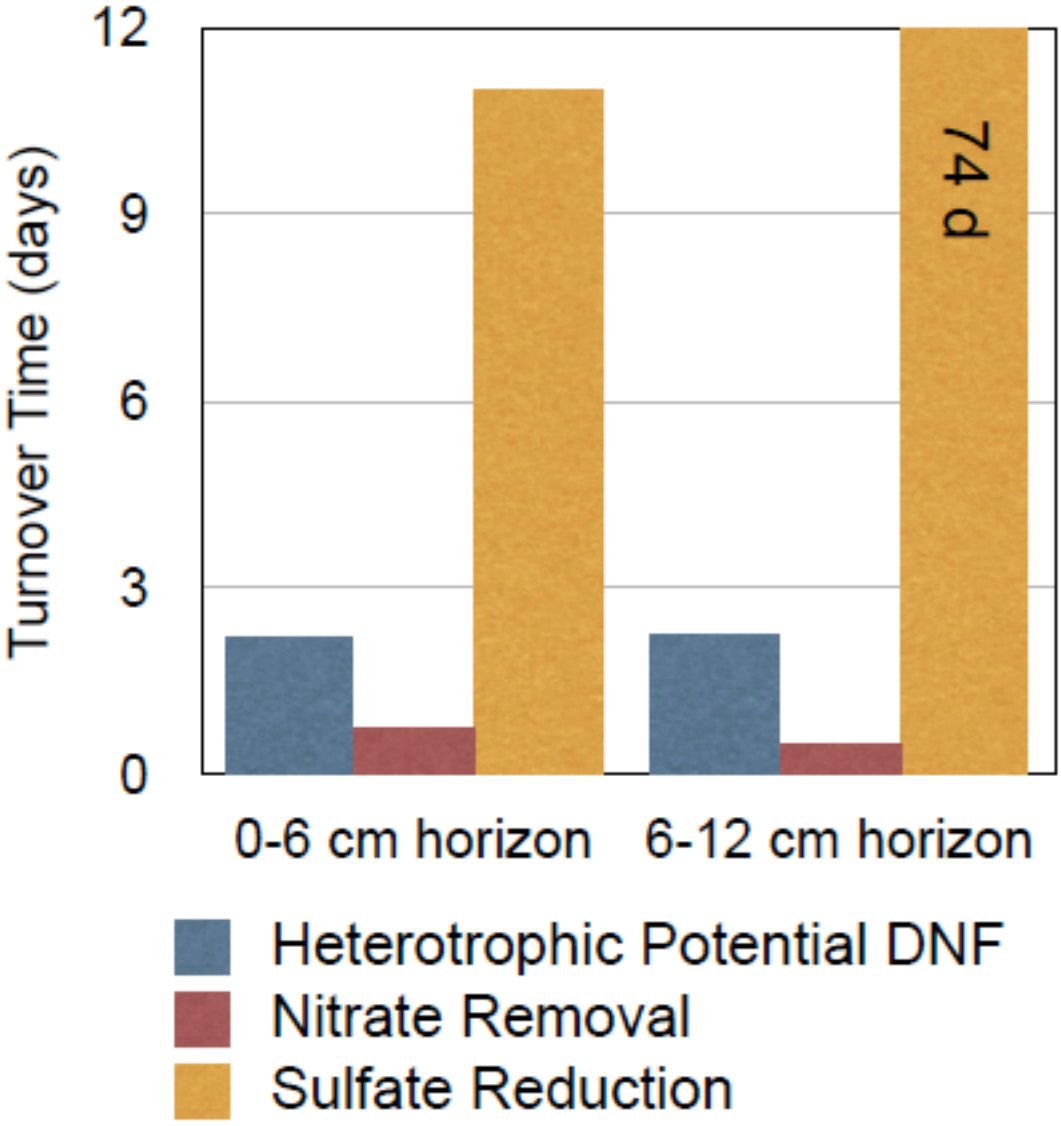
12
9
6
3
0
Turnover Time (days)
74 d
0-6 cm horizon
6-12 cm horizon
Heterotrophic Potential DNF
Nitrate Removal
Sulfate Reduction

References

Arvidson, R. S., Morse, J. W., and Joye, S. B., 2004. The sulfur biogeochemistry of chemosynthetic cold seep communities, Gulf of Mexico, USA. *Marine Chemistry* **87**, 97-119.

Bowles, M.W., Samarkin, V.A., Bowles, K.M., Joye, S.B., *in review*. Weak coupling between sulfate reduction and the anaerobic oxidation of methane in methane-rich seafloor sediments. *Geochimica et Cosmochimica Acta.*

Burgin, A.J. and Hamilton, S.K., 2007. Have we overemphasized the role of denitrification in aquatic ecosystems? A review of nitrate removal pathways. *Fron. Ecol. Environ.,* **5**(2), 89-96.

Joye, S. B., Boetius, A., Orcutt, B. N., Montoya, J. P., Schulz, H. N., Erickson, M. J., and Lugo, S. K., 2004. The anaerobic oxidation of methane and sulfate reduction in sediments from Gulf of Mexico cold seeps. *Chemical Geology* **205**, 219-238.

Joye, S. B., M.W. Bowles, V.A. Samarkin, K.S. Hunter and H. Niemann, 2010. Biogeochemical signatures and microbial activity of different cold seep habitats along the Gulf of Mexico lower slope. *Deep Sea Research*, in press.

Kana, T.M., Sullivan, M.B., Cornwell, J.C., Groszkowski, K.M., 1998. Denitrification in estuarine sediments determined by membrane inlet mass spectrometry. *Limnology and Oceanography* **43**(2), 334-339.

Lapham, L. L., Chanton, J.P., Martens, C.S., Higley, P.D., Jannasch, H.W., Woolsey, J.R., 2008. Measuring Temporal Variability in Pore-Fluid Chemistry To Assess

Gas Hydrate Stability: Development of a Continuous Pore-Fluid Array. *Environmental Science & Technology* **42**(19), 7368-7373.

Luther, G.W., Sunby, B., Lewis, B.L., Brendel, P.J., Silverberg, N., 1997. Interactions of manganese with the nitrogen cycle: Alternative pathways to dinitrogen. *Geochimica et Cosmochimica Acta* **61**(19), 4043-4052.

McHatton, S. C., Barry, J.P., Jannasch, H.W., Nelson, D.C., 1996. High Nitrate Concentrations in Vacuolate, Autotrophic Marine Beggiatoa spp., *Appl Environ Microbiol* **62**(3), 954-958.

Porubsky, W. P., Weston, N.B., Joye, S.B., 2009. Interactions between benthic primary production, denitrification and dissimilatory nitrate reduction to ammonium in intertidal sediments. *Estuarine Coastal and Shelf Science,* **83**(4), 392-402.

Sayama M, Risgaard-Petersen N, Nielsen LP, Fossing H, Christensen PB. 2005. Impact of bacterial NO_3 transport on sediment biogeochemistry. *Appl Environ Microbiol* **71**,7575–7577.

Seitzinger, S.P., 1988. Denitrification in freshwater and coastal marine ecosystems: ecological and geochemical significance. *Limnology and Oceanography* **33**(4), 702.

Teske, A. and Nelson, D.C., 2006. The Genera *Beggiatoa* and *Thioploca*. *Prokaryotes*. Springer, New York **3**, 784-810.

Weston, N. B., and S. B. Joye, 2005. Temperature driven accumulation of labile, dissolved organic matter in anoxic marine sediments. *Proceedings of the National Academy of Sciences (U.S.A.)*, **102**, 17036-17040.

Widdel, F. and Rabus, R., 2001. Anaerobic biodegradation of saturated and aromatic hydrocarbons. *Current Opinion in Biotechnology* **12**, 259-276.

CHAPTER 6

CONCLUSIONS

The broad goal of this work was to better assess microbial processes in deep-sea sediments. The initial approach was to use traditional methods and techniques to refine the knowledge of sulfate reduction (SR) and anaerobic methane oxidation (AOM) starting with cold seep sediments (**Chapter 2**). The findings in this initial work led to the realization that novel techniques were needed to more accurately address sulfate and methane cycling in cold seep sediments. To address this we developed a novel method allowing microbial activities to be determined at *in situ* pressures and methane concentrations (**Chapter 3**). Next we proceeded to utilize this method on sediments that are typically methane-rich, cold seep and hydrothermally-altered sediments (**Chapter 4**). Findings regarding SR, AOM, and methanogenesis (MOG), led to the suggestion for novel pathways to support methane oxidation in these methane rich environments. Finally a candidate process to support AOM could be denitrification (DNF) though this process was not known to occur in cold seep sediments. The reports of DNF here are the first for cold seep sediments (**Chapter 5**).

AOM was considered a process that was explicitly linked to SR, in a 1:1 ratio. In **Chapter 1** rates measured at a Gulf of Mexico cold seep and those compiled during a global survey (n = 53) of SR and AOM had a median ratio of 10.7 to 1. The median AOM rate from this global survey suggested that the cold seep AOM rate was only 5%

of the previous estimate. Regarding molecular microbiological observations at the study site, in spite of low AOM rates a substantial fraction (>90%) of clone libraries were made up of putative anaerobic methanotrophs (collectively called ANMEs). These findings led to critical assessment of the fundamental assumptions made that classify the archaea termed ANME as methanotrophs. In addition in the Gulf of Mexico study site extremely high rates of sulfate reduction (>20 μmol cm^{-3} d^{-1}) required novel explanations of sulfate replenishment to support such rates. I postulate that biological oxidation and downward moving, or into sediments, advection of sulfate-rich overlying water supports a substantial fraction of SR.

The findings of **Chapter 2** inspired the development of a novel method to more accurately assess microbial activities in methane-rich marine sediments. The method was applied to cold seep and hydrothermally altered sediments (**Chapter 3**) to quantify dissimilatory and assimilatory processes at *in situ* pressures and methane concentrations. Specifically rates of anaerobic oxidation of methane (AOM), sulfate reduction (SR), and bicarbonate-based methanogenesis (MOG) were measured at a range of elevated methane concentrations. In addition particulate organic carbon (POC) formation rates as a proxy for methane and separately bicarbonate assimilation, termed mPOC and bPOC for methane and bicarbonate derived POC were measured. In a reversal of the findings of **Chapter 2** in all sediments analyzed AOM was decoupled from SR as methane concentrations increased, at times becoming 10 times greater than SR. Rates of bPOC typically exceeded mPOC formation, and bPOC typically occurred on the same magnitude as MOG. Together these findings suggest that anaerobic methanotrophs are

predominantly supported by carbon assimilated from bicarbonate. The broader impacts of these findings suggest that novel mechanisms, or pathways, for methane oxidation exist in marine sediments. To clarify these mechanisms we measured the formation of volatile organics (e.g. acetate) and additionally postulate the release of hydrogen during AOM to support such elevated rates and stimulation of multiple processes like SR and MOG. In the contemporary ocean AOM rates exceeding SR rates and high rates of POC formation suggest significant oversights in carbon budgeting at cold seeps and hydrothermal vents. The potential for sulfate independent AOM reach much further than the contemporary ocean because during low sulfate ancient oceans (i.e. Proterozoic) methane oxidation might have been more pronounced than originally thought.

In **Chapter 5** rates of nitrate removal and DNF were measured for the first time in cold seep sediments. The rates of DNF were rapid and comparable to eutrophic freshwater ecosystems. In comparisons of SR to DNF and nitrate removal rates it was realized that nitrate pools were likely turned over at a much faster pace than sulfate pools. The nitrate removal rates are suggestive of an anaerobic mechanism that produces nitrate anaerobically.